Functional and Tunable Synthetic Hydrogel for Reproductive Tissue Engineering

By

Jiwon Kim

A dissertation submitted in partial fulfillment
of the requirements for the degree of
Doctor of Philosophy
(Macromolecular Science and Engineering)
in the University of Michigan
2016

Doctoral Committee:

Assistant Professor Ariella Shikanov, Chair
Assistant Professor Geeta Mehta
Professor Vasantha Padmanabhan
Professor Shuichi Takayama

© Jiwon Kim 2016
All Rights Reserved

DEDICATION

To my family, Shikanov lab, and my beloved, Cindy Yoonkyung Lee

ACKNOWLEDGEMENTS

I solely can not take all the credits myself, and I had met so many great peoples along the way. First, I would like to thank my advisor, Ariella Shikanov. Thanks to her, I have grown so much both as a person and as a scientist. She supported me throughout all difficulties and her passion for science and research has been my one of motivation to challenge myself during many endeavors. I am fortunate to have her as my advisor and I am honored to be her first Ph.D. student. Next, I would like to thank Shikanov lab members. Hong, Uzi, James and Amanda, thanks to you guys, it was fun to come into lab every day and I will cherish that time we spent together. And I would like to thank my undergraduate students, Steven and Jake. I hope you guys learned something from me as much as I learned from you guys. Finally and most importantly, I want to thank my family, friends, and my beloved, Cindy, for being with me every step of the way. Your support, faith, and love have always been there for me. None of this would have been possible and I always will remember. Thank you all and I love you guys so much.

TABLE OF CONTENTS

LIST OF FIGURES

Appendix – Supplemental Materials

Abstract

Many prepubertal girls and young women suffer from premature ovarian insufficiency induced by chemotherapy given for treatment of cancer and autoimmune diseases. Auto-transplantation of cryopreserved ovarian tissue could restore the lost ovarian endocrine function and fertility. Unfortunately, tissue ischemia, inconsistent graft quality and the risk of re-introducing malignant cells may stand in the way of the clinical translation of this approach. Therefore, isolation and re-implantation of multiple follicles may serve as a safer alternative; individual follicles can be isolated from the stromal environment in the ovarian tissue, and encapsulated in a hydrogel functioning as a supportive matrix for these isolated follicles. In the present study, we engineered an artificial ovarian tissue from the early stage follicles using a synthetic hydrogel, poly(ethylene glycol) vinyl-sulfone (PEG-VS), as a supportive matrix. The chemistry of the multi-arm PEG-VS formed by Michael-type addition allows: [1] modification with integrin binding peptides (such as RGD) for cell adhesion and migration and [2] a precise control over mechanical properties, making it suitable for reproductive tissue engineering applications. In this work, first we characterized the crosslinking kinetics of multi-arm PEG hydrogel. We investigated the role of PEG functionality on bioactive modification and mechanical properties of hydrogels, and the combined effect of mechano-biological properties on behavior of encapsulated cells. While the molar concentration of the reactive functional groups was identical in all the conditions, PEG with a larger number of functional groups on each unit allowed a greater degree of modification as well as a more precise control of mechanical properties, making it more suitable for supporting three-dimensional culture. Next, we modeled premature ovarian failure in mice to analyze the capability of PEG hydrogels to support folliculogenesis, vascularization, steroidogenesis and graft longevity *in vivo*. PEG hydrogels

supported folliculogenesis of enzymatically-isolated follicles, leading to repeating estrous cycles and functioning hypothalamus-pituitary-gonadal axis with physiological levels of follicle-stimulating hormone. Furthermore, we demonstrated re-vascularization of the hydrogel, suggesting its capability of undergoing remodeling process. In summary, this is the first study proving the concept of a fully functional artificial ovarian tissue transplant built on the platform of the synthetic PEG hydrogel.

CHAPTER I

Introduction

1.1 Understanding ovarian physiology

Ovarian tissue contains follicles at different developmental stages surrounded by stroma cells and rich vasculature. Follicles, the functional units of the ovary, are composed of a germ cell (the oocyte) and one or more layers of somatic cells (granulosa and theca cells), which are responsible for the production and metabolism of sex hormones, estradiol and progesterone. At birth, the human ovary contains approximately one million of immature follicles, called primordial follicles, which have the potential to develop and produce mature oocytes capable of fertilization. This number decreases to 300,000 follicles at puberty and continues to decline until menopause(1). The ovarian reserve declines rapidly with significantly decreasing fertility around the age of 38 in women due to follicle exhaustion, and eventually, leading to menopause. Premature depletion of the ovarian reserve in women exposed to chemotherapy causes premature ovarian failure (POF) and sterility.

Primordial follicles, the most immature and abundant class of follicles, constitute the ovarian reserve, and activation of a small portion of this reserve each cycle ensures ovarian function(1). Mammalian females are born with a set number of immature primordial follicles, which remain quiescent until puberty. Starting at puberty during each menstrual cycle a small cohort of primordial follicles gets activated and enters the pool of growing follicles(2). Upon activation, at

the primary stage of development, the oocyte expands and granulosa cells become cuboidal(3). Through the secondary stage of development, the granulosa cells proliferate rapidly along with the somatic theca cells on the exterior basement membrane and secrete sex hormones in response to circulating gonadotropins. The process of the selection and maturation of follicles depends on a complex set of systemic and local signals exchanged between follicles and the surrounding environment, which include circulating hormones(4), paracrine factors(5), extracellular matrix(6, 7), and vasculature(8-10). The final stage of follicle development into antral follicle culminates with the development of an antrum (a fluid-filled cavity adjacent to the oocyte), and it is followed by ovulation of an oocyte.

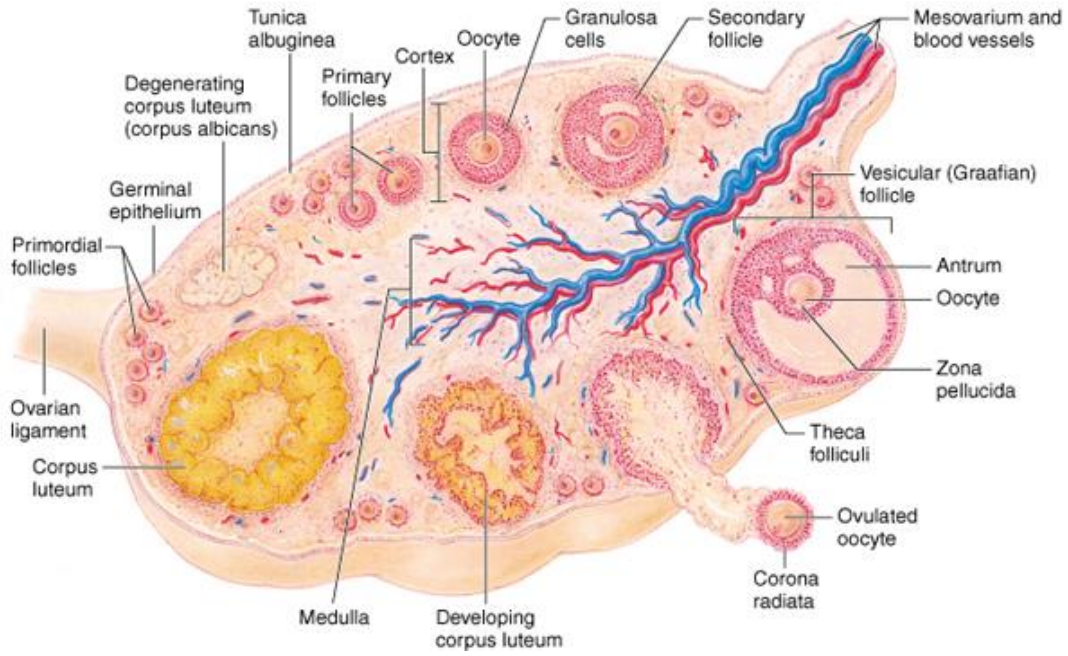

Fig. 1.1 – Ovarian Physiology. Ovary contains follicles at different developmental stages surrounded by stroma cells and rich vasculature. Follicles, the functional units of the ovary, are composed of a germ cell (the oocyte) and layers of somatic cells (granulosa and theca cells), which are responsible for the production and metabolism of sex hormones, estradiol and progesterone. *Copyright at Beniamin Cumminas.*

1.2 Fertility and ovarian endocrine function preservation

Progress in modern anticancer therapy has led to improved long-term survival rates of above 80% in most childhood malignancies(11). Unfortunately, chemotherapy and radiation have irreversible long-term side effects. Elimination of germline cells in the ovary and testes and resulting deficient reproductive and endocrine function is one of them. The rates of POF are very high; it occurs in up to 40% of the young women and girls treated with radiation and chemotherapy or combination of both(12, 13). In girls, POF has devastating consequences including late puberty, short stature and altered body image, interference with the physical and psychological development well into young adulthood(14). In young women, POF leads to a plethora of metabolic abnormalities; cripples cardiovascular system and causes premature aging(15, 16).

Currently, clinical strategies for fertility preservation exist only for women who can produce a fully mature egg. If the anticancer treatment can be delayed, patients can undergo hormonal induction for 2 to 3 weeks to stimulate follicle development and recover mature oocytes(17). The oocytes can then be fertilized *in vitro* post-treatment. However, pre-treatment egg preservation does not address the loss of ovarian endocrine function, and most importantly, egg preservation is not available to prepubescent girls or patients who require immediate treatment(18).

In vitro follicle culture and cryopreservation of ovarian tissue could address the loss of fertility and endocrine function, and expand options available to the patients (Fig.1.2). Multiple reports have shown successful survival and growth of mature mouse follicles *in vitro* using either two- or three-dimensional culture systems(19-23), yet this approach can not address the loss of the endocrine function. Another technique is autotransplantation, which is transplantation of cryopreserved ovarian tissue, which has shown promising results for fertility and ovarian

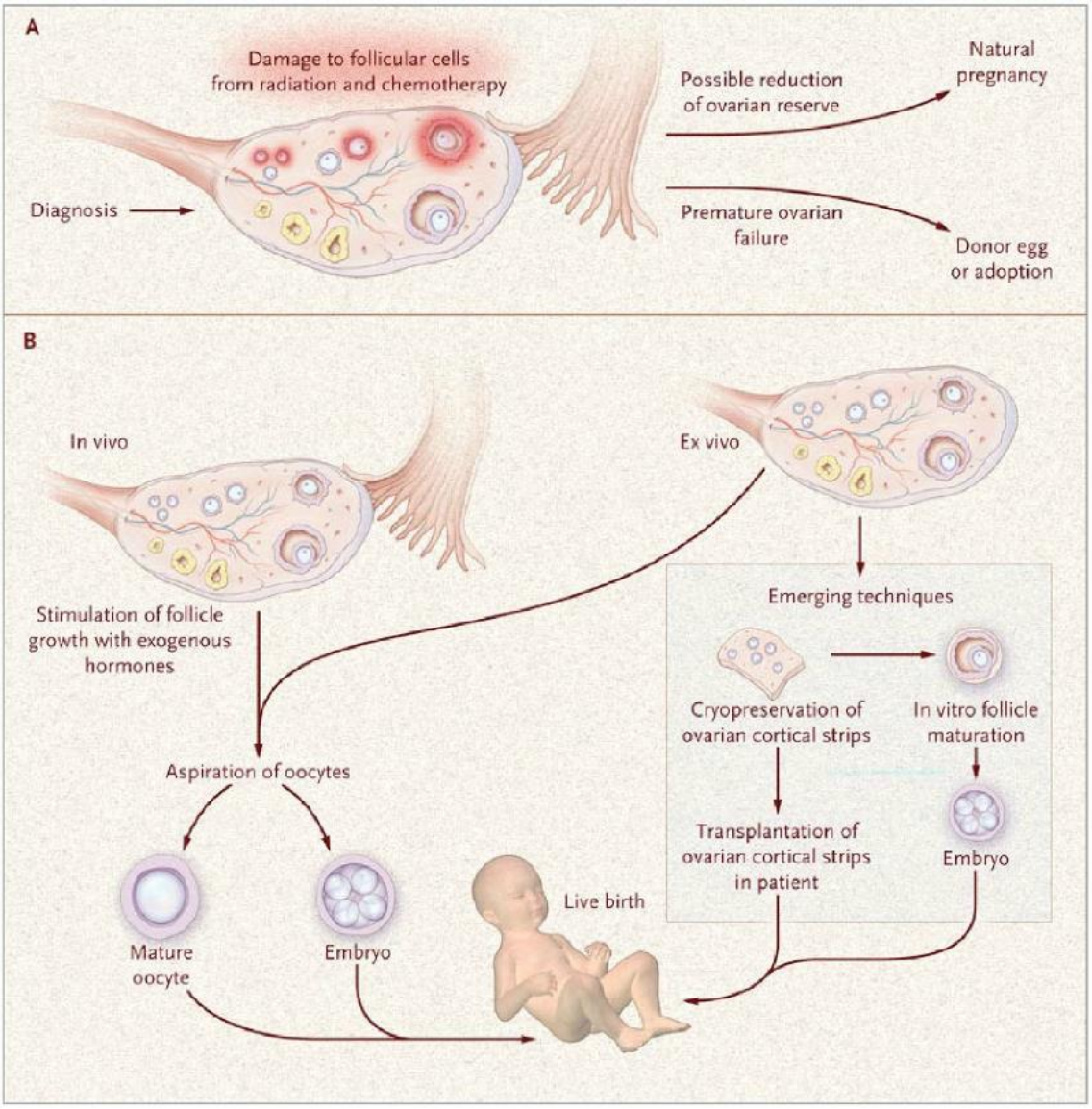

Fig.1.2 – Treatment Effects on Fertility and Options for Preserving Fertility in Women with Cancer. (A) A high-dose radiation and most chemotherapeutic agents damage the growing cells in mature and immature follicles and, depending on the type of drug, the dose, and the age of the patient, may result in depletion of many or all follicles. This depletion may result in a short-term loss of reproductive function and an inability to attain a natural pregnancy after treatment. **(B)** For patients who do not require immediate treatments, they can delay treatment and undergo hormonal induction for 2 to 3 weeks to stimulate follicle development and recover mature oocytes. The oocytes can be frozen or fertilized, depending on the wishes of the patient. If there is insufficient time or if there are contraindications, one ovary can be removed, and ovarian cortical strips can be cryopreserved for use in tissue transplantation or emerging techniques such as in vitro follicle maturation. *(According to Jeruss, JS. and Woodruff, TK. Preservation of fertility in patients with cancer. N.Engl.J.Med. 2009, 360. 9. 902 – 911.)*

function restoration. Autotransplantation does not require repeated cycles of hormone stimulation, thus reducing risk of ovarian carcinoma or ovarian hyperstimulation syndrome, and allowing immediate start of anti-cancer treatments(24).

A successful autotransplantation would require maintenance of a large primordial follicle population, which can maintain monthly cycles and provide healthy fertilizable eggs(17, 25-27). However, several groups reported that the size of the graft decreased (30 – 70% of the original size) after autotransplantation, and there was a significant loss of the follicular pool (50 – 90%) due to tissue ischemia and hypoxia as a result of oxidative stress(28-30). Furthermore, it was hypothesized that insufficient number of follicles secreting inhibitory factors led to a burst activation of premature follicles and shortened graft longevity(31). As a result, multiple invasive procedures are required to achieve ovarian function due to the short life span of ovarian tissue(28). More importantly, the elevated risk of re-introducing malignant cells when transplanting ovarian tissue from a patient with hematological cancer presents another limitation(32). Therefore, isolating individual follicles free from other ovarian cells and grafting a purified follicle population presents a safer alternative; individual follicles can be separated from the rest the ovarian tissue, while the artificial supportive matrix can prevent follicular loss and promote graft remodeling.

1.3 Tunable synthetic hydrogel as a platform for grafting of isolated follicles

The chemistry of the multi-arm PEG-VS cross-linked by MTA allows: [1] modification with integrin binding peptides (such as RGD) for cell adhesion and migration(33, 34), and [2] a precise control over mechanical properties(35). Also stepwise co-polymerization of end-functionalized multi-arm PEG-VS can be carried out at physiological temperature and pH(36),

making it suitable for reproductive tissue engineering applications. Multi-arm PEG hydrogels crosslinked with protease-sensitive peptides can degrade in response to enzymes secreted by the follicle, such as plasminogen activators (PA) and matrix metalloproteinases (MMPs) (Fig.1.3)(7, 37-39).

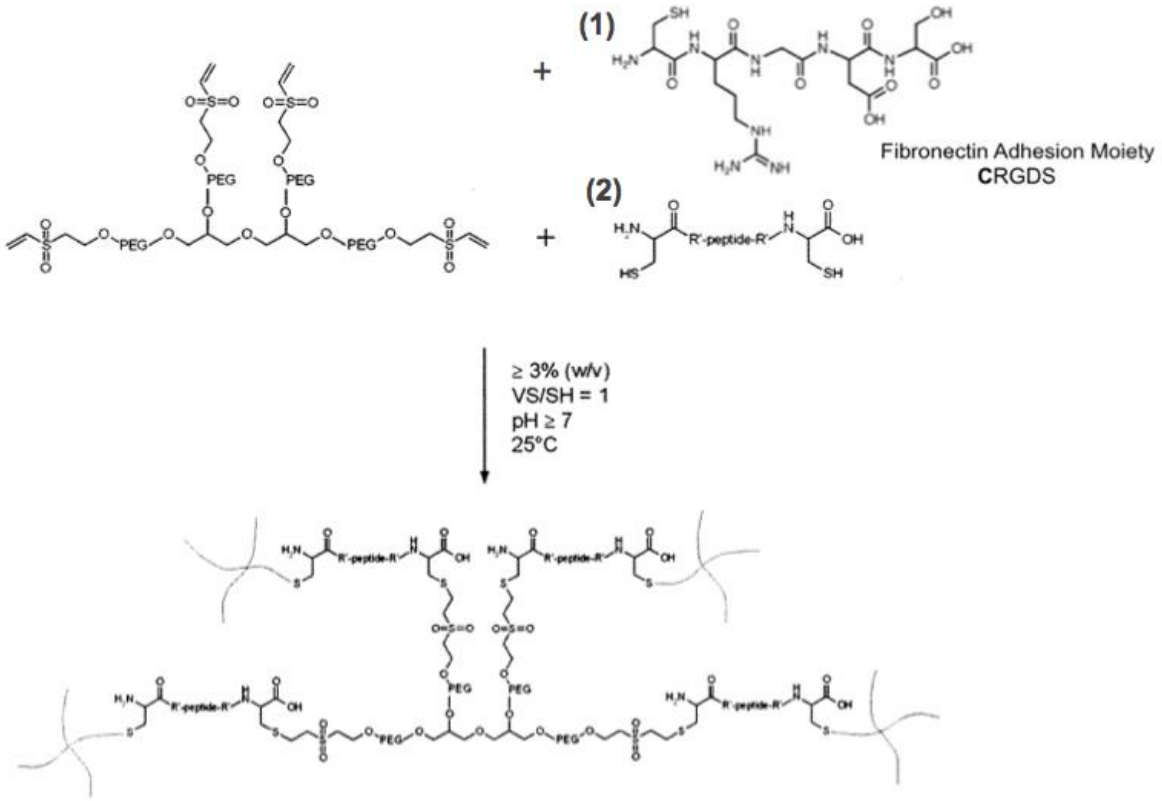

Fig. 1.3 – Synthesis scheme for the stepwise copolymerization of biomolecules containing free thiols on Cys residues with end-functionalized PEG macromers bearing conjugated unsaturated moieties. *(Adapted to Lutolf, MP. et al. Synthesis and physiochemical characterization of end-linked poly(ethylene glycol)-co-peptide hydrogels formed by Michael-type addition. Biomacromolecules. (2003) 4,713 –722.)*

Cell and follicle responsive proteolytic degradation is required for cell proliferation, migration, and expansion of the follicle encapsulated in a hydrogel. The mesh size of PEG hydrogels is in the range of tens to a hundred nanometers, which allows diffusion of oxygen and nutrients to the encapsulated tissues(40). Previous studies demonstrated that PEG-based matrices support folliculogenesis *in vitro*(22), vascularization of tissue constructs *in vivo*(41) and promote

matrix remodeling in bone defects(42, 43) through the control of the hydrogel degradation kinetics and their material properties.

Therefore, we hypothesized that a finely tuned and functional PEG hydrogel would serve as a biomimetic grafting material that supports folliculogenesis, remodeling and vascularization. These tunable biophysical and biochemical properties(35, 36) of PEG hydrogels would successfully mimic the native complexity of the extracellular matrix and function as a platform for artificial ovarian tissues.

1.4 Dissertation organization

The aims of this doctoral research are to develop, validate, and characterize functional and tunable 3D synthetic PEG hydrogel to mimic the components of extracellular matrix (ECM) for reproductive tissue engineering applications. This study was designed to understand the role of biomimetic 3D hydrogels in reconstruction and regeneration of ovarian tissues *in vivo*. In Chapter II, we address three different components of building an artificial ovarian tissue from enzymatic isolation and purification of the early stage follicles to encapsulation in natural hydrogels. The work investigating the enzymatic isolation and purification of isolated follicles using microfluidic device was published in *RSC Advances* in 2013. Chapter III presents the work of characterizing natural hydrogels, fibrin, collagen or fibrin-collagen, to design more dynamic environment for cells, and to understand how different mechanical and biological properties affect cellular growth and behavior. This work was published in *Journal of Biomedical Materials Research Part A* in 2015. Chapter IV reports the work of characterizing of a synthetic PEG hydrogel: [1] how increasing PEG functionality from 4 to 8, and the act of bioactive modification affect the kinetics of hydrogel formation and material properties, [2] the combined effect of

mechano-biological properties on cellular behavior. This work was published in *Soft Matter* in 2016. Chapter V describes the development of immature follicles encapsulated in PEG hydrogels and evaluates the graft function after orthotopic transplantation into ovariectomized mice. We demonstrated that PEG hydrogels with proteolytically-controlled degradation successfully supported follicle growth and promoted graft revascularization and remodeling. Regenerated artificial ovarian tissue successfully restored the cyclic hormonal changes in the reproductive tract as well as the function of Hypothalamus-Pituitary-Gonadal (HPG) axis. This work is currently under review. Lastly, chapter VI provides a summary of the findings and the future directions of this research in particular and the field in general.

1.5 References

1. Picton HM. Activation of follicle development: The primordial follicle. *Theriogenology.* 2001 Apr 1; 55(6): 1193-1210.

2. Gougeon A. Regulation of ovarian follicular development in primates: Facts and hypotheses. *Endocr Rev.* 1996 Apr; 17(2): 121-155.

3. Da Silva-Buttkus P, Jayasooriya GS, Mora JM, Mobberley M, Ryder TA, Baithun M, Stark J, Franks S, Hardy K. Effect of cell shape and packing density on granulosa cell proliferation and formation of multiple layers during early follicle development in the ovary. *J Cell Sci.* 2008 Dec 1; 121(Pt 23): 3890-3900.

4. de Kretser DM, Hedger MP, Loveland KL, Phillips DJ. Inhibins, activins and follistatin in reproduction. *Hum Reprod Update.* 2002 Nov-Dec; 8(6): 529-541.

5. Knight PG, Glister C. TGF-beta superfamily members and ovarian follicle development. *Reproduction.* 2006 Aug; 132(2): 191-206.

6. Berkholtz CB, Shea LD, Woodruff TK. Extracellular matrix functions in follicle maturation. *Semin Reprod Med.* 2006 Sep; 24(4): 262-269. PMCID: PMC2648384.

7. Rodgers RJ, Irving-Rodgers HF, Russell DL. Extracellular matrix of the developing ovarian follicle. *Reproduction.* 2003 Oct; 126(4): 415-424.

8. Acosta TJ, Hayashi KG, Ohtani M, Miyamoto A. Local changes in blood flow within the preovulatory follicle wall and early corpus luteum in cows. *Reproduction.* 2003 May; 125(5): 759-767.

9. Redmer DA, Reynolds LP. Angiogenesis in the ovary. *Rev Reprod.* 1996 Sep; 1(3): 182-192.

10. Fraser HM. Regulation of the ovarian follicular vasculature. *Reprod Biol Endocrinol.* 2006 Apr 12; 4: 18. PMCID: PMC1459163.

11. Smith MA, Altekruse SF, Adamson PC, Reaman GH, Seibel NL. Declining childhood and adolescent cancer mortality. *Cancer.* 2014 Aug 15; 120(16): 2497-2506. PMCID: PMC4136455.

12. Shuster LT, Rhodes DJ, Gostout BS, Grossardt BR, Rocca WA. Premature menopause or early menopause: Long-term health consequences. *Maturitas.* 2010 Feb; 65(2): 161-166. PMCID: PMC2815011.

13. Rocca WA, Grossardt BR, Miller VM, Shuster LT, Brown RD,Jr. Premature menopause or early menopause and risk of ischemic stroke. *Menopause.* 2012 Mar; 19(3): 272-277. PMCID: PMC3258468.

14. Resetkova N, Hayashi M, Kolp LA, Christianson MS. Fertility preservation for prepubertal girls: Update and current challenges. *Curr Obstet Gynecol Rep.* 2013 Dec 1; 2(4): 218-225. PMCID: PMC4125124.

15. Schover LR. Premature ovarian failure and its consequences: Vasomotor symptoms, sexuality, and fertility. *J Clin Oncol.* 2008 Feb 10; 26(5): 753-758.

16. Schover LR. Premature ovarian failure is a major risk factor for cancer-related sexual dysfunction. *Cancer.* 2014 Aug 1; 120(15): 2230-2232.

17. Jeruss JS, Woodruff TK. Preservation of fertility in patients with cancer. *N Engl J Med.* 2009 Feb 26; 360(9): 902-911. PMCID: PMC2927217.

18. Desai N, Alex A, AbdelHafez F, Calabro A, Goldfarb J, Fleischman A, Falcone T. Three-dimensional in vitro follicle growth: Overview of culture models, biomaterials, design parameters and future directions. *Reprod Biol Endocrinol.* 2010 Oct 14; 8: 119-7827-8-119. PMCID: PMC2967553.

19. Eppig JJ. Mouse oocyte development in vitro with various culture systems. *Dev Biol.* 1977 Oct 15; 60(2): 371-388.

20. Hornick JE, Duncan FE, Shea LD, Woodruff TK. Isolated primate primordial follicles require a rigid physical environment to survive and grow in vitro. *Hum Reprod.* 2012 Jun; 27(6): 1801-1810. PMCID: PMC3357191.

21. Tagler D, Tu T, Smith RM, Anderson NR, Tingen CM, Woodruff TK, Shea LD. Embryonic fibroblasts enable the culture of primary ovarian follicles within alginate hydrogels. *Tissue Eng Part A.* 2012 Jun; 18(11-12): 1229-1238. PMCID: PMC3360509.

22. Shikanov A, Smith RM, Xu M, Woodruff TK, Shea LD. Hydrogel network design using multifunctional macromers to coordinate tissue maturation in ovarian follicle culture. *Biomaterials.* 2011 Apr; 32(10): 2524-2531. PMCID: PMC3040241.

23. Brito IR, Lima IM, Xu M, Shea LD, Woodruff TK, Figueiredo JR. Three-dimensional systems for in vitro follicular culture: Overview of alginate-based matrices. *Reprod Fertil Dev.* 2013 Jul 19.

24. Fauser BC, Devroey P, Yen SS, Gosden R, Crowley WF,Jr, Baird DT, Bouchard P. Minimal ovarian stimulation for IVF: Appraisal of potential benefits and drawbacks. *Hum Reprod.* 1999 Nov; 14(11): 2681-2686.

25. Smitz J, Dolmans MM, Donnez J, Fortune JE, Hovatta O, Jewgenow K, Picton HM, Plancha C, Shea LD, Stouffer RL, Telfer EE, Woodruff TK, Zelinski MB. Current achievements and future research directions in ovarian tissue culture, in vitro follicle development and transplantation: Implications for fertility preservation. *Hum Reprod Update.* 2010 Jul-Aug; 16(4): 395-414. PMCID: PMC2880913.

26. Nieman CL, Kazer R, Brannigan RE, Zoloth LS, Chase-Lansdale PL, Kinahan K, Dilley KJ, Roberts D, Shea LD, Woodruff TK. Cancer survivors and infertility: A review of a new problem and novel answers. *J Support Oncol.* 2006 Apr; 4(4): 171-178.

27. West ER, Zelinski MB, Kondapalli LA, Gracia C, Chang J, Coutifaris C, Critser J, Stouffer RL, Shea LD, Woodruff TK. Preserving female fertility following cancer treatment: Current options and future possibilities. *Pediatr Blood Cancer.* 2009 Aug; 53(2): 289-295. PMCID: PMC3081672.

28. Donnez J, Dolmans MM, Pellicer A, Diaz-Garcia C, Sanchez Serrano M, Schmidt KT, Ernst E, Luyckx V, Andersen CY. Restoration of ovarian activity and pregnancy after transplantation of cryopreserved ovarian tissue: A review of 60 cases of reimplantation. *Fertil Steril.* 2013 May; 99(6): 1503-1513.

29. Kim SS, Soules MR, Battaglia DE. Follicular development, ovulation, and corpus luteum formation in cryopreserved human ovarian tissue after xenotransplantation. *Fertil Steril.* 2002 Jul; 78(1): 77-82.

30. Donnez J, Squifflet J, Dolmans MM. Frozen-thawed ovarian tissue retransplants. *Semin Reprod Med.* 2009 Nov; 27(6): 472-478.

31. McGee EA, Hsueh AJ. Initial and cyclic recruitment of ovarian follicles. *Endocr Rev.* 2000 Apr; 21(2): 200-214.

32. Dolmans MM, Luyckx V, Donnez J, Andersen CY, Greve T. Risk of transferring malignant cells with transplanted frozen-thawed ovarian tissue. *Fertil Steril.* 2013 May; 99(6): 1514-1522.

33. Hern DL, Hubbell JA. Incorporation of adhesion peptides into nonadhesive hydrogels useful for tissue resurfacing. *J Biomed Mater Res.* 1998 Feb; 39(2): 266-276.

34. Howe A, Aplin AE, Alahari SK, Juliano RL. Integrin signaling and cell growth control. *Curr Opin Cell Biol.* 1998 Apr; 10(2): 220-231.

35. Morpurgo M, Veronese FM, Kachensky D, Harris JM. Preparation of characterization of poly(ethylene glycol) vinyl sulfone. *Bioconjug Chem.* 1996 May-Jun; 7(3): 363-368.

36. Lutolf MP, Hubbell JA. Synthesis and physicochemical characterization of end-linked poly(ethylene glycol)-co-peptide hydrogels formed by michael-type addition. *Biomacromolecules.* 2003 May-Jun; 4(3): 713-722.

37. Li M, Karakji EG, Xing R, Fryer JN, Carnegie JA, Rabbani SA, Tsang BK. Expression of urokinase-type plasminogen activator and its receptor during ovarian follicular development. *Endocrinology.* 1997 Jul; 138(7): 2790-2799.

38. Liu YX. Plasminogen activator/plasminogen activator inhibitors in ovarian physiology. *Front Biosci.* 2004 Sep 1; 9: 3356-3373.

39. Ny T, Wahlberg P, Brandstrom IJ. Matrix remodeling in the ovary: Regulation and functional role of the plasminogen activator and matrix metalloproteinase systems. *Mol Cell Endocrinol.* 2002 Feb 22; 187(1-2): 29-38.

40. Sokic S, Papavasiliou G. Controlled proteolytic cleavage site presentation in biomimetic PEGDA hydrogels enhances neovascularization in vitro. *Tissue Eng Part A.* 2012 Dec; 18(23-24): 2477-2486. PMCID: PMC3501121.

41. Vigen M, Ceccarelli J, Putnam AJ. Protease-sensitive PEG hydrogels regulate vascularization in vitro and in vivo. *Macromol Biosci.* 2014 Oct; 14(10): 1368-1379. PMCID: PMC4198447.

42. Pratt AB, Weber FE, Schmoekel HG, Muller R, Hubbell JA. Synthetic extracellular matrices for in situ tissue engineering. *Biotechnol Bioeng.* 2004 Apr 5; 86(1): 27-36.

43. Lutolf MP, Weber FE, Schmoekel HG, Schense JC, Kohler T, Muller R, Hubbell JA. Repair of bone defects using synthetic mimetics of collagenous extracellular matrices. *Nat Biotechnol.* 2003 May; 21(5): 513-518.

CHAPTER II

A first step toward building an artificial ovarian tissue – follicle isolation, purification and encapsulation

2.1 Introduction

Autotransplantation of ovarian tissue has shown promising results for fertility and ovarian function restoration, resulting in 60 live human births reported since 2004(1). Following ovarian tissue transplantation, patients resume menstrual cycles and can conceive naturally. The transplanted tissues vary in size, follicle numbers and efficiency of revascularization, which contributes to a number of limitations, such as premature follicle activation, burnout and graft failure. Yet, the greatest limitation of autotransplantation of ovarian tissue is the potential risks of re-introducing malignant cells when transplanting ovarian tissue from a patient with hematological cancers(2). Therefore, isolating and grafting a purified population of ovarian follicles presents a safer alternative to autotransplantation of ovarian tissue removed from a patient before the treatments. Enzymatic isolation serves as a gentle tool for harvesting a large population of the early stage follicles. Yet, the survival and function of the enzymatically harvested follicles is inadequate without the support from stromal cells and native extracellular matrix.

To provide three-dimensional (3D) support of these isolated follicles, naturally derived hydrogels can be used to preserve oocyte-somatic cell connections and the overall architecture of encapsulated follicles while enabling follicular expansion through degradation. They provide a 3D environment similar to soft tissues, allow diffusion of nutrients, present critical biological signals, and degrade via endogenous enzymatic mechanisms(3).

Natural hydrogels, such as fibrin and collagen, provide a biophysical and biochemical environment and allow interaction among embedded cells due to their endogenous biological activity. Fibrin gel, which is the main component in blood clots, has been characterized extensively as a plausible 3D hydrogel for various tissue-engineering applications(4, 5). Cell and follicle secreted enzymes, such as plasmin and matrix metalloproteinases (MMPs), can degrade fibrin, and allow cell migration and proliferation(6), making suitable for *in vitro* follicle culture.

However, the survival rate of cultured primordial follicles, the most immature and abundant class of follicles in the ovary, is very low *in vitro*. Therefore, several groups have investigated an approach of grafting enzymatically-isolated immature follicles encapsulated in naturally derived hydrogels, such as alginate(13), fibrin(10-12), vascular endothelial growth factor (VEGF) releasing fibrin(9, 12), for delivery of isolated follicles and demonstrated complete folliculogenesis showing the potential of this approach *in vivo*(7-12).

In this chapter, we addressed three different components of building an artificial ovarian tissue, from enzymatic isolation and purification of the early stage follicles to encapsulation in fibrin hydrogels. The viability and quality of the early stage follicles isolated using a cocktail of digestive enzymes, Liberase DH, and how these follicles were separated from stromal and cancer cells using microfluidic device are shown. We further discussed the previous studies of using fibrin hydrogels for grafting and their limitations for the design of artificial ovarian tissue.

2.2 Enzymatic isolation of the early stage follicles

Enzymatic digestion allows isolation of primordial follicles from ovarian tissue. Primordial follicles have the greatest potential to survive cryopreservation and transplantation(14) due to their relative small size (30μm) compared to activated follicles (80 – 500μm in mice). It has been shown that hundreds of viable primordial and primary follicles can be isolated from fresh and cryopreserved ovarian cortical biopsies from young women using enzyme treatment(15, 16). Primordial follicles have high cryotolerance, which makes them more attractive for both *in vivo* and *in vitro* culture. The survival rate of gametes during the cryopreservation and subsequent transplantation was improved by dissociating the tissue into individual cells before cryopreservation(17, 18). For example, 70 – 80% of the initial number of gametes present at the resting primordial stages was recovered by using slow freezing protocols(15, 19). However, collagenase type I and DNAse I can cause partial disaggregation and damages to the basement membrane due to its high endotoxin levels(15, 20).

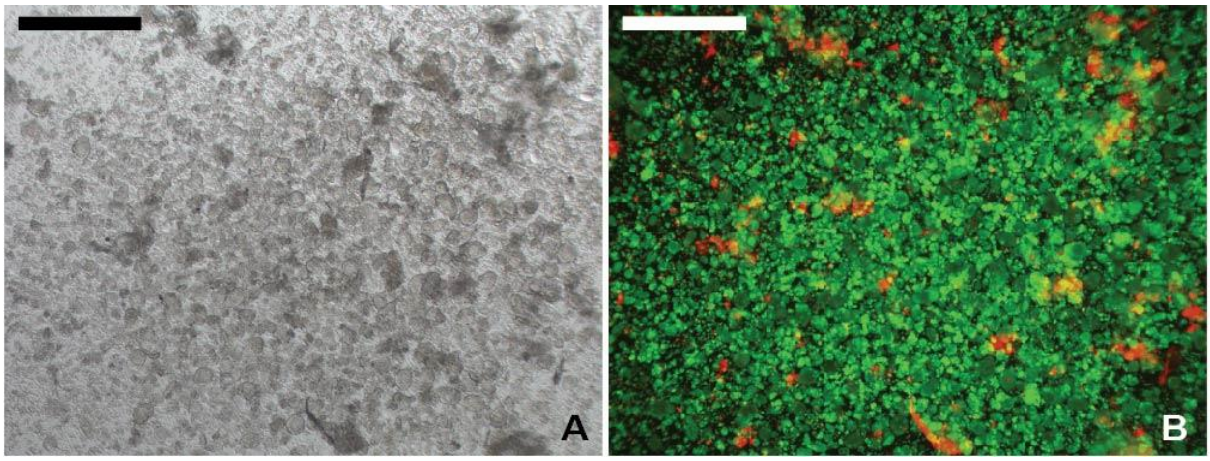

Figure 2.1 - LIVE/DEAD staining of enzymatically isolated follicles using Liberase DH. To determine deleterious effects of isolation procedure on the viability of enzymatically isolated follicle (A), double fluorescent labeling LIVE/DEAD Cell Imaging Kit (Invitrogen) was performed. The enzymatically isolated follicle's viability was confirmed by high Calcien AM (Green) staining (B). *(According to Kim J et al. Synthetic hydrogel supports the function and regeneration of artificial ovarian tissue in mice. Unpublished Data.)*

To address the limitations of collagenase type I, a purified blend of digestive enzymes, Liberase DH, was implemented to improve the quality of enzymatic isolation (Fig. 2.1)(21). Compared to collagenase, Liberase DH allowed isolation of a higher percentage of viable follicles with good morphology(22, 23). Overall, the isolation process can disrupt the oocyte-follicular cell interface and lead to dispersion of granulosa or theca cells, causing detachment of oocytes(22, 24), which requires optimization of the follicle isolation protocol. However, there was no noticeable difference in oocyte maturation and embryo development rates between enzymatically and mechanically isolated follicles(25), and the connections between oocytes and somatic cells were reformed when enzymatically isolated follicles were encapsulated within three-dimensional gels(18, 26), supporting the idea of encapsulating within hydrogels.

2.3 Purification of enzymatically isolated follicles using microfluidics

Ovarian tissue can be removed prior to the whole body exposure to toxic chemotherapy, cryopreserved and later transplanted back to the patient to restore fertility. The major drawback of the tissue autotransplantation is the potential risk of reintroduction of cancer cells back to the patient. Ovarian follicles can be mechanically or enzymatically isolated from other cell types and transplanted back into the patient as a pure population of the reproductive units using current tissue engineering techniques. Smith, RM et al. and Kniazeva, E. et al. showed cell-size based separation of different cell types followed by enzymatic follicle isolation poses a potential application in the field of fertility preservation in cancer survivors, but did not completely removed stromal and cancer cells (Fig. 2.2)(10, 12). Soares et al. recently showed an approach of simple rinsing of the human follicles to remove leukemic cells(27); however, this method required manual pick up of isolated follicles. While purification of enzymatically isolated

follicles showed a promise of reducing residual cancer cells, further development of the isolation and purification is needed to eliminate cancer cells more effectively and efficiently.

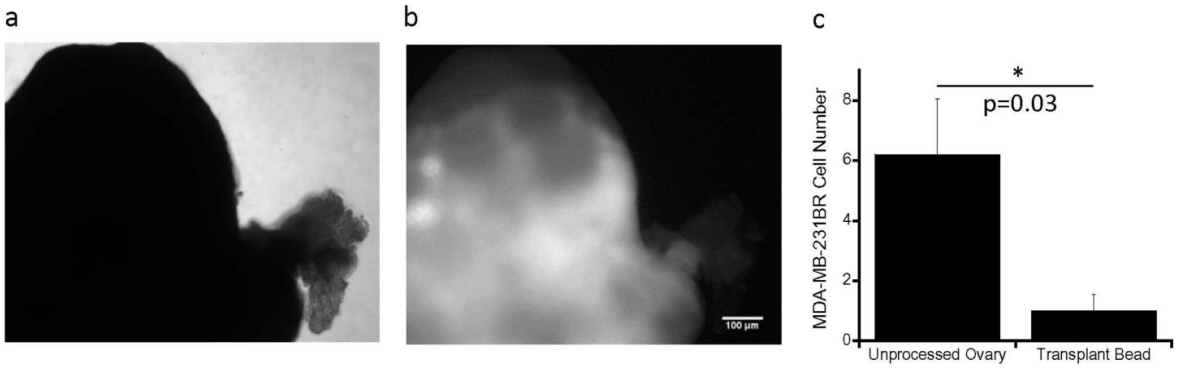

Figure 2.2 - Tumor Burden Evaluation within Unprocessed Ovary and Prepared Transplantation Bead. Cancerous ovarian tissue extracted from a mouse 28 days post-inoculation (phase contrast in (a)) is showing a strong red fluorescent signal (b); (c) flow cytometry results for TdTomato+ MD-MBA-231BR cells within unprocessed ovary and transplant bead made from processed ovary, where tissue was extracted 5 days postinoculation; data shown represent average cell number± s.e.m., n= 5 and p= 0.03 by two-tailed Student's t-test, * indicates statistical significance, where $p \leq 0.05$. *(According to Kniazeva, E. et al. Primordial follicle transplantation within designer biomaterial grafts produce live birth in a mouse infertility model. Scientific Report. (2015) 5, 17709.)*

To effectively and efficiently remove residing cancer cells within the ovarian tissue, we used pseudo-grayscale (pGS) photomasks in combination with backside diffused light lithography (BDLL) to create a mold with a wide structure for soft lithography to produce a PDMS device with increased separation capacity to isolate the large ovarian follicles from the smaller cancer cells(28). Our design was effective at sorting of follicles from stromal and cancer cells. In these trials, 88% of the cancer cells were removed while 84% of ovarian follicles were recovered, as shown from examination of cell mixture before and after sorting by a microfluidic device (Fig. 2.3). Our experimental observations suggest a fraction of cancer cells failed to be isolated from follicles due to the cancer cells adhering to the leftover extracellular matrix around the follicles. More experimentation will reveal the collagenase and liberase activity for the optimum cancer cell removal. In a clinically relevant scenario, we anticipate that an 88% contaminant removal

may be enough to eliminate all cancer cells. This study would serve as future potential applications of clinical treatment-scale separation of ovarian follicles from cancer cells.

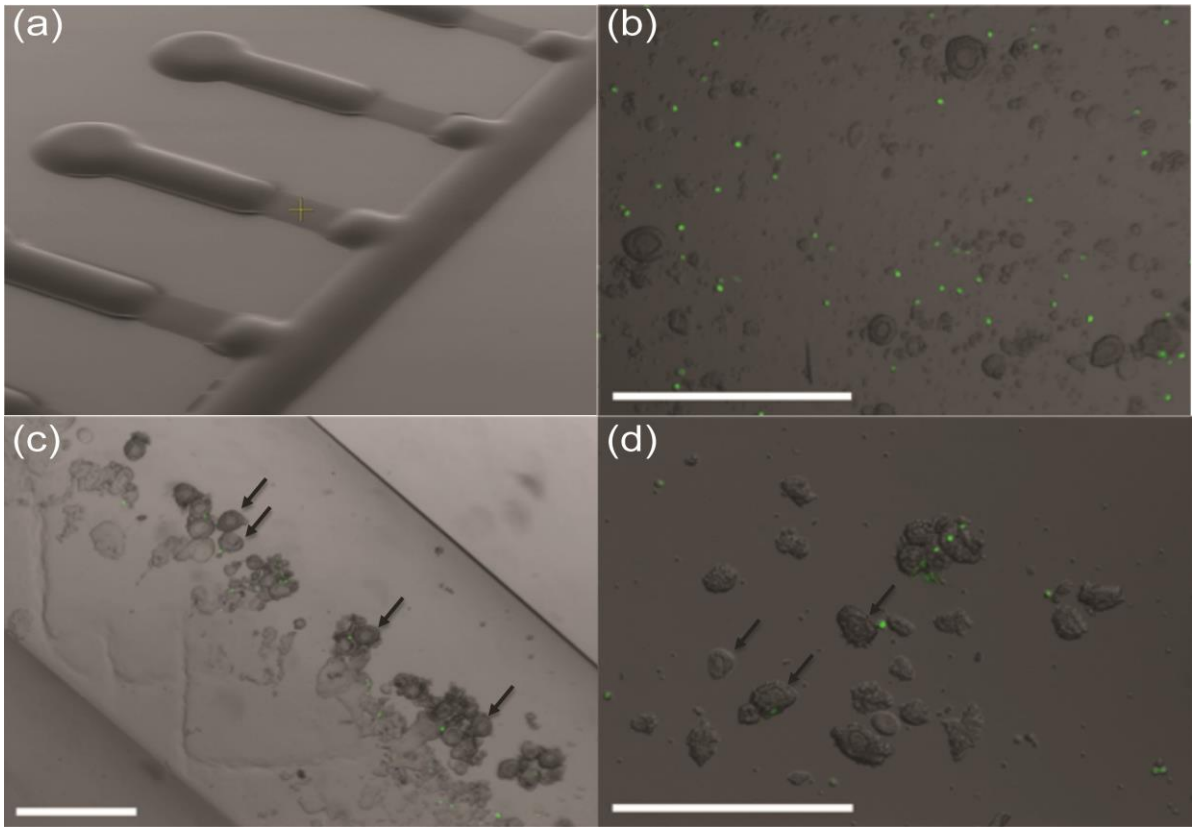

Fig. 2.3 - Follicle sorting from GFP-MDA-MB-231 cancer cells. To further demonstrate the range of possible channel heights and their applications, a separate larger PDMS weir-type trap was produced with unspun SU-8 molds using pGS BDLL. Scale bar: 500 mm. a) Multi-layered microfluidic channels. b) Cancer cells were added into a solution containing primordial follicles within a petri dish. c) Follicles are trapped by weir-type traps while undigested collagen matrix squeezes through and cancer cells freely pass through. Flow was passive driven by a 7 cm height differential via suction of the outlet. d) The trapped follicles can be extracted from the device onto another petri dish by reversing the height differential of the inlet/outlet after a short flushing period with culture medium. The efficiency of cancer cell elimination is 88% and follicle recovery is 84%. *(According to Lai, D. et al. Simple multi-level microchannel fabrication by pseudo-grayscale backside diffused light lithography. RSC Adv. (2013) 3, 19467.)*

2.4 Grafting of isolated follicles using fibrin hydrogels

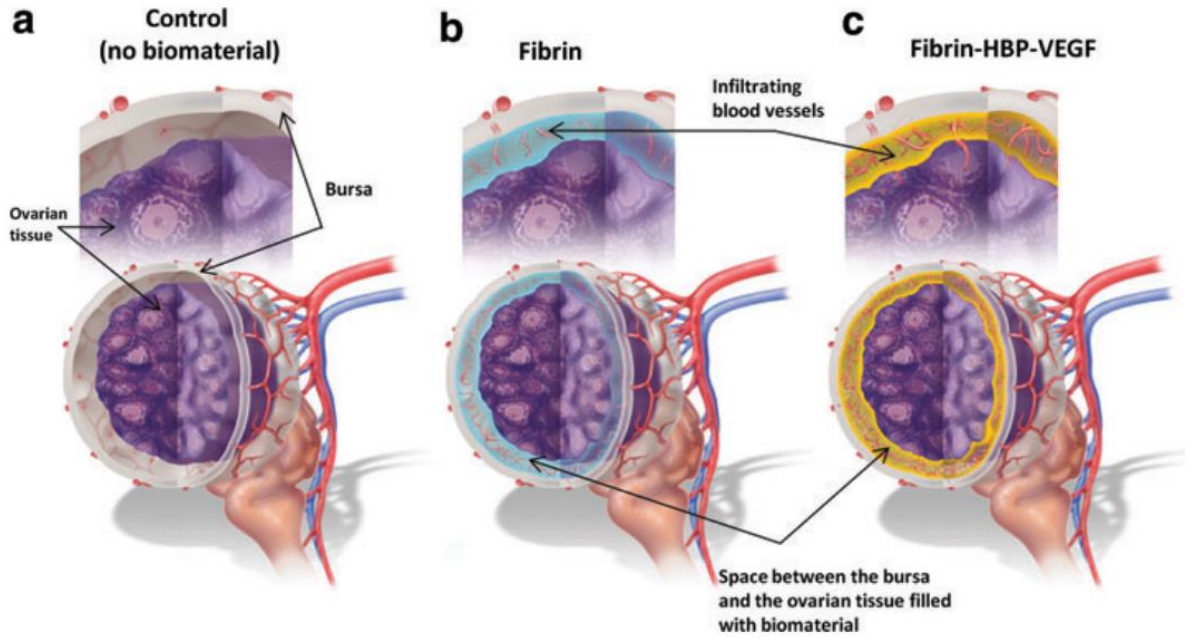

Fig. 2.4 – Schematic presentation of the hypothesis: (a) ovarian tissue transplanted in the bursal cavity lack the spatial connection to the host; (b) ovarian tissue encapsulation in degradable fibrin allows physical connectivity that may result in improved communication between the host and the graft and serve a continuous path for cell infiltration; (c) additionally to the described advantages of (b) controlled release of VEGF promoted revascularization. *(According to Shikanov, A. et al. Fibrin encapsulation and vascular endothelial growth factor delivery promotes ovarian graft survival in mice. Tissue Eng. Part.A. (2011)17, 3095 – 3104)*

Implantation of individually isolated follicles reduces the risk of re-implanting malignant cells, but it lacks the stromal support, which is the essential component for follicle survival and development. Isolated follicles need to maintain their 3D structure in order to prevent disruption of the metabolic link between granulosa cells (GCs) and oocytes, which are directly related to growth and survival(29). Therefore, naturally derived biomaterials, such as alginate(30), collagen(31) and fibrin(32, 33), have been employed to provide a temporary support due to their intrinsic biological activity, three-dimensionality, and biodegradability. These 3D grafts can function as a bridge between the host and the transplanted follicles and also as a supportive matrix for follicle development and cell infiltration to initiate the graft remodeling (Fig.2.4)(9).

Alginate hydrogels support follicle growth and 3D culture of rodent follicles. However, the non-degradable nature of the alginate hydrogel was prohibitive in supporting the complete development of a human follicle, which typically reaches a diameter of 20 mm at the final stages of growth(34). On the other hand, fibrin has been extensively investigated as a grafting material for isolated follicles, because it can degrade in response to enzymes secreted by the follicle such as plasminogen activators (PA) and matrix metalloproteinases (MMPs)(35).

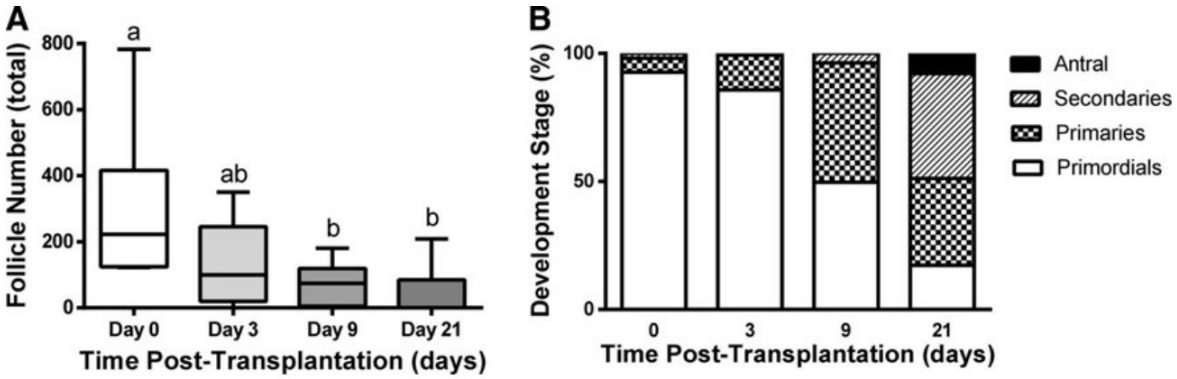

Fig. 2.5 – Follicle development and attrition in fibrin. (A) Number of follicles as a function of time in the graft during 21 days post-transplantation. Different letters above bars indicate significant differences ($p < 0.05$). **(B)** Percentage of follicles in each developmental stage within the graft (n = 6, 6, 10, and 12 for day 0, 3, 9, and 21, respectively) *(Adapted from Smith, RM. et al. Fibrin-mediated delivery of an ovarian follicle pool in a mouse model of infertility. Tissue Eng. Part.A. (2014) 20(21), 3021 – 3029)*

Multiple previous studies successfully demonstrated the use of fibrin hydrogels for the transplantation of ovarian tissue or isolated ovarian follicles, resulting in complete follicular development(9-12). Smith, RM. et al. reported successful development of transplanted early-stage follicles into fully-grown antral follicles during 21 days *in vivo*. However, fibrin failed to support longer graft function due to significant reduction in follicle pool as a result of matrix degradation(10) and poor support of the graft structure(36) (Fig.2.5). Shikanov, A. et al.(9) and Kniazeva, E. et al.(12) demonstrated extended longevity and function by incorporating vascular endothelial growth factor (VEGF) (Fig.2.4). The controlled release of VEGF initiated functional vascularization promoting follicle survival(9). These studies showed the potential of grafting of

isolated follicles for delivery *in vivo*. However, the poor control of physical properties of naturally derived biomaterials, such as degradation rate and matrix stiffness, and lot-to-lot compositional and structural variability(37, 38) limits their applications and clinical translations.

2.5 Conclusion

In summary, we addressed three different components toward building an artificial ovary, from enzymatic isolation and purification of the early stage follicles to encapsulation in natural hydrogels. The large populations of early stage follicles isolated and encapsulated were viable, which were separated from stromal and cancer cells using microfluidic device with high efficiency. Follicle sorting using microfluidic device would serve as future potential applications of clinical treatment-scale separation of ovarian follicles from cancer cells. Encapsulating isolated follicles in fibrin hydrogels has shown promising results; however, the rapid degradation and coupled mechanical and biological properties of fibrin hydrogels resulted in early graft failure, limiting their long-term applications. This result further confirmed the importance of dynamic hydrogel design for reproductive tissue engineering applications.

2.6 Materials and methods

2.6.1. Enzymatic follicle isolation and viability assessment

For all experiments, ovaries were isolated from 6 or 7-day-old female mice (F1 CBA/J x C57BL/6N), separated from the connective tissues and enzymatically digested in 50 μL (13 Wünsch units/mL) Liberase DH (Roche, Indianapolis, IN) in 500 μL L15 (Leibovitz's) media (Sigma-Aldirch) (Fig.2.1B). The total digestion time was 50min at 37 ^{o}C, followed by 20min gentle pipetting of enzyme-digested pieces. The enzyme digestion was arrested by adding 10%

fetal bovine serum and the digest was transferred to a tube for sedimentation. The sedimentation velocity of primordial and primary follicles was calculated according to a previously published report(10). After 15 min of sedimentation, the top half of the total media containing slower sinking arbitrary cells was removed. The rest of the media volume remaining follicular suspension was removed by centrifuging at 100G for 5min. To determine any deleterious effecst of the isolation procedure on the viability of enzymatically isolated follicles, double fluorescent labeling LIVE/DEAD Cell Imaging Kit (Invitrogen) was performed according to the manufacturer's protocol.

2.6.2. Follicle sorting using pseudo-grayscale (pGS) photomasks in combination with backside diffused light lithography (BDLL)(28)

Devices were fabricated using pGS BDLL with channel heights of 58 mm and weir-type traps of 21 to 8 mm in height for blood sorters and channel heights of 120 mm and 20 mm traps for the follicle sorters. Five thousand MDA-MB-231 human breast cancer cells (5 µL of 10^6 mL^{-1} suspension) were added to the follicle-stromal cell suspension to mimic the scenario of cancer cell contaminated tissue. A dramatically higher amount of cancer cells than what is clinically expected was used to facilitate calculation of isolation efficiency. Cells and follicles were sorted using multi-level channels to produce weir-type traps.

2.7 References

1. Donnez J, Dolmans MM. Ovarian cortex transplantation: 60 reported live births brings the success and worldwide expansion of the technique towards routine clinical practice. J Assist Reprod Genet. 2015 Aug;32(8):1167-70.

2. Dolmans MM, Luyckx V, Donnez J, Andersen CY, Greve T. Risk of transferring malignant cells with transplanted frozen-thawed ovarian tissue. Fertil Steril. 2013 May;99(6):1514-22.

3. Shea LD, Woodruff TK, Shikanov A. Bioengineering the Ovarian Follicle Microenvironment. Annu Rev Biomed Eng. 2014 May 14.

4. Kaibara M, Fukada E. Effect of temperature on dynamic viscoelasticity during the clotting reaction of fibrin. Biochim Biophys Acta. 1977 Oct 25;499(3):352-61.

5. Blomback B, Carlsson K, Fatah K, Hessel B, Procyk R. Fibrin in human plasma: gel architectures governed by rate and nature of fibrinogen activation. Thromb Res. 1994 Sep 1;75(5):521-38.

6. Mosesson MW. Fibrinogen and fibrin structure and functions. J Thromb Haemost. 2005 Aug;3(8):1894-904.

7. Hovatta O, Wright C, Krausz T, Hardy K, Winston RM. Human primordial, primary and secondary ovarian follicles in long-term culture: effect of partial isolation. Hum Reprod. 1999 Oct;14(10):2519-24.

8. Abir R, Fisch B, Nitke S, Okon E, Raz A, Ben Rafael Z. Morphological study of fully and partially isolated early human follicles. Fertil Steril. 2001 Jan;75(1):141-6.

9. Shikanov A, Zhang Z, Xu M, Smith RM, Rajan A, Woodruff TK, et al. Fibrin encapsulation and vascular endothelial growth factor delivery promotes ovarian graft survival in mice. Tissue Eng Part A. 2011 Dec;17(23-24):3095-104.

10. Smith RM, Shikanov A, Kniazeva E, Ramadurai D, Woodruff T, Shea LD. Fibrin-mediated delivery of an ovarian follicle pool in a mouse model of infertility. Tissue Eng Part A. 2014 May 7.

11. Chiti MC, Dolmans MM, Orellana R, Soares M, Paulini F, Donnez J, et al. Influence of follicle stage on artificial ovary outcome using fibrin as a matrix. Hum Reprod. 2016 Feb;31(2):427-35.

12. Kniazeva E, Hardy AN, Boukaidi SA, Woodruff TK, Jeruss JS, Shea LD. Primordial Follicle Transplantation within Designer Biomaterial Grafts Produce Live Births in a Mouse Infertility Model. Sci Rep. 2015 Dec 3;5:17709.

13. Vanacker J, Dolmans MM, Luyckx V, Donnez J, Amorim CA. First transplantation of isolated murine follicles in alginate. Regen Med. 2014;9(5):609-19.

14. Donnez J, Martinez-Madrid B, Jadoul P, Van Langendonckt A, Demylle D, Dolmans MM. Ovarian tissue cryopreservation and transplantation: a review. Hum Reprod Update. 2006 Sep-Oct;12(5):519-35.

15. Oktay K, Nugent D, Newton H, Salha O, Chatterjee P, Gosden RG. Isolation and characterization of primordial follicles from fresh and cryopreserved human ovarian tissue. Fertil Steril. 1997 Mar;67(3):481-6.

16. Oktay K, Newton H, Aubard Y, Salha O, Gosden RG. Cryopreservation of immature human oocytes and ovarian tissue: an emerging technology? Fertil Steril. 1998 Jan;69(1):1-7.

17. Carroll J, Whittingham DG, Wood MJ, Telfer E, Gosden RG. Extra-ovarian production of mature viable mouse oocytes from frozen primary follicles. J Reprod Fertil. 1990 Sep;90(1):321-7.

18. Carroll J, Gosden RG. Transplantation of frozen-thawed mouse primordial follicles. Hum Reprod. 1993 Aug;8(8):1163-7.

19. Hovatta O, Silye R, Abir R, Krausz T, Winston RM. Extracellular matrix improves survival of both stored and fresh human primordial and primary ovarian follicles in long-term culture. Hum Reprod. 1997 May;12(5):1032-6.

20. Torrance C, Telfer E, Gosden RG. Quantitative study of the development of isolated mouse pre-antral follicles in collagen gel culture. J Reprod Fertil. 1989 Sep;87(1):367-74.

21. Linetsky E, Bottino R, Lehmann R, Alejandro R, Inverardi L, Ricordi C. Improved human islet isolation using a new enzyme blend, liberase. Diabetes. 1997 Jul;46(7):1120-3.

22. Dolmans MM, Michaux N, Camboni A, Martinez-Madrid B, Van Langendonckt A, Nottola SA, et al. Evaluation of Liberase, a purified enzyme blend, for the isolation of human primordial and primary ovarian follicles. Hum Reprod. 2006 Feb;21(2):413-20.

23. Vanacker J, Camboni A, Dath C, Van Langendonckt A, Dolmans MM, Donnez J, et al. Enzymatic isolation of human primordial and primary ovarian follicles with Liberase DH: protocol for application in a clinical setting. Fertil Steril. 2011 Aug;96(2):379,383.e3.

24. Smitz JE, Cortvrindt RG. The earliest stages of folliculogenesis in vitro. Reproduction. 2002 Feb;123(2):185-202.

25. Demeestere I, Delbaere A, Gervy C, Van Den Bergh M, Devreker F, Englert Y. Effect of preantral follicle isolation technique on in-vitro follicular growth, oocyte maturation and embryo development in mice. Hum Reprod. 2002 Aug;17(8):2152-9.

26. Eppig JJ, Wigglesworth K, Pendola FL. The mammalian oocyte orchestrates the rate of ovarian follicular development. Proc Natl Acad Sci U S A. 2002 Mar 5;99(5):2890-4.

27. Soares M, Sahrari K, Amorim CA, Saussoy P, Donnez J, Dolmans MM. Evaluation of a human ovarian follicle isolation technique to obtain disease-free follicle suspensions before safely grafting to cancer patients. Fertil Steril. 2015 Sep;104(3):672,80.e2.

28. Lai D, Labuz J, Kim J, Luker G, Shikanov A, Takayama S. Simple multi-level micochannel fabrication by pseudo-grayscale backside diffused light lithography. RSC Advances. 2013 July, 29th, 2013;3(42):19467-73.

29. Picton HM, Gosden RG. In vitro growth of human primordial follicles from frozen-banked ovarian tissue. Mol Cell Endocrinol. 2000 Aug 15;166(1):27-35.

30. Xu M, Barrett SL, West-Farrell E, Kondapalli LA, Kiesewetter SE, Shea LD, et al. In vitro grown human ovarian follicles from cancer patients support oocyte growth. Hum Reprod. 2009 Oct;24(10):2531-40.

31. Steffens GC, Yao C, Prevel P, Markowicz M, Schenck P, Noah EM, et al. Modulation of angiogenic potential of collagen matrices by covalent incorporation of heparin and loading with vascular endothelial growth factor. Tissue Eng. 2004 Sep-Oct;10(9-10):1502-9.

32. Hall H. Modified fibrin hydrogel matrices: both, 3D-scaffolds and local and controlled release systems to stimulate angiogenesis. Curr Pharm Des. 2007;13(35):3597-607.

33. Rao RR, Peterson AW, Ceccarelli J, Putnam AJ, Stegemann JP. Matrix composition regulates three-dimensional network formation by endothelial cells and mesenchymal stem cells in collagen/fibrin materials. Angiogenesis. 2012 Jun;15(2):253-64.

34. Gougeon A. Regulation of ovarian follicular development in primates: facts and hypotheses. Endocr Rev. 1996 Apr;17(2):121-55.

35. Ny T, Wahlberg P, Brandstrom IJ. Matrix remodeling in the ovary: regulation and functional role of the plasminogen activator and matrix metalloproteinase systems. Mol Cell Endocrinol. 2002 Feb 22;187(1-2):29-38.

36. Donnez J, Squifflet J, Dolmans MM. Frozen-thawed ovarian tissue retransplants. Semin Reprod Med. 2009 Nov;27(6):472-8.

37. Yu W, Datta A, Leroy P, O'Brien LE, Mak G, Jou TS, et al. Beta1-integrin orients epithelial polarity via Rac1 and laminin. Mol Biol Cell. 2005 Feb;16(2):433-45.

38. Hughes CS, Postovit LM, Lajoie GA. Matrigel: a complex protein mixture required for optimal growth of cell culture. Proteomics. 2010 May;10(9):1886-90.

CHAPTER III

Characterizing natural hydrogels - towards more dynamic hydrogel design

3.1 Introduction

The extracellular matrix (ECM) provides the three-dimensional structure and paracrine signals that regulate and promote cell adhesion and directs the cellular processes leading to tissue development(1, 2). ECM also affects morphology(3), cell communication(4, 5), survival(6, 7), proliferation(8) and steroidogenesis(9). *In vivo,* cells are embedded within a complex environment that contains multiple ECM components and cell-secreted factors(10). In addition to complexity, cell morphology and orientation with respect to matrix architecture can affect cellular response and their function(11). The ECM is a highly dynamic structure that undergoes continuous controlled remodeling, and in order to promote appropriate development, precise control and regulation of ECM assembly, modification and degradation are needed(12).

Naturally derived materials mimicked some components of ECM, but they were still limited to modeling static environments compared to complex tissue processes. For example, in applications focused on supporting ovarian follicle *in vitro*, a hydrogel must accommodate the significant increase in follicle volume through degradation. The volumetric expansion of the growing follicle is approximately 300 folds in mice and about 10^5 fold in humans(13, 14) along with massive recruitment of cells and vessels to support follicle development(15). Alginate

hydrogels restricted and compressed the expansion of a human follicle, which typically reaches a diameter of 20mm(16), beyond 700μm due to the non-degradability of the hydrogel. This proves that the degradation and elasticity of the matrix are important factors to accommodate the follicle growth.

Therefore, Shikanov, A et al. investigated the fibrin-alginate interpenetrating networks (FA-IPN), which combined the degradable and non-degradable components, to provide more dynamic cell-responsive hydrogel design to culture follicles *in vitro*(17). Alginate provided the physical support while fibrin degraded to create a space for follicle growth and expansion. The fibrin degradation rate was also controlled by using a monomeric serine protease inhibitor, aprotinin, which extended the period of follicle culture and mechanical integrity *in vitro*(18).

In this chapter, to further explore how different mechanical properties and degradation rate of natural hydrogels affect cellular phenotype and behavior, we encapsulated human bone marrow derived stromal cells (HS-5) in fibrin, collagen or fibrin-collagen hydrogels. We explored different concentrations of aprotinin to the culturing media to control the fibrin degradation rate and to extend the period when the stromal network architecture is supported. The fast degradation rate of fibrin was controlled with aprotinin; however, high concentration of aprotinin slowed down fibrinolysis significantly, which slowed down cell growth as well. Among the different gel systems, more cell growth and more interconnected stromal network formation were observed when cells were in less rigid and more degradable environments, allowing branching and cell remodeling. This study further discusses how the kinetics of fibrin degradation and stiffness significantly affected cell proliferation, migration and cell-mediated matrix remodeling.

3.2 Results

3.2.1 Stromal network formation in fibrin gel

To design a 3D hydrogel system that can support and mimic a lymphoid stromal network, fibrin gel was investigated. The encapsulated HS-5 cells in fibrin gel (6 mg/mL) demonstrated fibroblast-like spindle morphology at Day 2, and stromal networks began to form through branching and joining with other adjacent cell populations by Day 6 (Fig.3.1A). However, due to the rapid fibrinolysis along with cell growth, fibrin degraded completely by Day 8, leading to the loss of the structural support and contraction of the stromal network architecture (Fig.3.1A). Inability to maintain the matrix architecture after complete network formation restricted T-cell penetration into the network due to the high density of the cells and the collapse of the fibrin structure.

3.2.2 Optimal aprotinin concentration controls fibrin degradation and cell spreading

We hypothesized that the kinetics of fibrin degradation would affect cell proliferation, migration and cell-mediated matrix remodeling. We used a monomeric serine protease inhibitor, aprotinin, added to the culturing media to control the fibrin degradation rate and to extend the period when the stromal network architecture is supported. Higher concentration of aprotinin (0.1 TIU/mL) slowed down fibrinolysis significantly (Fig.3.1B, 3.1C), but also restricted cell growth (Fig.3.1A). As a result, we concluded that in order for HS-5 cells to proliferate and connect with other surrounding cells, these cells have to be able to migrate and remodel their microenvironment. Reducing the aprotinin concentration to 0.05 TIU/mL resulted in sufficient cell proliferation for network formation, and slow enough fibrin degradation (Fig.3.1A).

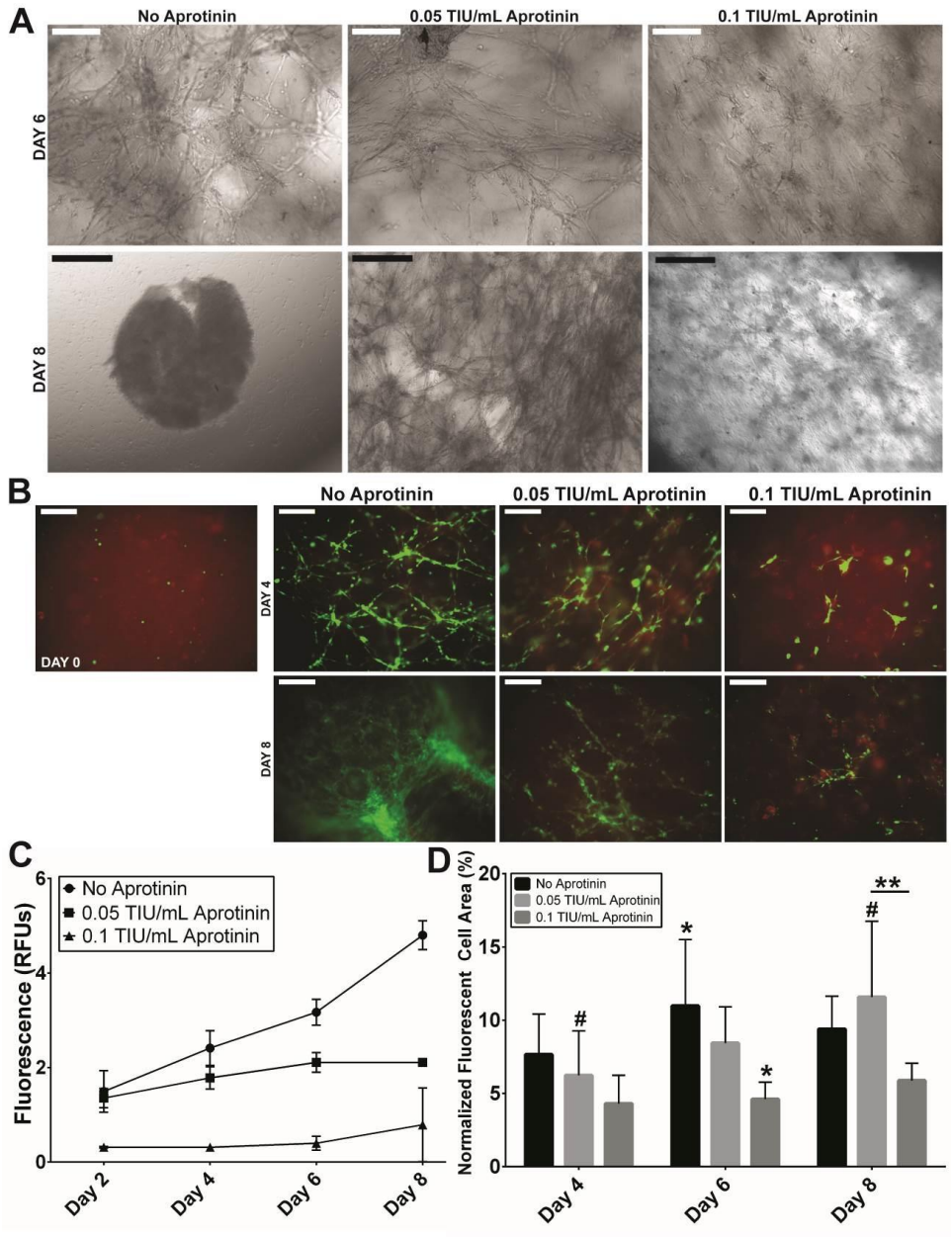

Figure 3.1. Effects of aprotinin on HS-5 stromal network formation and fibrin degradation rate. (A) HS-5 cells encapsulated in fibrin (6 mg/mL) gel [220,000 cells/ml gels] and two different concentrations of aprotinin (0.1 TIU/mL and 0.05 TIU/mL) were supplemented with media. Scale Bar: White = 200 μm, Black = 500 μm **(B)** GFP labeled HS-5 were encapsulated in fibrin gels copolymerized with 2% w/w AlexaFluor 546 (558/573 nm) labeled fibrinogen to measure the fibrin degradation during the stromal network formation. Scale Bar: 200 μm **(C)** Fluorescence was measured in the media that was collected every 2 days from fibrin gels labeled with 2% w/w AlexaFluor 546. Stronger fluorescence was detected in media collected from more degraded fibrin gels, verifying the effect of aprotinin concentration on fibrinolysis. No autofluorescence was detected in the media. Values are reported as mean ± S.D. (n = 5) **(D)** The area occupied by cells was quantified as the area corresponding with GFP fluorescence within 100x images (Fig.S3). Only fibrin gel supplemented with aprotinin (0.05 TIU/mL) showed significant increase in normalized fluorescent cell area from day 4 to day 8. However, there was statistical difference only between fibrin gel with 0.05 TIU/mL aprotinin and fibrin gel with 0.1 TIU/mL aprotinin at day 8 throughout the culture. Values are reported as mean ± S.D. (n = 5). Significance was determined by a Two-way ANOVA followed by Tukey post-tests (*,**,# $p < 0.05$).

After identifying the optimal aprotinin concentration that allows both control over fibrinolysis and maintenance of the stromal network, the ability to support cell growth and network formation was assessed quantitatively by measuring the fluorescent area occupied by the cells in the hydrogel (Fig.3.1D). Compared to no-aprotinin control condition, fibrin gels supplemented with aprotinin (0.05 TIU/mL) showed slower cell proliferation rate and lower cell area in the beginning stage of culture, which then significantly increased, by Day 8 (Fig.3.1D). On the other hand, the cell area in fibrin gel without aprotinin slightly decreased at Day 8 due to accelerated fibrinolysis and its inability to maintain the architecture leading to the collapse of the stromal network (Fig.3.1D). Only fibrin gel supplemented with aprotinin (0.05 TIU/mL) showed significant increase in normalized fluorescent cell area from day 4 to day 8, proving the importance of a balance between fibrin degradation and cell proliferation in the stromal network formation (Fig.3.1D). There was no statistical difference in normalized cell area between fibrin gel supplemented with 0.05 TIU/mL aprotinin and fibrin gel alone throughout any day of the culture; however, the ability to maintain the structural architecture after complete network formation was significantly improved with the addition of 0.05 TIU/mL aprotinin (Fig.3.1A).

3.2.3 Comparison between three different hydrogel systems: fibrin, fibrin-collagen, and collagen

Based on results from the aprotinin test with fibrin gels, we hypothesized that combining the faster degrading fibrin and slow degrading collagen gel would provide optimal degradation rate and structural rigidity to promote cell growth and network formation. Fibrin concentration was kept constant at 6 mg/mL and only collagen concentration was varied (Collagen concentration: 2 mg/mL and 4 mg/mL) to identify the optimal concentration for HS-5 cells.

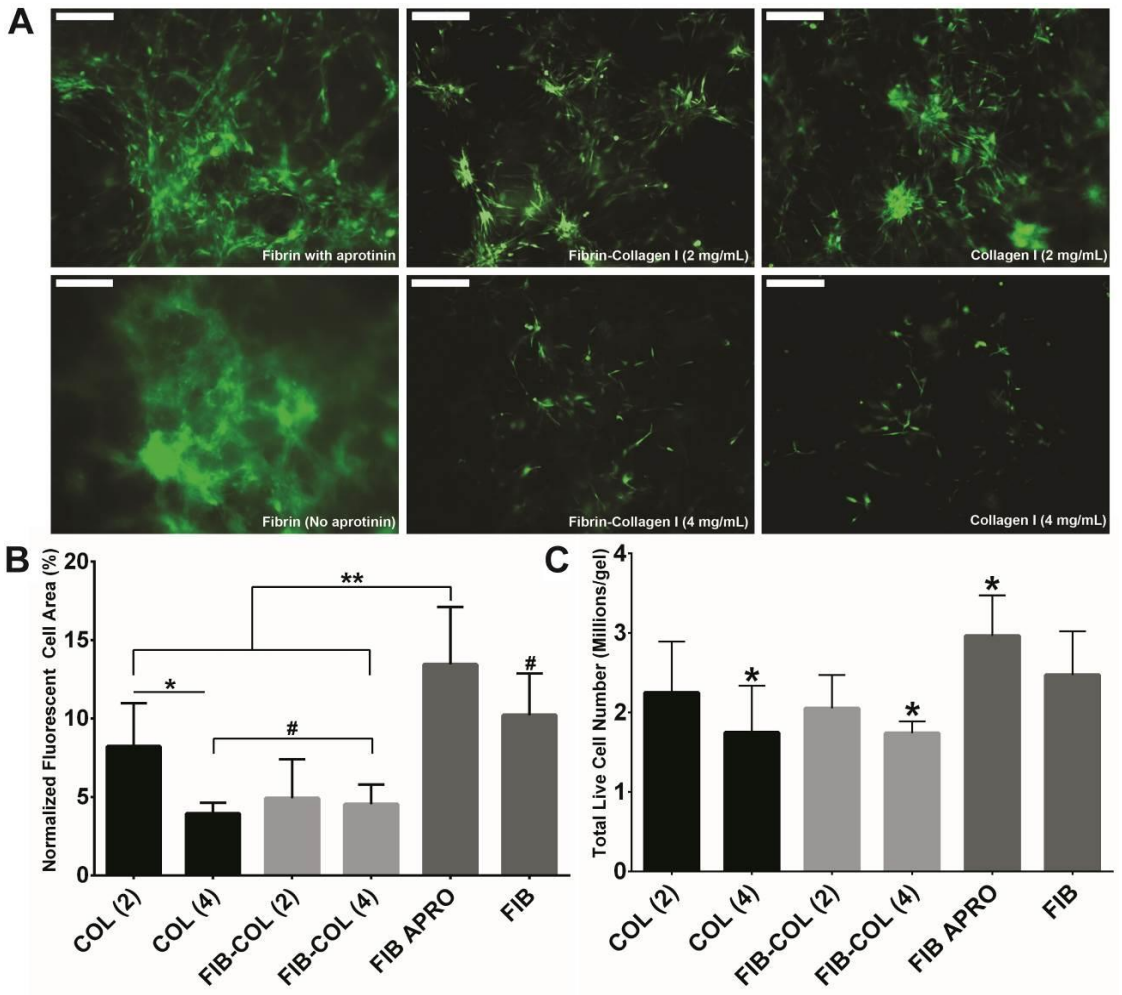

Figure 3.2. Comparison between three different hydrogel systems: Fibrin, Fibrin-Collagen, and Collagen. **(A)** GFP labeled HS-5 cells [220,000 cells/ml gels] encapsulated in six different hydrogel conditions: fibrin with and without aprotinin, fibrin-collagen, and pure collagen at various concentrations. Fibrin concentration was kept at 6 mg/mL for all gels and only collagen concentration was varied from 2 mg/mL to 4 mg/mL. HS-5 formed more interconnected and complete network in Fibrin gel with aprotinin (0.05 TIU/mL). Scale Bar: 200 μm. **(B)** The normalized fluorescent cell area was quantified as the area corresponding with the GFP fluorescence within 100x images and compared between the different hydrogel systems. Fibrin gel supplemented with aprotinin (0.05 TIU/mL) showed significantly greater values of total cell area at day 8 compared to all compositions of collagen and fibrin-collagen. However, there was no statistical difference between fibrin gel supplemented with aprotinin and fibrin gel alone. **(C)** CellTiter-Glo Luminescent Cell Viability Assays was used to determine the total number of viable cells per gel based on quantification of ATP. Fibrin gel supplemented with aprotinin (0.05 TIU/mL) showed significantly greater values of viable cells at Day 8 compared to collagen (4 mg/mL) and fibrin-collagen (4 mg/mL). There was no statistical difference between fibrin gel supplemented with aprotinin and fibrin gel alone in both cell area and viable cell number. Values are reported as mean ± S.D. (n = 5). Significance was determined by a Two-way ANOVA followed by Tukey post-tests. (* $p < 0.05$)

In general, both the degree of stromal network formation and the number of viable cells clearly increased with decreasing collagen concentration in collagen and fibrin-collagen gels. Fibrin gel supplemented with aprotinin (0.05 TIU/mL) showed significantly higher values of cell

area (Fig.3.2B) as well as viable cell number (Fig.3.2C) at Day 8 compared to all concentrations of collagen and fibrin-collagen and supported 67-fold increase in the number of viable cells. This could be because compact environments restrict cell growth. There was no statistical difference between fibrin gel supplemented with aprotinin and fibrin gel alone in both normalized cell area and viable cell number; however, a dense mass of cells formed in fibrin gel without aprotinin (Fig.3.2A) due to the collapse of the fibrin structure.

3.3 Discussion

Natural hydrogels provide a 3D mechanical and biochemical environment and allow interaction among embedded cells due to their endogenous biological activity. Fibrin and collagen gels undergo cell-mediated degradation through cell-secreted enzymes, such as plasmin and matrix metalloproteinase (MMPs) allowing cell migration, proliferation and remodeling of the encapsulating matrix(19). We have characterized each hydrogel system and its ability to support the 3D stromal network formation. Among the different gel systems, more cell growth and more interconnected stromal network formation were observed when cells were in less rigid and more degradable environments, allowing branching and cell remodeling. The fast degradation rate of fibrin can be controlled with aprotinin, making it a potential material for *in vitro* 3D hydrogel system. High concentration of aprotinin slowed down fibrinolysis significantly; however, it slowed down cell growth as well. In order for cells to proliferate and connect with other surrounding cells, these cells have to be in a microenvironment where they can migrate and remodel. After reducing the aprotinin concentration to 0.05 TIU/mL, the level of proliferation and network formation were recovered while slowing down the fibrin degradation.

To better mimic the *in vivo* microenvironment, we further investigated fibrin-collagen by incorporating naturally degradable fibrin into collagen gel to allow more cell growth and better stromal network support. Surprisingly, fibrin-collagen showed lower values of normalized fluorescent cell area and viable cell number compared to both pure fibrin and collagen. This could be due to the overall mechanics of fibrin-collagen and collagen gels being influenced by changes in the network architecture. Multiple studies have shown the trend of increase in the stiffness of fibrin-collagen compared to that of pure fibrin or collagen gel(20-22). Depending on protein concentrations, the storage modulus of the gel varied; however, the trend of fibrin-collagen having a greater modulus compared to pure fibrin or collagen was consistent throughout these studies. The increase in the microstructure stiffness is likely due to the greater amount of protein in fibrin-collagen gels and the combinatory effect of highly connected bundles of collagen and inter-fibrillar bonding of fibrin(21, 23). Also it has been shown that the permeability correlates with the overall collagen content and decrease in the collagen resulted in an increase in overall permeability(24).

Gel contraction of both collagen and fibrin-collagen gels over time also could have restricted stromal cell growth and network formation. Collagen-containing gels are known to contract over time due to cells attaching and pulling on fibers as well as the force generated from cell-to-cell contact(25, 26). Fibrin-collagen underwent more significant contraction compared to pure collagen gels as fibrin degraded away. Fibrin gel also contracts, but the addition of optimal aprotonin concentration resulted in balanced matrix degradation and cell proliferation, making it more suitable for three dimensional cell culture and tissue engineering applications.

3.4 Conclusion

Throughout the different gel systems, more cell growth and more interconnected stromal network formation were observed when cells were in less rigid and more degradable environments, which allowed branching and cell-driven remodeling. Unlike slow degrading collagen-containing gel systems, fibrin degradation rate can be controlled with aprotinin, which allows better control of microenvironment. We further investigated fibrin-collagen by incorporating naturally degradable fibrin into collagen gel to allow both degradation and structural support; however, cellular growths in fibrin-collagen gels were more restricted due to higher stiffness. These results demonstrated the importance of controlled degradation rate and the stiffness, which affects the cellular capabilities to remodel their surrounding environment. Controlling the degradation rate of fibrin hydrogel using aprotinin was successful in both 3D cell and follicle cultures and extended the period of culture; however, this approach is only applicable for *in vitro* systems. Our findings further confirmed the importance of a precise and local control of hydrogel properties, such as degradation kinetics and stiffness, to design the optimum environment for cells as well as ovarian follicles, increasing the needs of synthetic hydrogels with tunable properties.

3.5 Materials and methods

3.5.1 Cell isolation and culture

Human bone marrow stromal cell lines, HS-5 (ATCC CRL-11882) were cultured in DMEM (Dulbecco's modified Eagle's medium) culture medium (ATCC) supplemented with 10% fetal heat inactivated bovine serum (FBS) (Biowest). HS-5 cells, which resemble FRCs in that they are podoplanin-positive and CD31-negative, were cultured in T-75 flasks and split in a 1:5 ratio

every 3-4 days. CD4+ T cells used in this study, P2 cells(27), were isolated from A3.01 cells (a subclone of the CEM cell line) based on its high propensity to adopt a polarized shape. These T cells were cultured in RPMI-1640 medium (Gibco Life Technologies) supplemented with 10% heat inactivated FBS in T-25 flasks, placed upright, and split in a 1:10 ratio every 3-4 days. All culture media were supplemented with 1% PenStrep (Lonza) and incubated in 5% CO_2 atmosphere at 37°C.

3.5.2 Gel preparation and cell encapsulation

3.5.2.1 Fibrin gel

Dialyzed sterile bovine fibrinogen (Sigma Aldrich) (12.0 mg/mL), HS-5 cells, and bovine thrombin (Sigma) (50 IU/mL) were mixed and extruded homogeneously using the extruder from the Hemaseel APR™ Sealer Protein Kit (Haemacure) to obtain a fibrin gel with the final fibrinogen of 6 mg/mL and 220,000 cells/mL gel concentrations. Fibrin gels (each with 200 μL volume) with encapsulated stromal cells were allowed to gel in 48 well plates for 10 min in the incubator (37°C, 5% CO_2). Fibrin coagulated and formed solid gels after 10 min and the addition of 200 μL media did not disturb the morphology of the gel. A timeframe of 10 min was selected to maximize the cell viability during the polymerization process. Media was changed every 2 days and cells were cultured up to 8 days. Each experiment was repeated five times and the results were reproducible.

3.5.2.2 Type I collagen gel

Type I Collagen rat tail (Col I) (8.56 mg/mL) (BD Biosciences) was mixed with the appropriate amounts of 10x PBS, 1N NaOH and dH_2O to make the final concentration of 2 mg/mL or 4 mg/mL. This was quickly followed by the addition of cells to reach a final concentration of 220,000 cells/mL. Constructs (each with 200 μL volume) were allowed to gel in

48 well plates for 10 min in the incubator (37°C, 5% CO_2). Collagen coagulated and formed solid gels after 10 min and the addition of 200 μL media did not disturb the morphology of the gel. Media was changed every 2 days and cells were cultured up to 8 days. Each experiment was repeated five times and the results were reproducible.

3.5.2.3 Fibrin-collagen I gel

To reach a final concentration of 6 mg/mL fibrinogen and 2 mg/mL or 4 mg/mL Type I Collagen in a gel, we added the appropriate amounts of Col I (8.56 mg/mL), fibrinogen (12.0 mg/mL), 10x PBS, 1N NaOH, dH_2O and 50 IU/ml bovine Thrombin (Sigma). Each concentration of fibrinogen, thrombin, and collagen were selected based on previous *in vitro* 3D cell culture studies(20-22), which have shown to support cell growth and proliferation. Cells were harvested and resuspended in fibrinogen to reach a final concentration of 220,000 cells/mL. Constructs (each with 200 μL volume) were allowed to gel in 48 well plates for 10 min in the incubator (37°C, 5% CO_2). Fibrin-collagen coagulated and formed solid gels after 10 min and the addition of 200 μL media did not disturb the morphology of the gel. Media was changed every 2 days and cells were cultured up to 8 days. Each experiment was repeated five times and the result were reproducible.

3.5.3 GFP transfection

To visualize HS-5 stromal networks up to 8 days in culture and to quantify cell area using fluorescence, HS-5 cells were stably transfected to express green fluorescent protein (GFP). 24 hours prior to transfection, HS-5 cells were seeded in 6-well plate to reach 60% confluency on the day of transfection. Plasmid DNA vector (pLenti-III-CMV-GFP-Puro, LV590, Applied Biological Materials) was mixed with Fugene 6 transfection reagent (Promega) and Opti-MEM® (Life Technologies) according to manufacturer's instructions. DNA/Fugene6/Opti-MEM®

mixture was added dropwise to the well of 6-well plate containing growth medium. Cells were then incubated at 37°C for 48 hours. The GFP plasmid construct contains a puromycin resistance gene, which allows selecting stably transfected cells by culturing in a medium supplemented with 1 μg/ml puromcyin (Sigma-Aldrich). After 48 hours, incubated HS-5 cells were subcultured 1:3 in selection medium. Selection medium were replaced every 3 days for 14 days. Successful selection was confirmed by the observation of 100% distinct colonies of surviving GFP-positive HS-5 cells.

3.5.4 Fluorescent area measurement

A MATLAB® code was created using the Image Processing Toolbox in order to determine the approximate area of GFP expressing cells. Specifically, the green channel was parsed out from each image before using image segmentation functions to create a gradient picture. Image segmentation relies upon differences in contrast in order to create a binary mask of the image. Once the binary mask image contained outlines of the cells, the mask was dilated and filled in order to cover the full area of each cell. Within the binary mask, white spots denoted cells, and cell area was calculated by determining the number of white pixels per image and converting the number to a size in microns (Fig.3S1). Additionally, the binary mask outline was superimposed onto the original image to ensure that cell area was detected appropriately. All the analyzed images were taken at 100x magnification by the inverted microscope Leica DMI3000B and images were screened, selected and analyzed using a double-blind method (n = 5).

3.5.5 Aprotinin test

To slow down fibrinolysis, the culturing media (DMEM with 10% FBS) was supplemented with monomeric serine protease inhibitor, aprotinin (Sigma-Aldrich). Aprotinin was added in the medium to reach and to maintain sufficient concentration levels throughout the 8 days of culture

and to be able to easily modify the concentration if necessary. Before addition, 1 TIU/mL aprotinin was diluted with culturing media to the desired aprotinin concentration (0.1 TIU/mL and 0.05 TIU/mL). Aprotinin was added beginning on Day 2 and continued until Day 8 of culture. At Day 4, Day 6, and Day 8 of the culture, its effects on HS-5 stromal network formation were examined by measuring the fluorescent cell area as described previously (n = 5).

3.5.6 Fibrin degradation assays

To measure the degradation rate of fibrin gels, we mixed unlabeled fibrinogen with AlexaFluor546 conjugate (558/573 nm) labeled fibrinogen with (Invitrogen), resulting in 2% w/w labeling. HS-5 cells were encapsulated in the fluorescently labeled fibrin gels and cultured in DMEM without phenol red and supplemented with 4 mM L-Glutamine (ATCC). A plate reader (Fluoroskan Ascent FL) was used to measure the levels of soluble degradation products, AlexaFluor conjugate, released from the labeled fibrinogen as a result of the fibrin degradation (n = 5). Media was collected every 2 days for up to 8 days of culture. As a control, we measured the release of the AlexaFluor conjugate to the media from fibrin gels without cells to ensure that the fibrin degradation is driven by the cells. We did not detect fluorescent signal when fibrin gels were cultured without the cells and no autofluorescence was detected from the media.

3.5.7 Stromal cell viability

CellTiter-Glo Luminescent Cell Viability Assays (Promega) was used to determine the number of viable cells based on quantification of ATP present, which indicates the presence of metabolically active cells. This procedure was carried out on Day 8 for all conditions as described by the manufacturer's protocol. The luminescence values were recorded by using a platereader (Fluoroskan Ascent FL) after 10 minutes of incubation at room temperature to stabilize the luminescent signals. Standard curves were generated for each gel condition to

identify the linear relationship between the luminescent signal and the number of cells in the hydrogel, ranging from 0 to 2 million cells per gel in the 96-well format (n = 5).

3.5.8 Statistical analysis

All statistical analyses were performed using GraphPad Prism (GraphPad Prism Software, La Jolla, CA). Data are reported as mean ± standard deviation of measurements, and analyzed with Two-way ANOVA followed by Tukey post-test. Statistical significance was assumed when $p < 0.05$.

3.6 References

1. Giancotti FG, Ruoslahti E. Integrin signaling. *Science.* 1999 Aug 13; 285(5430): 1028-1032.

2. De Arcangelis A, Georges-Labouesse E. Integrin and ECM functions: Roles in vertebrate development. *Trends Genet.* 2000 Sep; 16(9): 389-395.

3. Ben-Ze'ev A, Amsterdam A. Regulation of cytoskeletal proteins involved in cell contact formation during differentiation of granulosa cells on extracellular matrix. *Proc Natl Acad Sci U S A.* 1986 May; 83(9): 2894-2898. PMCID: PMC323413.

4. Albertini DF, Kravit NG. Isolation and biochemical characterization of ten-nanometer filaments from cultured ovarian granulosa cells. *J Biol Chem.* 1981 Mar 10; 256(5): 2484-2492.

5. Anderson E, Albertini DF. Gap junctions between the oocyte and companion follicle cells in the mammalian ovary. *J Cell Biol.* 1976 Nov; 71(2): 680-686. PMCID: PMC2109751.

6. Adams JC, Watt FM. Regulation of development and differentiation by the extracellular matrix. *Development.* 1993 Apr; 117(4): 1183-1198.

7. Irving-Rodgers HF, Mussard ML, Kinder JE, Rodgers RJ. Composition and morphology of the follicular basal lamina during atresia of bovine antral follicles. *Reproduction.* 2002 Jan; 123(1): 97-106.

8. Rodgers HF, Irvine CM, van Wezel IL, Lavranos TC, Luck MR, Sado Y, Ninomiya Y, Rodgers RJ. Distribution of the alpha1 to alpha6 chains of type IV collagen in bovine follicles. *Biol Reprod.* 1998 Dec; 59(6): 1334-1341.

9. Kreeger PK, Woodruff TK, Shea LD. Murine granulosa cell morphology and function are regulated by a synthetic arg-gly-asp matrix. *Mol Cell Endocrinol.* 2003 Jul 31; 205(1-2): 1-10.

10. Baker BM, Chen CS. Deconstructing the third dimension: How 3D culture microenvironments alter cellular cues. *J Cell Sci.* 2012 Jul 1; 125(Pt 13): 3015-3024. PMCID: PMC3434846.

11. Kurpinski K, Chu J, Hashi C, Li S. Anisotropic mechanosensing by mesenchymal stem cells. *Proc Natl Acad Sci U S A.* 2006 Oct 31; 103(44): 16095-16100. PMCID: PMC1637542.

12. Bonnans C, Chou J, Werb Z. Remodelling the extracellular matrix in development and disease. *Nat Rev Mol Cell Biol.* 2014 Dec; 15(12): 786-801. PMCID: PMC4316204.

13. Picton HM. Activation of follicle development: The primordial follicle. *Theriogenology.* 2001 Apr 1; 55(6): 1193-1210.

14. Shikanov A, Smith RM, Xu M, Woodruff TK, Shea LD. Hydrogel network design using multifunctional macromers to coordinate tissue maturation in ovarian follicle culture. *Biomaterials.* 2011 Apr; 32(10): 2524-2531. PMCID: PMC3040241.

15. Amorim CA. Artificial ovary. In: Donnez J, Kim S, editors. *Principles and Practice of Fertility Preservation.*. Cambridge, UK: Cambridge University press; 2011. p. 448-458.

16. Gougeon A. Regulation of ovarian follicular development in primates: Facts and hypotheses. *Endocr Rev.* 1996 Apr; 17(2): 121-155.

17. Shikanov A, Xu M, Woodruff TK, Shea LD. Interpenetrating fibrin-alginate matrices for in vitro ovarian follicle development. *Biomaterials.* 2009 Oct; 30(29): 5476-5485. PMCID: PMC2906124.

18. Shikanov A, Xu M, Woodruff TK, Shea LD. A method for ovarian follicle encapsulation and culture in a proteolytically degradable 3 dimensional system. *J Vis Exp.* 2011 Mar 15; (49). pii: 2695. doi(49): 10.3791/2695. PMCID: PMC3197327.

19. Mosesson MW. Fibrinogen and fibrin structure and functions. *J Thromb Haemost.* 2005 Aug; 3(8): 1894-1904.

20. Rao RR, Peterson AW, Ceccarelli J, Putnam AJ, Stegemann JP. Matrix composition regulates three-dimensional network formation by endothelial cells and mesenchymal stem cells in collagen/fibrin materials. *Angiogenesis.* 2012 Jun; 15(2): 253-264. PMCID: PMC3756314.

21. Rowe SL, Stegemann JP. Interpenetrating collagen-fibrin composite matrices with varying protein contents and ratios. *Biomacromolecules.* 2006 Nov; 7(11): 2942-2948. PMCID: PMC1795649.

22. Lai VK, Lake SP, Frey CR, Tranquillo RT, Barocas VH. Mechanical behavior of collagen-fibrin co-gels reflects transition from series to parallel interactions with increasing collagen content. *J Biomech Eng.* 2012 Jan; 134(1): 011004. PMCID: PMC3717315.

23. Lewis JL, Johnson SL, Oegema TR,Jr. Interfibrillar collagen bonding exists in matrix produced by chondrocytes in culture: Evidence by electron microscopy. *Tissue Eng.* 2002 Dec; 8(6): 989-995.

24. Helm CL, Zisch A, Swartz MA. Engineered blood and lymphatic capillaries in 3-D VEGF-fibrin-collagen matrices with interstitial flow. *Biotechnol Bioeng.* 2007 Jan 1; 96(1): 167-176.

25. McGuigan AP, Bruzewicz DA, Glavan A, Butte MJ, Whitesides GM. Cell encapsulation in sub-mm sized gel modules using replica molding. *PLoS One.* 2008 May 21; 3(5): e2258. PMCID: PMC2376064.

26. Roy P, Petroll WM, Chuong CJ, Cavanagh HD, Jester JV. Effect of cell migration on the maintenance of tension on a collagen matrix. *Ann Biomed Eng.* 1999 Nov-Dec; 27(6): 721-730.

27. Llewellyn GN, Hogue IB, Grover JR, Ono A. Nucleocapsid promotes localization of HIV-1 gag to uropods that participate in virological synapses between T cells. *PLoS Pathog.* 2010 Oct 28; 6(10): e1001167. PMCID: PMC2965768.

CHAPTER IV

Characterization of the crosslinking kinetics of multi-arm poly(ethylene glycol) hydrogels formed via Michael-type addition

4.1 INTRODUCTION

Naturally derived and synthetic hydrogels have been extensively exploited in biomedical materials research due to their abilities in directing cellular behavior and function(1, 2). Natural hydrogels, such as collagen(3) and fibrin(4), are compatible with live cells, support cell attachment, migration and remodeling; however, the mechanical and biological properties of these materials are closely tied. For example, altering the Matrigel or collagen concentration in hydrogels changes the stiffness of the gel and also affects the concentration of bioactive factors, such as integrin binding and protease sensitive sites. This interdependence of mechanical properties and the biological activity in natural hydrogels makes it challenging to prepare matrices suitable for the diverse requirements of biomedical applications. In contrast to natural hydrogels, biologically inert synthetic hydrogels, such as poly(ethylene glycol) (PEG), have tunable physical properties independent of their biological activity(5-10). These properties are important for regulating cellular differentiation and function(11-13) and can be manipulated through PEG hydrogel composition, solid concentration, and crosslinking chemistry.

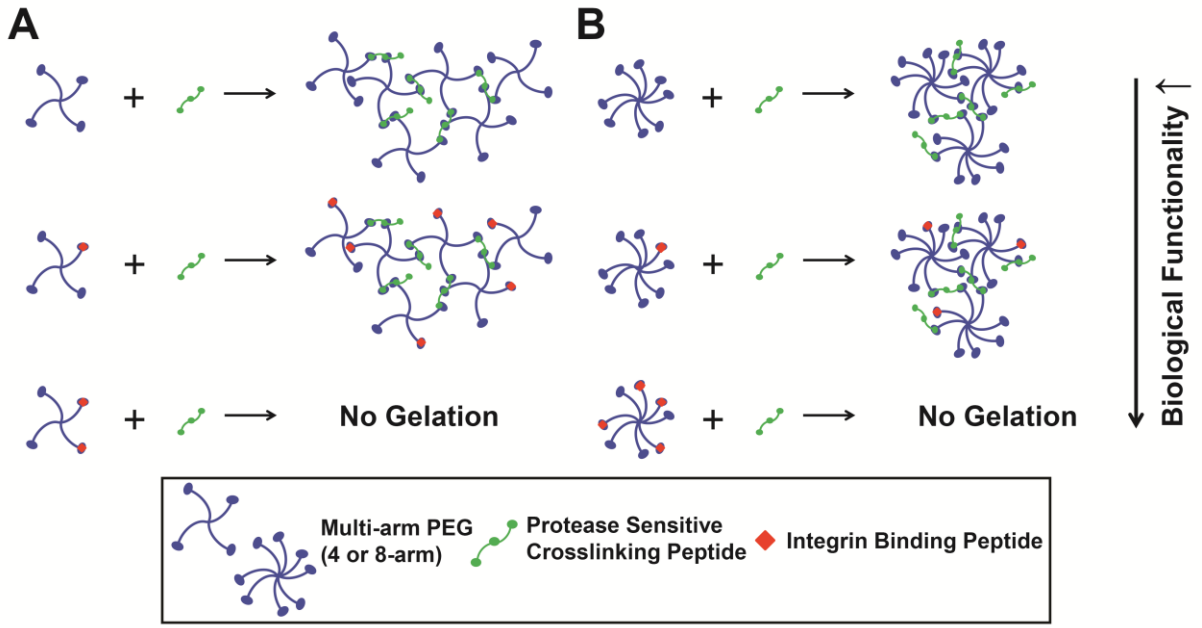

Figure 4.1. Crosslinking mechanism for RGD modified multi-arm PEG and YKNR crosslinking peptides. This schematic shows the crosslinking kinetics between **(A)** 4-arm PEG and **(B)** 8-arm PEG that are modified with integrin binding peptides, RGD, and trifunctional protease sensitive crosslinking peptide, YKNR, through Michael-type addition. Intermolecular reactions and the presence of a third binding site allowed continuation of the network formation. However, bioactive modification with integrin binding peptides, RGD, affected crosslinking kinetics by binding to the reactive sites on the PEG molecules, preventing network growth at those binding sites. L-Cysteine hydrochloride monohydrate (L-Cys) was substituted on a molar basis as a biologically inactive surrogate molecule for RGD.

PEG hydrogels are prepared using Michael-type addition (MTA) chemistry, where cysteine-containing peptides react with the unsaturated groups of the multi-arm PEG(14, 15). The biocompatible chemistry of the MTA reaction allows bioactive modification of the inert PEG hydrogels through the incorporation of integrin binding sequences, like RGD, followed by crosslinking with protease sensitive peptides. Modification of PEG with monofunctional RGD peptides promotes cell adhesion, and crosslinking with di- or trifunctional protease sensitive peptides allow migration and proliferation of the encapsulated cells(5, 8, 16, 17). Specifically for tissue engineering applications, cysteine containing peptides react with the unsaturated groups of the end-functionalized multi-arm PEG to form PEG hydrogels(14, 15). As a result, the modification with RGD, or any other monofunctional peptide, leaves fewer “free” reactive arms

available for crosslinking (Fig.4.1). We have demonstrated previously that adding a third reactive site to bifunctional crosslinking peptides permits continuation of the hydrogel network, improving crosslinking density(18) (Fig.4.1). Despite the improved crosslinking density of hydrogels prepared with 4-arm PEG and tri-functional crosslinkers, there are still limitations on the extent of modification with RGD. Furthermore, a higher concentration of monofunctional peptides results in a greater degree of swelling, which contributes to dilution of the incorporated bioactive molecule concentrations in the hydrogel(19).

The crosslinking kinetics and macroscopic properties of MTA PEG hydrogels depend on pH, PEG solid concentration, and the presence of charged amino acid residues(15, 20). However, it has not been fully explored how the PEG functionality and the consequences of bioactive modification with monofunctional peptides affect the crosslinking kinetics, mechanical properties, and the behavior of encapsulated cells. In this study, we investigated the effects of increasing the number of reactive groups around the core of the PEG macromer from 4 to 8 on the macroscopic properties of the hydrogel, such as swelling and storage modulus. The total molar concentration of the reactive functional groups in the conditions comparing 4 and 8-arm PEG was identical (e.g. 10mM [–VS] for 5% 4 and 8-arm PEGs), yet we demonstrated that a greater local concentration of reactive arms around the core of the PEG macromer resulted in improved crosslinking efficiency and reduced network defects stemming from incomplete gelation. These findings support our hypothesis that PEG macromers with increased functionality allow a greater degree of bioactive modification without compromising the mechanical properties of the hydrogel and result in an improved hydrogel design for various biomedical applications.

4.2 RESULTS

4.2.1 Storage Modulus of 5% PEG Hydrogels

First, we studied how the addition of 1.25, 2.5, and 3mM L-Cys affected the storage modulus (G') compared to unmodified hydrogels (0mM L-Cys). Addition of up to 3mM L-Cys to 5% 4-arm PEG hydrogels allowed complete gelation, which was determined to be the maximal concentration of the monofunctional peptide. The storage modulus of unmodified 4 and 8-arm PEG hydrogels showed no significant difference after 15min of gelation (Fig.4.2A) or after 60min (Fig.4.2B). However, upon the addition of L-Cys, storage moduli at 15min and at 60min of 4-arm PEG hydrogels were significantly lower compared to those of 8-arm PEG gels modified with L-Cys (Fig.4.2A,B). The final G' of 4-arm PEG hydrogels modified with 3mM L-Cys modification only attained 0.8kPa compared to the 1.8kPa of 8-arm PEG gels, and 4.7kPa for unmodified 4-arm PEG hydrogels (Fig.4.2B). Modification with L-Cys had a pronounced negative effect on gelation and storage modulus of 4-arm PEG hydrogels, especially when the reaction was quenched after 15min. In that case, the storage modulus of 4-arm PEG hydrogels modified with 1.25mM L-Cys reached only 1.6kPa compared to the 2.9kPa of 8-arm PEG hydrogels, and 3.8kPa for unmodified 4-arm PEG hydrogels (Fig.4.2A). This negative effect was also observed for the G' of 8-arm PEG hydrogels with the addition of L-Cys; yet, less pronounced compared to 4-arm PEG hydrogels.

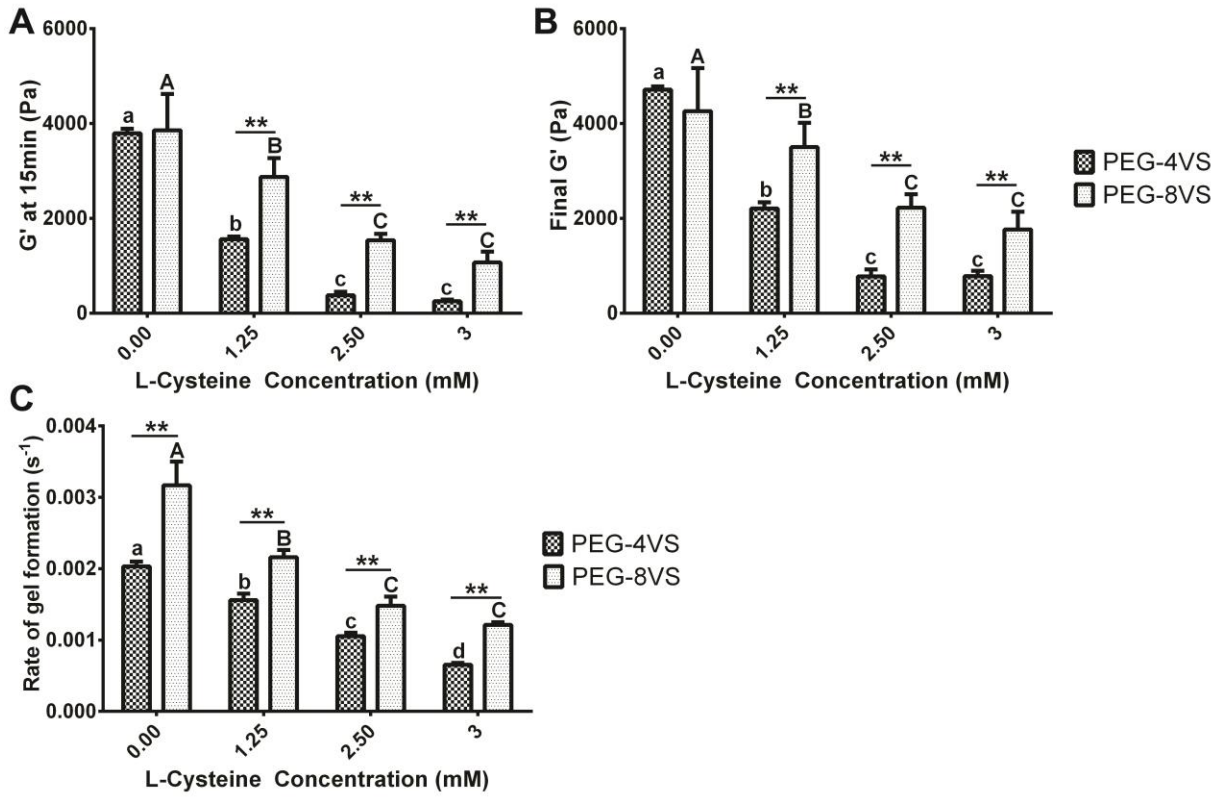

Figure 4.2. The effect of the L-Cysteine concentration on storage modulus and rate constant of gel formation. Time sweep tests were performed at 1 rad/sec and 10% strain to measure storage modulus (G') of 5% 4 and 8-arm PEGs modified with 0, 1.25, 2.5 and 3mM L-Cysteine **(A)** after 15min and **(B)** after 60min of gelation. There were no significant differences between G' of unmodified 4 and 8-arm PEGs (0mM L-Cys). However, G' of 4 and 8-arm PEG **(A)** at 15min and **(B)** at 60min was significantly different at all other L-Cys concentrations. **(C)** Rate constant of gel formation of 5% 4 and 8-arm PEGs were significantly different at all conditions. All data is reported as mean ± S.D. (n = 3). Significance was determined by a two-way ANOVA followed by Bonferroni post-tests with $p < 0.05$. Double asterisks (**) denoted significance between PEG-4VS and PEG-8VS at all L-Cys concentration. Different lower (4-arm) and uppercase (8-arm) letter represent statistically significant difference within modified PEG-4VS and PEG-8VS conditions.

4.2.2 Rate Formation of PEG Hydrogels

We performed a time sweep test to determine the rate constant of gelation rate and investigate how the addition of bioactive moieties affects the crosslinking kinetics. Overall, the rate constant of gel formation was dependent on the number of arms available for crosslinking. The rate constant of gel formation of the 8-arm PEG hydrogel was significantly higher than those of 4-arm PEG hydrogel at all L-Cys concentrations (Fig.4.2C). The incorporation of L-Cys in both 4 and 8-arm PEG hydrogels resulted in a decrease in the rate constant of gel formation and

the decrease was more significant when L-Cys concentration increased. For example, the incorporation of 3mM L-Cys caused the rate constant of gel formation to decrease one order of magnitude (from 2.0 x 10^{-3} sec^{-1} to 6.5 x 10^{-4} sec^{-1}) for 4-arm PEG hydrogels. The decrease in the rate constant of gel formation of 8-arm PEG hydrogels also occurred; however, it was less significant compared to 4-arm PEG hydrogels.

4.2.3 Swelling of PEG-VS Hydrogels

4 and 8-arm PEG hydrogels modified with increasing concentrations of L-Cys demonstrated significantly increased swelling ratios and a reduced concentration of elastically active chains (Fig.4.4B); however, the swelling ratio of 8-arm PEG hydrogels was less affected by the incorporation of L-Cys than relative to 4-arm PEG hydrogels (Fig.4.3B). In 5% PEG hydrogels with 1.25mM L-Cys modification, 4-arm PEG hydrogels had a swelling ratio 1.4 times greater than 8-arm PEG hydrogels. When no L-Cys was added or at a L-Cys concentration of 1.25mM, there was no significant difference in the swelling ratio in 5% 8-arm PEG hydrogels in contrast to 5% 4-arm PEG hydrogels. Furthermore, 8-arm PEG hydrogels supported efficient network crosslinking up to 3.75mM L-Cys modification (Fig.4.3B) when 4-arm PEG hydrogels could form with up to 3mM L-Cys content (Fig.4.3A).

We also compared the equilibrium mass swelling ratio of 4 and 8-arm PEG-VS hydrogels with varying solid concentrations from 4 to 10% w/v when the crosslinking reaction was quenched after 15min. Gels with PEG concentrations of less than 4% did not form after 15min, and gels with PEG concentration above 10% were not investigated due to the small mesh size and high storage modulus, which are less suitable for applications involving cells(6). We found that a higher concentration of PEG resulted in less swelling for both 4 and 8-arm PEG hydrogels

(Fig.4.3C). For example, the lowest Q_m values, which are indicative of higher crosslinking density, were obtained for unmodified 4 and 8-arm at the 10% PEG concentrations. Even though both 4 and 8-arm PEG conditions had the same molar concentrations of reactive groups, significantly lower Q_m values were observed in 8-arm PEG hydrogels compared to 4-arm PEG hydrogels at all PEG concentrations. Similar trends were observed for concentration of elastically active chains calculated by using the Flory-Rehner equation (Fig.4.4).

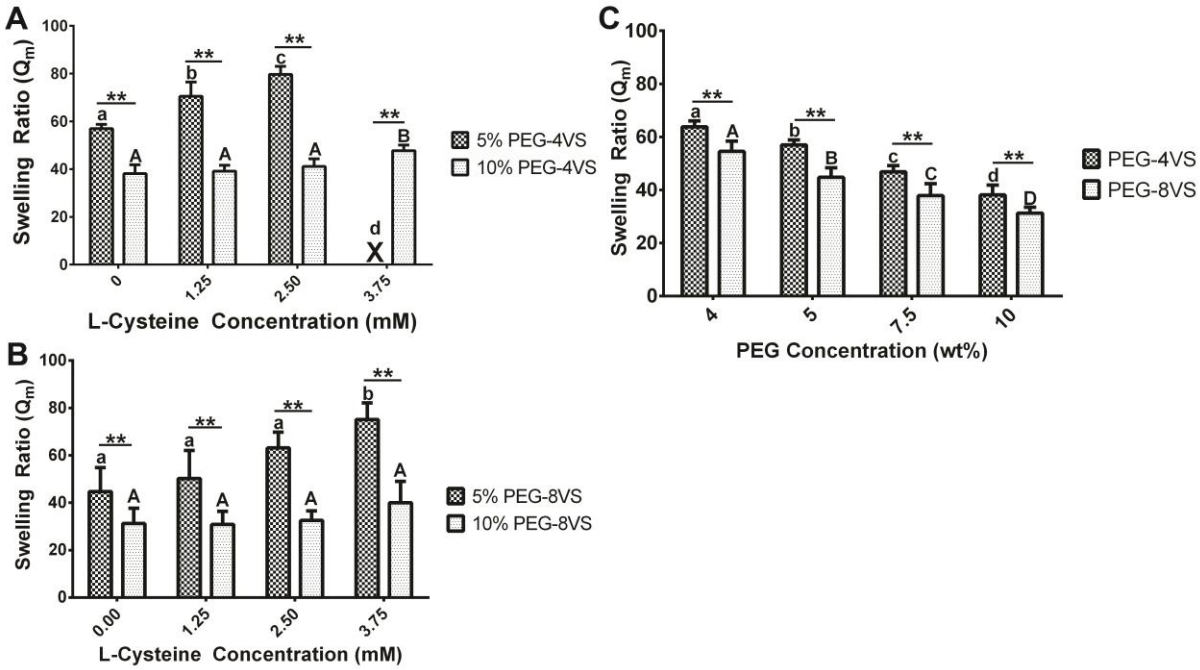

Figure 4.3. The effects of L-Cysteine and PEG-VS concentration on swelling ratio. Swelling ratios were compared between **(A)** 5% and 10% 4-arm PEG and **(B)** 8-arm PEG modified with 0, 1.25, 2.5 and 3.75mM L-Cys. **(A)** Swelling ratios of 5% 4-arm PEG hydrogels were significantly different from those of 10% 4-arm PEGs at all L-Cys concentrations. Swelling ratios of 5% 4-arm PEGs with 0mM L-Cys were significantly different from those of 5% 4-arm PEGs modified with 1.25 and 2.5mM L-Cys. However, swelling ratios of 10% 4-arm PEGs with 3.75mM L-Cys was only significantly different from those of all 10% 4-arm PEGs. ($P<0.001$) An 'X' denotes conditions that did not form gels. **(B)** For 8-arm PEG hydrogels, swelling ratios of 5% 8-arm PEGs were significantly different from those of 10% 8-arm PEGs at all L-Cys concentrations. However, there was no significant difference among any 10% 8-arm PEGs at all L-Cys concentrations ($P<0.01$) **(C)** Swelling ratios of 4-arm PEGs were significantly different from those of 8-arm PEGs at all PEG concentrations. All data is reported as mean ± standard deviation (n = 8). Significance was determined by a two-way ANOVA followed by Bonferroni post-tests. Double asterisks (**) denoted significance between PEG-4VS and PEG-8VS at all L-Cys concentration ($p < 0.01$). Different lower (4-arm) and uppercase (8-arm) letter represented statistically significant difference within modified PEG-4VS and PEG-8VS conditions ($p < 0.05$).

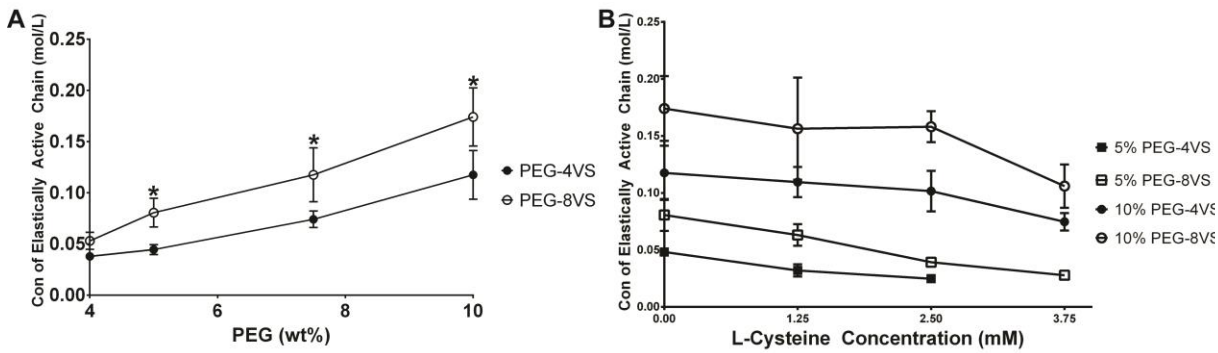

Figure 4.4. Concentration of elastically active chains. (A) Concentrations of elastically active chains of 8-arm PEG were greater than those of 4-arm PEG at all biologically relevant PEG solids concentration, indicating a higher PEG functionality would favor intermolecular reactions between elastically active binding sites. **(B)** Concentrations of elastically active chains of 8-arm PEG were available up to 3.75mM L-Cysteine modification when they were only available up to 3mM L-Cysteine modification in 4-arm PEG hydrogels, confirming experimental data on how PEG with higher number of functional binding sites allowed greater degree of biological modification.

4.2.4 Material Properties Comparisons Between 5% PEG-VS and PEG-A Hydrogel

Different reactive end groups, such as acrylate (PEG-A) and vinylsulfone (PEG-VS), have the ability affect the mechanical properties of PEG MTA hydrogels. We investigated whether PEG functionality and the degree of modification demonstrate similar trends across various end groups of PEG in crosslinking efficiency and macroscopic properties. The PEG-VS and PEG-A macromers are identical in structure besides their reactive end groups. The considerable differences in resulting material properties among different MTA reactive groups arise from differences in electronegativity of the end groups affecting the crosslinking efficiency(21). The main difference between the two functional end groups was the range of possible L-Cys modification in 5% 4-arm PEG hydrogels. PEG-4A hydrogels could form with a maximum of 1.25mM when PEG-4VS supported efficient network crosslinking up to 3mM L-Cys modification (Fig.4.5A). Overall, both PEG-8VS and PEG-8A demonstrated more efficient crosslinking compared to either 4-arm PEGs. As an example, the rate constant of gel formation of both PEG-8VS and PEG-8A was significantly higher than those of both PEG-4VS and PEG-4A at all L-Cys concentrations (Fig.4.5B). Also G' of both 4-arm PEG hydrogels modified with

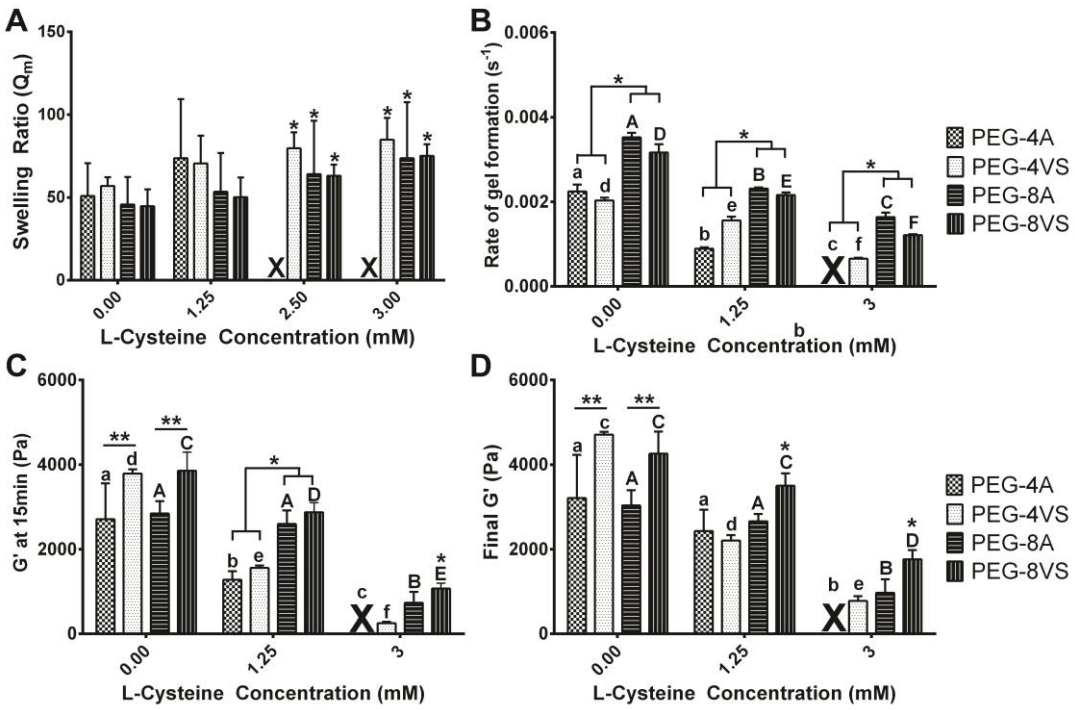

Figure 4.5. Comparison of PEG-VS and PEG-A. (A) Swelling ratio, **(B)** the rate constant of gel formation, storage modulus **(C)** after 15min of gelation and **(D)** after 60min were compared between 5% 4-arm PEG and 8-arm PEG hydrogels (PEG-VS and PEG-A) modified with 0, 1.25, and 3mM L-Cys. For swelling ratio, there was no statistical difference between PEG-VS and PEG-A at all conditions. However, PEG-4A gels could form with a maximum of 1.25mM when PEG-4VS supported efficient network crosslinking up to 3mM modification. The rate constant of gel formation of both PEG-8VS and PEG-8A was significantly higher than those of PEG-4VS and PEG-4A at all L-Cys concentration. G' of both unmodified 8-arm PEGs after **(C)** 15min and **(D)** 60min was significantly higher from G' of both unmodified 4-arm PEGs; however, upon addition of L-Cys, there were no significant differences between G' of PEG-8A and both 4-arm PEGs. An 'X' denotes conditions that did not form gels. All data is reported as mean ± S.D. (A) n = 8, (B – D) n = 3. Significance was determined by a two-way ANOVA followed by Bonferroni post-tests. A single asterisk (*) denoted significance among groups of PEG-VS and PEG-A (both 4 and 8-arm) modified with a same L-Cys concentration. Different lower (4-arms) and uppercase (8-arms) letter represented statistically significant difference within modified PEG-VS and PEG-A groups (both 4 and 8-arm) ($p < 0.05$).

1.25mM L-Cys at 15min was significantly lower than G' of both 8-arm PEG hydrogels modified with 1.25mM L-Cys at 15min (Fig.4.5C). However, there was no significant difference between any measurements of swelling ratio (Fig.4.5A). Overall, the trend of an increase in swelling ratio and a decrease in storage modulus with the addition of L-Cys was similar in PEG-A.

Modification with L-Cys had a less pronounced negative effect on gelation and storage modulus

of both PEG-8VS and PEG-8A compared to PEG-4VS and PEG-4A, especially when the reaction was quenched after 15min (Fig.4.5C).

4.2.5 PEG Functionality and the Bioactive Modification Affect Cellular Growth and Behavior

PEG hydrogels with the same solid concentrations, but modified with different RGD concentrations, exhibit different mechanical properties. Here, we encapsulated and cultured HS-5 cells in 5% 4 and 8-arm PEG hydrogels modified with 0.25mM and 1.25mM RGD (Fig.4.6). To isolate the effect of the concentration of biological cues, we incorporated 1mM L-Cys to PEG hydrogels modified with 0.25mM RGD to mimic the same mechanical properties of PEG gels modified with 1.25mM RGD by blocking the same number of reactive arms. These hydrogels were crosslinked with the plasmin sensitive tri-functional crosslinking peptide composed of fibrin-derived sequences, YKNR, to allow proteolytic degradation(18).

HS-5 cells cultured in 5% 8-arm PEG hydrogels modified with 1.25mM RGD exhibited fibroblast-like spindle morphology starting at Day 4 and stromal networks began to form through affixing with other adjacent cell populations by Day 12 (Fig.4.6B). In 5% 4-arm PEG hydrogels modified with 1.25mM RGD, HS-5 cells started to express fibroblast-like spindle morphology at Day 8; however, stromal networks were not as dense nor interconnected as those observed in 5% 8-arm PEG modified with 1.25mM RGD (Fig.4.6A). Despite a less dense network, spheroid formation was still observed in 5% 4 and 8-arm PEG gels modified with 0.25mM RGD, which was confirmed by multiple nuclei DAPI staining (Fig.4.6A,B). In addition, although a reduction in the concentration of RGD limited cell network growth, cells were viable in gels modified with 0.25mM RGD (Fig.4.7).

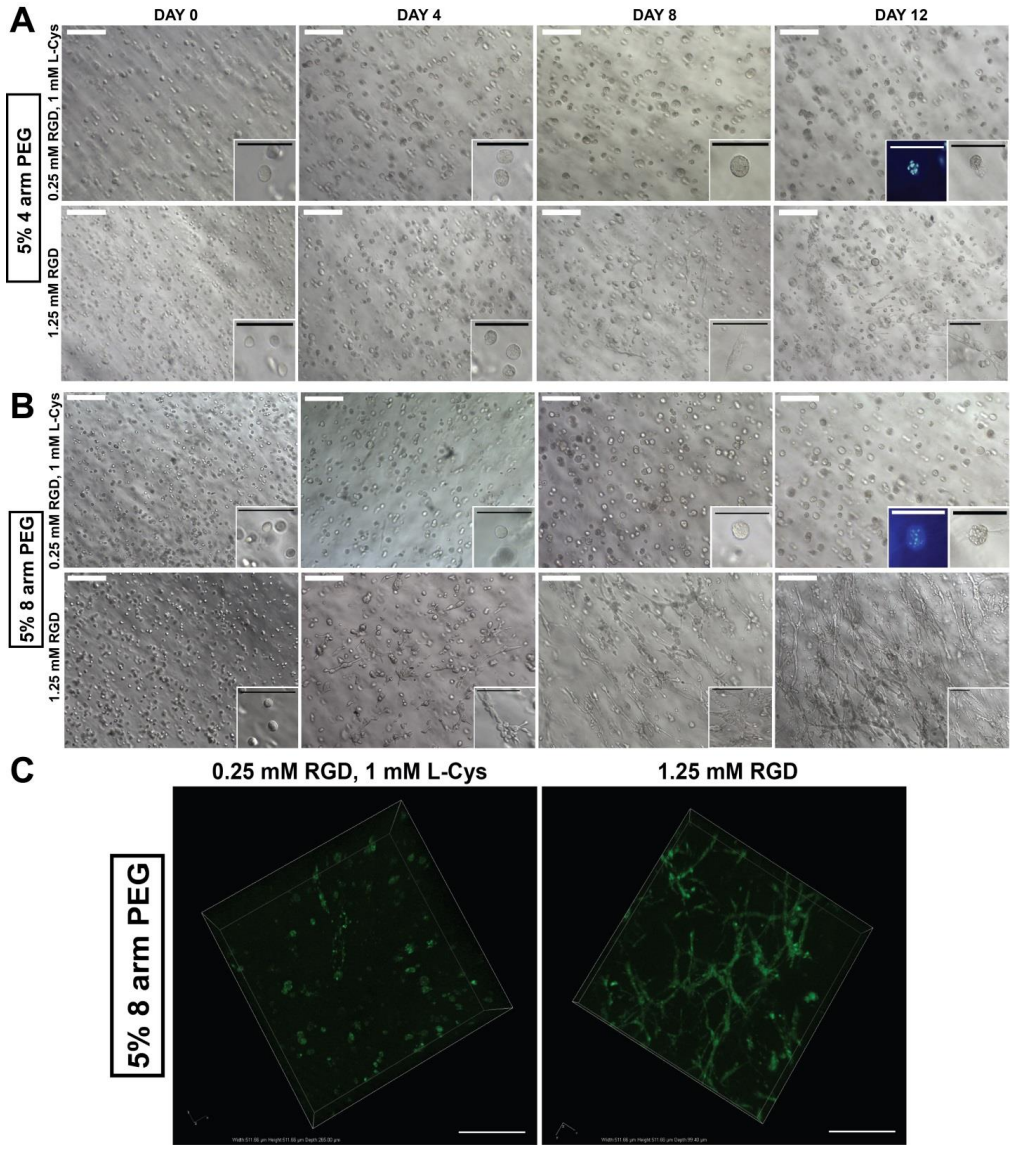

Figure 4.6. The effect of the RGD concentration on human bone marrow stromal cells growth and the network formation. Stromal cells derived from human bone marrow (HS-5) [2 x 10^6 cells/mL] were encapsulated in 5% **(A)** 4-arm and **(B)** 8-arm PEG-VS modified with 0.25mM RGD and 1.25mM RGD and cultured up to Day 12. HS-5 cultured in 5% 8-arm PEG-VS modified with 1.25mM RGD formed more interconnected and complete network. In contrast, HS-5 cultured in 4-arm PEG-VS and 8-arm PEG-VS modified with 0.25mM RGD + 1mM L-Cysteine formed spheroids confirmed by multiple nuclei observed using DAPI staining due to insufficient cell adhesion. Scale bar: White = 200µm, Black/DAPI = 100µm **(C)** GFP transfected Human bone marrow stromal cells (GFP HS-5) [2 x 10^6 cells/mL gels] were encapsulated in 5% 8-arm PEG-VS modified with 0.25mM RGD + 1mM L-Cysteine and 1.25mM RGD and cultured up to Day 12. GFP HS-5 cultured in 5% 8-arm PEG-VS modified with 1.25mM RGD formed more interconnected and complete network. Images were taken using a confocal microscope Nikon A1. Scale bar: 100µm.

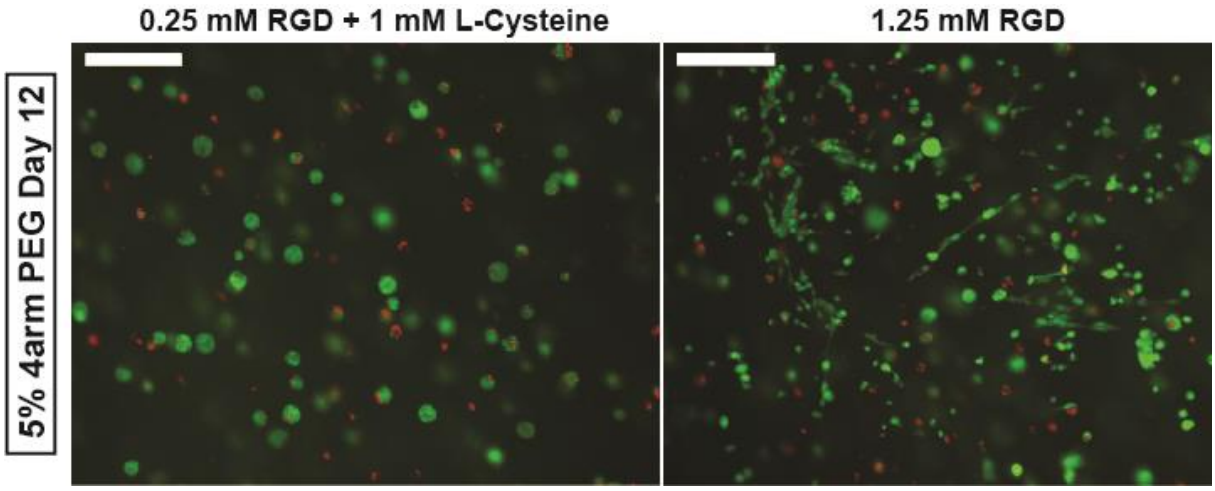

Figure 4.7. LIVE/DEAD assay on 5% 4-arm PEG-VS on Day 12. Human bone marrow stromal cells (HS-5) viability was confirmed by LIVE/DEAD assay. High Calcien AM (Green) staining confirmed the cell viability was not significantly affected by the RGD concentration. Scale bar: 200μm.

4.3 DISCUSSION

In this study, we aimed to investigate how the modification of PEG macromers with monofunctional groups affects the material properties. Considering that there are equal molar concentrations of reactive end groups participating in the reaction, we hypothesized that a greater number of arms per molecule core would allow a greater degree of bioactive modification without affecting the mechanical properties of the hydrogel. Interestingly, the crosslinking kinetics and the storage modulus of unmodified 4 and 8-arm PEG gels were not affected by the spatial distribution of arms around the core of the PEG macromer. In contrast, incorporation of biological cues dramatically affected the storage modulus and the crosslinking kinetics of modified 4-arm PEG gels compared to the 8-arm PEG gels.

The rate constant of gel formation of 4 and 8-arm PEG gels was significantly different at all L-Cys concentrations and the most significant differences were observed during the first 15min of crosslinking. These results indicate that increasing the spatial distribution of arms around the

core of the PEG macromer attenuates the negative effect of modification on the crosslinking kinetics and storage modulus.

We also investigated whether PEG functionality and the degree of modification demonstrate similar trends across various end groups of PEG in crosslinking efficiency and macroscopic properties. The PEG-VS and PEG-A macromers are identical in structure besides their reactive end groups; however, the considerable differences in resulting material properties were observed. The significant differences in the gel formation kinetics and the storage modulus of PEG-VS and PEG-A resulted from the differences in reactivity of the end groups. A sulfone group of PEG-VS has a higher electron withdrawing capability than a carbonyl group of PEG-A, making the vinyl moiety more electron deficient, and more reactive with the electron rich thiol group compared to the acrylate(22). Due to more reactive vinyl sulfone moiety, unmodified PEG-VS demonstrates higher storage modulus after 15 and 60min compared to PEG-A regardless of the number of reactive end groups. Also, the bioactive modification had a less pronounced negative effects on the properties of PEG-VS compared to PEG-A due to the same reason. Importantly, increasing bioactive modification resulted in similar trends of decreased storage modulus, reduced rate of gel formation, and increased swelling in both PEG-A and PEG-VS hydrogels.

According to the MTA chemistry of the hydrogel formation, the number of reactive arms, elastically inactive loop formation, and entropy are related to this phenomenon. First, the formation of elastically inactive loops is more critical in PEG with lower functionality because the effective crosslink functionality must be greater than two in order for networks between any elastically active chains to occur(20). Second, based on previous studies involving Monte Carlo simulation of many-chain star polymers(23, 24), an increase in the number of arms causes an expansion of the arms due to the influence of three-body effects in the central regions of the

"core". As a result, when the number of arms is high, the segment density near the core is much higher than in the periphery, as described by the model of Daoud and Cotton(25). Therefore, this core effect reduces the interpenetration and overlap of other macromer's arms; thus, there is a higher probability for a greater number of the end functional groups to be exposed at a given time for efficient crosslinking to occur(26). Finally, the mobile tip of the chain encounters an entropic potential barrier that penalizes deep fluctuations needed to bring the tip to the tethering point(27). As the number of arms on the macromer increases, there is progressively less space left for the local fluctuation of the chains(25), meaning that 8-arm PEG would encounter a lower entropic potential barrier compared to 4-arm PEG.

Bioactive modification of PEG hydrogels is done by incorporating integrin binding sequences like RGD; however, monofunctional RGD occupies the same reactive sites on the PEG molecules used for the crosslinking reaction, thus affecting its material properties. In this study, we measured the equilibrium swelling ratio (Q_m) of 4 and 8-arm PEG hydrogels because Q_m correlates with crosslinking density and serves as an indication of overall hydrogel network structural defects, such as multiple primary loops and dangling ends(15, 20). Q_m is also relevant in biological applications since high swelling is known to mitigate the effects of incorporated RGD due to dilution(28). Overall, a greater PEG solid concentration resulted in less swelling and better network formation regardless of the number of arms. Even with the presence of added biological cues, 8-arm PEG hydrogels had significantly lower Q_m values and demonstrated a greater range of modification compared to 4-arm PEG at all concentrations. Lower Q_m values of modified 8-arm PEG hydrogels compared to those of 4-arm PEG hydrogels indicated a more densely crosslinked networks, which also correlated with a higher storage modulus. Similarly, the calculations using the Flory-Rehner equation of the concentration of elastically active chains

predicted more elastically active chains in 8-arm PEG at all biologically relevant PEG solid concentrations (4 – 10% w/v) compared to 4-arm PEG (Fig.B1A). Both experimental data and theoretical calculations confirmed how functionality is directly related to effective crosslinking and the concentration of elastically active chains. This implies that additional types and concentrations of biological cues, such as growth factors, can be incorporated into 8-arm PEG hydrogels for further modification(7, 8, 29).

To investigate how the changes in macroscopic properties induced by bioactive modification affect cellular behavior and function, we encapsulated and cultured HS-5 cells in 4 and 8-arm PEG hydrogels. Cell growth and stromal network formation were observed in 8-arm PEG hydrogels modified with 1.25mM RGD. We also found that HS-5 cells cultured in both 4-arm and 8-arm PEG hydrogels modified with 0.25mM RGD formed spherical multicellular aggregates (spheroids). Spheroid formations were previously described in anchorage-dependent cell lines on non-adherent surfaces or in bio-inert polymers(30, 31). Multiple reports have shown that spheroid formation is directly related to cell-cell contacts that regulate cell survival and growth, which was shown to be dependent on integrin-mediated cell contacts and RGD peptides(32, 33). As a result, we concluded that 0.25mM was an insufficient RGD concentration to promote appropriate cell adhesion and growth. More importantly, HS-5 cells cultured in 4-arm PEG hydrogels modified with 1.25mM RGD did not form as dense and interconnected stromal networks as they did in the 8-arm PEG modified with 1.25mM RGD. The 4-arm PEG gel, in this case, had a swelling ratio 1.4 times greater than the 8-arm PEG, demonstrating the negative effect of swelling on cell growth and matrix remodeling. The more swollen matrix of the 4-arm PEG hydrogel was inferior because swelling is known to mitigate the effects of incorporated RGD due to dilution(28) (e.g. 1.25mM RGD gets diluted to 0.34mM after swelling for 4-arm

PEG gels). These results demonstrate that bioactive modification not only affects the PEG hydrogel's macroscopic properties, but also regulates cellular behavior and function.

4.4 CONCLUSIONS

Bioactive modification affected the mechanical properties of multi-arm PEG gels, such as storage modulus and swelling, as a consequence of the macroscopic network changes. These changes were dependent on PEG functionality (4 vs. 8-arm) and PEG solid concentrations, which are directly related to the concentration of elastically active chains and the overall amount of binding sites. Overall, 8-arm PEG allowed a greater degree of modification and its macroscopic properties and crosslinking kinetics were less affected by the act of modification or quenching compared to 4-arm PEG. These advantages provide a finely tuned design for various biological applications with broad range of bioactive modification.

4.5 Materials & Methods

4.5.1 Hydrogel Materials

Hydrogels for mechanical and physical characterization studies were prepared with 4 and 8-arm PEG vinyl sulfone (PEG-VS, 20kDa and 40kDa, >99% purity, Jenkem Technology). The hydrogels were formed via MTA with plasmin sensitive tri-functional crosslinking peptides A-G**C**<u>*YK*↓*NR*</u>G**C**<u>*YK*↓*NR*</u>**C**G (YKNR) (1663.91 g mol^{-1}, >90% purity, GenScript, cleavage site indicated by ↓) for all experiments. The stoichiometric ratio of -VS to thiol (-SH) groups was kept constant at 1:1 ratio for all experiments. PEG hydrogels were modified with the integrin binding peptide G**C**GYG<u>*RGD*</u>SPG (RGD) (1067.10 g mol^{-1}, GenScript) to allow attachment of

the encapsulated cells. For experiments without cells, L-Cysteine hydrochloride monohydrate (L-Cys) (98.5-101.0%, F.W. 175.64 g mol^{-1}, Fisher BioReagents) was substituted on a molar basis as a biologically inactive model compound for RGD(7). All methods and conditions for 4 and 8-arm PEG acrylate (PEG-A, 20kDa and 40kDa, >99% purity, Jenkem Technology) hydrogels were identical.

4.5.2 Rheology – Storage Modulus and the Rate Constant of Gel Formation

The storage modulus (G') and the rate constant of gel formation were studied using AR-G2 rheometer (TA Instruments, New Castle, DE) equipped with 20mm parallel plates and a Peltier stage was utilized for mechanical testing. We compared 4 and 8-arm PEG-VS hydrogels (5% w/v) crosslinked with YKNR peptide and modified with varying concentration of L-Cys, ranging from 0 to 3mM. After 100µl of the PEG solution was mixed with YKNR peptide, the mixture was directly pipetted between the rheometer's plates and each test was conducted at 37^{o}C for a 60min time sweep at 10% strain and 1 rad/sec. The rate constant of gel formation was calculated from G' curves by using the curve fit tool in MATLAB (Natick, MA). A non-linear regression was performed using the equation:

$$Y = Y_0 + (Plateau - Y_0) \times (1 - \exp(-K \times t))$$

The storage modulus at the initial time, t=0, is defined as Y_0. In the above equation, the term *Plateau* is the storage modulus, G', after complete gelation, *K* represents the rate constant for gel formation in unit of reciprocal time, and *t* represents time.

4.5.3 Swelling of the PEG hydrogels

Hydrogels (4 and 8-arm PEG) at various final concentrations (4 – 10% w/v) were crosslinked with YKNR and modified with L-Cys at concentrations ranging from 0 to 3.75mM. Hydrogels were prepared by dissolving each precursor in 0.05M HEPES buffer at pH 7.4. For example, to

make 100µl of PEG-8A 5% gel with 1.25mM L-Cys, 5mg of PEG-8VS/PEG-8A was dissolved in 45µl of HEPES buffer and mixed with 0.022mg of L-Cys in 10µl of HEPES buffer. Larger volumes of stock solutions were prepared to minimize weighing error. L-Cys was allowed to bind to the PEG macromer's reactive sites at 37^{o}C for 15min. Next, 0.49mg of YKNR was dissolved in 40µl HEPES buffer at a 1:1 molar ratio of the functional groups in PEG. Afterwards, the YKNR solution was pipetted into the modified PEG solution and mixed, vortexed, and pipetted into 20µl gels. After 1min, the reaction was quenched and PEG gels were submerged in 15ml of MilliQ water for 24h. After 24h, excess water was removed and the gels were weighed. The mass swelling ratio (Q_m) was calculated by dividing the mass of the swollen hydrogels (m_s) by the mass of the dry gel components (m_d)(34, 35).

$$Q_m = \frac{m_s}{m_d}$$

4.5.4 Elastically Active Chain Concentration

Elastically active chain concentration in the PEG network was calculated by using the modified Flory-Rehner equation that shows a direct relation between the PEG precursor weight percent and associated Q_m(15).

$$v_e = -\frac{V_d}{v_1}\frac{[\ln(1-v_{2,s}) + v_{2,s} + X_1 v_{2,s}^2]}{v_{2,c}\left[\left(\frac{v_{2,s}}{v_{2,c}}\right)^{\frac{1}{3}} - \frac{1}{2}\left(\frac{v_{2,s}}{v_{2,c}}\right)\right]}$$

In the Flory-Rehner equation, X_1, polymer-solvent interaction parameter, is equal to 0.43 for PEG in water, V_d is the polymer volume in the dry state, and v_1 is the molar volume of water in cm^3/mol. $v_{2,s}$ is the equilibrium polymer volume fraction after swelling has occurred ($1/Q_m$)(36), and $v_{2,c}$ is the polymer volume fraction at crosslinking.

4.5.5 HS-5 Green Fluorescent Protein (GFP) Transfection and Culture

Human bone marrow stromal cell line, HS-5 cells (ATCC) were cultured in DMEM (Dulbecco's modified Eagle's medium, ATCC) supplemented with 10% fetal bovine serum (FBS) (Biowest) and 1% PenStrep (Lonza). The cells were cultured in T-75 flasks in 5% CO_2 atmosphere at 37^{o}C and split in a 1:5 ratio every 3-4 days. For confocal fluorescent imaging HS-5 cells were transfected with Green Fluorescent Protein (GFP)(37). Briefly, 24 hours prior to transfection, HS-5 cells were seeded and cultured in 6 well plates. Once cell confluency reached 60% a transfection reagent Fugene 6 (Promega), was first mixed with serum-free Opti-Mem media (Invitrogen) and sequentially with DNA (pLenti-GIII-GFP) (Applied Biological Materials) according to the manufacturer's instructions. This mixture was carefully added dropwise and then incubated at 37°C for 24 – 48 hours. After verifying HS-5 was successfully transfected with GFP, transfected cells were selected and cultured in media supplemented with puromyocin (1μg/ml) (Sigma-Aldrich).

4.5.6 HS-5 Cell Encapsulation and 3D Culture in PEG Hydrogels

Prior to *in situ* crosslinking and encapsulation, HS-5 cells were suspended at a concentration of 2 x 10^{6}cells/mL and centrifuged for 5min at 300G to remove excess media. In order to investigate the effects of RGD concentration on 3D cell behavior without inducing changes in hydrogel mechanical properties, the total concentration of monofunctional cysteine groups composed of L-Cys and RGD peptide was kept constant at 1.25mM. We prepared 5% PEG-4VS or PEG-8VS by dissolving PEG in the appropriate amount of 0.05M HEPES Buffer at pH 7.4, followed by modification with 1.25mM RGD or 0.25mM RGD plus 1mM L-Cys. The monofunctional agents were allowed to bind to the PEG macromers at 37^{o}C for 15min. Then, the cell pellet was reconstituted with modified 4-arm or 8-arm PEG and formed gels by the addition

of trifunctional plasmin sensitive crosslinking peptide, YKNR. The stoichiometric ratio VS:SH was kept 1:1 for all experiments. Each 50µl gel was crosslinked between two glass slides at 37^{o}C for 15min and flipped at 7min to prevent cell sedimentation and clustering. After 15min, gels were placed in a 48 well plate and covered with 400µl of DMEM. Media was changed every 2 days and cells were cultured up to 12 days. All images were taken using Leica DMI3000B and a confocal microscope Nikon A1 was used for imaging GFP transfected HS-5 cells.

4.5.7 DAPI Staining and Cell Viability Assay

Cells were stained with DAPI (Invitrogen) and LIVE/DEAD kit (488/570) (Invitrogen) at Day 12 to evaluate cell viability as described by the manufacturer's protocol. DAPI stain was added directly to cells in full media and incubated for 15 min. Spheroid formation was identified by multiple nuclei staining. All images were taken using Leica DMI3000B.

4.5.8 Statistical Analysis

All statistical analyses were performed using GraphPad Prism (GraphPad Prism Software, La Jolla, CA). Data are reported as mean ± standard deviation of measurements, and statistical analyses were performed with Two-way ANOVA followed by Bonferroni post-test.

4.6 References

1. Peppas NA, Langer R. New challenges in biomaterials. *Science.* 1994 Mar 25; 263(5154): 1715-1720.

2. Hubbell JA. Biomaterials in tissue engineering. *Biotechnology (N Y).* 1995 Jun; 13(6): 565-576.

3. Wolf K, Alexander S, Schacht V, Coussens LM, von Andrian UH, van Rheenen J, Deryugina E, Friedl P. Collagen-based cell migration models in vitro and in vivo. *Semin Cell Dev Biol.* 2009 Oct; 20(8): 931-941. PMCID: PMC4021709.

4. Mosesson MW. Fibrinogen and fibrin structure and functions. *J Thromb Haemost.* 2005 Aug; 3(8): 1894-1904.

5. Hern DL, Hubbell JA. Incorporation of adhesion peptides into nonadhesive hydrogels useful for tissue resurfacing. *J Biomed Mater Res.* 1998 Feb; 39(2): 266-276.

6. Lutolf MP, Lauer-Fields JL, Schmoekel HG, Metters AT, Weber FE, Fields GB, Hubbell JA. Synthetic matrix metalloproteinase-sensitive hydrogels for the conduction of tissue regeneration: Engineering cell-invasion characteristics. *Proc Natl Acad Sci U S A.* 2003 Apr 29; 100(9): 5413-5418. PMCID: PMC154359.

7. Pratt AB, Weber FE, Schmoekel HG, Muller R, Hubbell JA. Synthetic extracellular matrices for in situ tissue engineering. *Biotechnol Bioeng.* 2004 Apr 5; 86(1): 27-36.

8. Lutolf MP, Hubbell JA. Synthetic biomaterials as instructive extracellular microenvironments for morphogenesis in tissue engineering. *Nat Biotechnol.* 2005 Jan; 23(1): 47-55.

9. van de Wetering P, Metters AT, Schoenmakers RG, Hubbell JA. Poly(ethylene glycol) hydrogels formed by conjugate addition with controllable swelling, degradation, and release of pharmaceutically active proteins. *J Control Release.* 2005 Feb 16; 102(3): 619-627.

10. Weiss MS, Bernabe BP, Shikanov A, Bluver DA, Mui MD, Shin S, Broadbelt LJ, Shea LD. The impact of adhesion peptides within hydrogels on the phenotype and signaling of normal and cancerous mammary epithelial cells. *Biomaterials.* 2012 May; 33(13): 3548-3559. PMCID: PMC3288720.

11. Engler AJ, Sen S, Sweeney HL, Discher DE. Matrix elasticity directs stem cell lineage specification. *Cell.* 2006 Aug 25; 126(4): 677-689.

12. Huebsch N, Arany PR, Mao AS, Shvartsman D, Ali OA, Bencherif SA, Rivera-Feliciano J, Mooney DJ. Harnessing traction-mediated manipulation of the cell/matrix interface to control stem-cell fate. *Nat Mater.* 2010 Jun; 9(6): 518-526. PMCID: PMC2919753.

13. Burdick JA, Murphy WL. Moving from static to dynamic complexity in hydrogel design. *Nat Commun.* 2012; 3: 1269.

14. Morpurgo M, Veronese FM, Kachensky D, Harris JM. Preparation of characterization of poly(ethylene glycol) vinyl sulfone. *Bioconjug Chem.* 1996 May-Jun; 7(3): 363-368.

15. Lutolf MP, Hubbell JA. Synthesis and physicochemical characterization of end-linked poly(ethylene glycol)-co-peptide hydrogels formed by michael-type addition. *Biomacromolecules.* 2003 May-Jun; 4(3): 713-722.

16. Hersel U, Dahmen C, Kessler H. RGD modified polymers: Biomaterials for stimulated cell adhesion and beyond. *Biomaterials.* 2003 Nov; 24(24): 4385-4415.

17. Fittkau MH, Zilla P, Bezuidenhout D, Lutolf MP, Human P, Hubbell JA, Davies N. The selective modulation of endothelial cell mobility on RGD peptide containing surfaces by YIGSR peptides. *Biomaterials.* 2005 Jan; 26(2): 167-174.

18. Shikanov A, Smith RM, Xu M, Woodruff TK, Shea LD. Hydrogel network design using multifunctional macromers to coordinate tissue maturation in ovarian follicle culture. *Biomaterials.* 2011 Apr; 32(10): 2524-2531. PMCID: PMC3040241.

19. Singh SP, Schwartz MP, Lee JY, Fairbanks BD, Anseth KS. A peptide functionalized poly(ethylene glycol) (PEG) hydrogel for investigating the influence of biochemical and biophysical matrix properties on tumor cell migration. *Biomater Sci.* 2014 Jul 1; 2(7): 1024-1034. PMCID: PMC4120072.

20. Metters A, Hubbell J. Network formation and degradation behavior of hydrogels formed by michael-type addition reactions. *Biomacromolecules.* 2005 Jan-Feb; 6(1): 290-301.

21. Phelps EA, Enemchukwu NO, Fiore VF, Sy JC, Murthy N, Sulchek TA, Barker TH, Garcia AJ. Maleimide cross-linked bioactive PEG hydrogel exhibits improved reaction kinetics and cross-linking for cell encapsulation and in situ delivery. *Adv Mater.* 2012 Jan 3; 24(1): 64-70, 2. PMCID: PMC3517145.

22. Chatani S, Nair DP, Bowman CN. Relative reactivity and selectivity of vinyl sulfones and acrylates towards the thiol-michael addition reaction and polymerization. *Polymer Chemistry.* 2013; 4(4): 1048-1055.

23. Molina LA, Freire JJ. Monte carlo simulation of many-chain star polymer solutions. *Macromolecules.* 1999; 32: 499-505.

24. Cecca AD, Freire JJ. Monte carlo simulation of star polymer systems with the bond fluctuation model. *Macromolecules.* 2002; 35: 2851-2858.

25. Daoud M, Cotton JP. Star shaped polymers : A model for the conformation and its concentration dependence. *J Physics.* 1982; 43: 531-538.

26. Pakula T, Vlassopoulos D, Fytas G, Roovers J. Structure and dynamics of melts of multiarm polymer stars. *Macromolecules.* 1998; 31: 8931-8940.

27. Shanbhag S, Larson RG. Chain retraction potential in a fixed entanglement network. *Phys Rev Lett.* 2005 Feb 25; 94(7): 076001.

28. Jongpaiboonkit L, King WJ, Murphy WL. Screening for 3D environments that support human mesenchymal stem cell viability using hydrogel arrays. *Tissue Eng Part A.* 2009 Feb; 15(2): 343-353. PMCID: PMC2788994.

29. Seliktar D, Zisch AH, Lutolf MP, Wrana JL, Hubbell JA. MMP-2 sensitive, VEGF-bearing bioactive hydrogels for promotion of vascular healing. *J Biomed Mater Res A.* 2004 Mar 15; 68(4): 704-716.

30. Koide N, Sakaguchi K, Koide Y, Asano K, Kawaguchi M, Matsushima H, Takenami T, Shinji T, Mori M, Tsuji T. Formation of multicellular spheroids composed of adult rat

hepatocytes in dishes with positively charged surfaces and under other nonadherent environments. *Exp Cell Res.* 1990 Feb; 186(2): 227-235.

31. Ijima H, Nakazawa K, Mizumoto H, Matsushita T, Funatsu K. Formation of a spherical multicellular aggregate (spheroid) of animal cells in the pores of polyurethane foam as a cell culture substratum and its application to a hybrid artificial liver. *J Biomater Sci Polym Ed.* 1998; 9(7): 765-778.

32. Korff T, Augustin HG. Integration of endothelial cells in multicellular spheroids prevents apoptosis and induces differentiation. *J Cell Biol.* 1998 Nov 30; 143(5): 1341-1352. PMCID: PMC2133072.

33. Bates RC, Edwards NS, Yates JD. Spheroids and cell survival. *Crit Rev Oncol Hematol.* 2000 Nov-Dec; 36(2-3): 61-74.

34. Sokic S, Papavasiliou G. Controlled proteolytic cleavage site presentation in biomimetic PEGDA hydrogels enhances neovascularization in vitro. *Tissue Eng Part A.* 2012 Dec; 18(23-24): 2477-2486. PMCID: PMC3501121.

35. Rizzi SC, Hubbell JA. Recombinant protein-co-PEG networks as cell-adhesive and proteolytically degradable hydrogel matrixes. part I: Development and physicochemical characteristics. *Biomacromolecules.* 2005 May-Jun; 6(3): 1226-1238.

36. Metters AT, Anseth KS, Bowman CN. Fundamental studies of a novel, biodegradable PEG-b-PLA hydrogel. *Polymer.* 2000(41): 3993-4004.

37. Kim J, Wu B, Niedzielski SM, Hill MT, Coleman RM, Ono A, Shikanov A. Characterizing natural hydrogel for reconstruction of three-dimensional lymphoid stromal network to model T-cell interactions. *J Biomed Mater Res A.* 2015 Feb 3.

CHAPTER V

Synthetic hydrogel supports the function and regeneration of artificial ovarian tissue in mice

5.1 Introduction

The number of cancer survivors has been growing due to advancements in anticancer treatments, and the long-term survival rates improved above 80% in most childhood malignancies(1, 2). Yet, cytotoxic chemotherapy, radiotherapy and bone marrow transplantation treatments often cause infertility and premature ovarian failure(3, 4). Clinically approved fertility preservation options exist only for adult patients who can produce a fully mature egg(5). If the anticancer treatment can be delayed, these patients can undergo hormonal stimulation to stimulate follicle development and recover mature oocytes(6). The retrieved oocytes can then be cryopreserved and used later for *in vitro* fertilization (IVF) treatments. Unfortunately, the option of egg preservation is not applicable to patients who require immediate treatment or prepubescent girls, whose dormant ovaries cannot produce mature eggs(6). Furthermore, the cytotoxic chemotherapy affects the ability of the prepubescent girls to undergo complete and physiological puberty(7). This eventually leads to a variety of long-term clinical complications, such as delayed growth of bones, impaired cognitive development, cardiovascular and metabolic complications(8).

Autotransplantation of cryopreserved ovarian tissue has shown promising results for fertility and ovarian function restoration and has resulted in 60 reported live human births since 2004(9). Unlike *in vitro* maturation and fertilization of mature eggs, transplantation of ovarian tissue does not require repeated cycles of hormone stimulation, thus reducing risk of ovarian hyperstimulation syndrome and delay in chemotherapy treatments(10). Despite promising results, there is a significant loss of the follicular pool due to tissue ischemia and it requires multiple invasive procedures to extend ovarian function because of the short life span of autografts(11-13). Yet, the most prohibitive limitation of the ovarian tissue autotransplantation is a potential risk for re-introducing malignant cells, especially in patients with leukemia and other blood-borne cancers(14). Therefore, grafting of multiple isolated follicles presents a safer alternative because individual follicles are separated from the stromal environment before being encapsulated in a three-dimensional supportive matrix.

Ovarian tissue contains follicles at different developmental stages surrounded by stroma cells and rich vasculature. Follicles, the functional units of the ovary, are composed of a germ cell (the oocyte) and layers of somatic cells (granulosa and theca cells), which are responsible for the production and metabolism of gonadal hormones, estradiol and progesterone. At birth, the human ovary contains approximately one million of immature follicles, called primordial follicles, which have the potential to develop and produce mature oocytes capable of fertilization. This number decreases to 300,000 follicles at puberty and continues to decline until menopause(15). Because of the non-regenerative nature of follicles, a sufficient number of follicles must be present in the ovary in order to sustain ovarian endocrine function.

Primordial follicles, the most immature and most abundant class of follicles, constitute the ovarian reserve, and activation of a small portion of this reserve each cycle ensures ovarian

function(15). Activated primordial follicles enter the growing pool of preantral follicles and secrete sex hormones. A burst activation of premature follicles can shorten the longevity of the graft. A successful transplantation would require significant primordial follicle population, which can contribute to monthly cycles and provide healthy, fertilizable eggs(6, 16-18). Several reports have investigated an approach of grafting enzymatically-isolated immature follicles encapsulated in naturally derived hydrogels, such as alginate(19), fibrin(20-22), fibrin and vascular endothelial growth factor (VEGF)(21, 23), for delivery of isolated follicles and demonstrated complete folliculogenesis *in vivo* showing the potential of this approach. Here, for the first time, we report the application of synthetic hydrogels with defined degradation kinetics and tunable physical properties(24) to support long-term engraftment and function of the artificial ovarian tissue.

To address the limitations of fertility preservation options available only to a small subset of patients, we investigated whether an engineered ovarian tissue supports the ovarian endocrine function in sterile mice. We constructed an artificial ovary from pre-antral follicles encapsulated in a tunable synthetic hydrogel, poly(ethylene glycol) vinyl-sulfone (PEG-VS), as a supportive matrix. The tunable biophysical and biochemical properties(24, 25) of PEG hydrogels successfully mimic the native complexity of the extracellular matrix. End-functionalized multi-arm PEG-VS allows modification with integrin-binding peptides (such as RGD) to allow cell-matrix interactions(26, 27) and crosslinking with protease-sensitive peptides to allow cell-driven degradation and remodeling of the matrix. PEG-based matrices support folliculogenesis *in vitro*(28), vascularization of tissue constructs *in vivo*(29) and promote matrix remodeling in bone defects(30, 31). We hypothesized that PEG-VS hydrogels modified with RGD and crosslinked with MMP-sensitive peptide can serve as a supportive matrix for an engineered artificial ovarian tissue. Matrix with MMP sensitive peptide would allow cell and follicle driven remodeling as the

abundance of collagen in the natural ovarian tissues undergoes remodeling during follicular development and ovulation(32). We evaluated the development of immature follicles encapsulated in PEG hydrogels and assessed the graft function after orthotopic transplantation into ovariectomized mice. Our results demonstrated for the first time that synthetic PEG hydrogels with proteolytically-controlled degradation successfully supported follicle growth and promoted graft remodeling *in vivo*.

5.2. Results

5.2.1. Development of encapsulated immature follicles

Histological analysis of PEG hydrogels explanted 14, 30, and 60 days after transplantation was performed to evaluate the development of the implanted follicles. The initial population of the follicles (day 0) was mostly primordial follicles (67.6%) with 30.8% primary and a small percentage (1.6%) of secondary follicles (Fig.5.2E). Antral follicles appeared 14 days after transplantation (Tx), which is consistent with the fact that the transition from primordial to antral takes 14 to 18 days during normal folliculogenesis in mice(33)(Fig.5.2F). Multiple fully mature pre-ovulatory follicles were observed in the grafts retrieved after 30 (Fig.5.2G) and 60 days (Fig.5.2H) post-Tx, which indicated the progression and the extent of the follicle development during this period. From day 14 to day 60, the proportion of secondary and antral follicles increased by 7.7 times and 36 times, respectively (Fig.5.3B), and tissue regeneration progressed as encapsulated follicles were going through follicle development (Fig.5.2B – D).

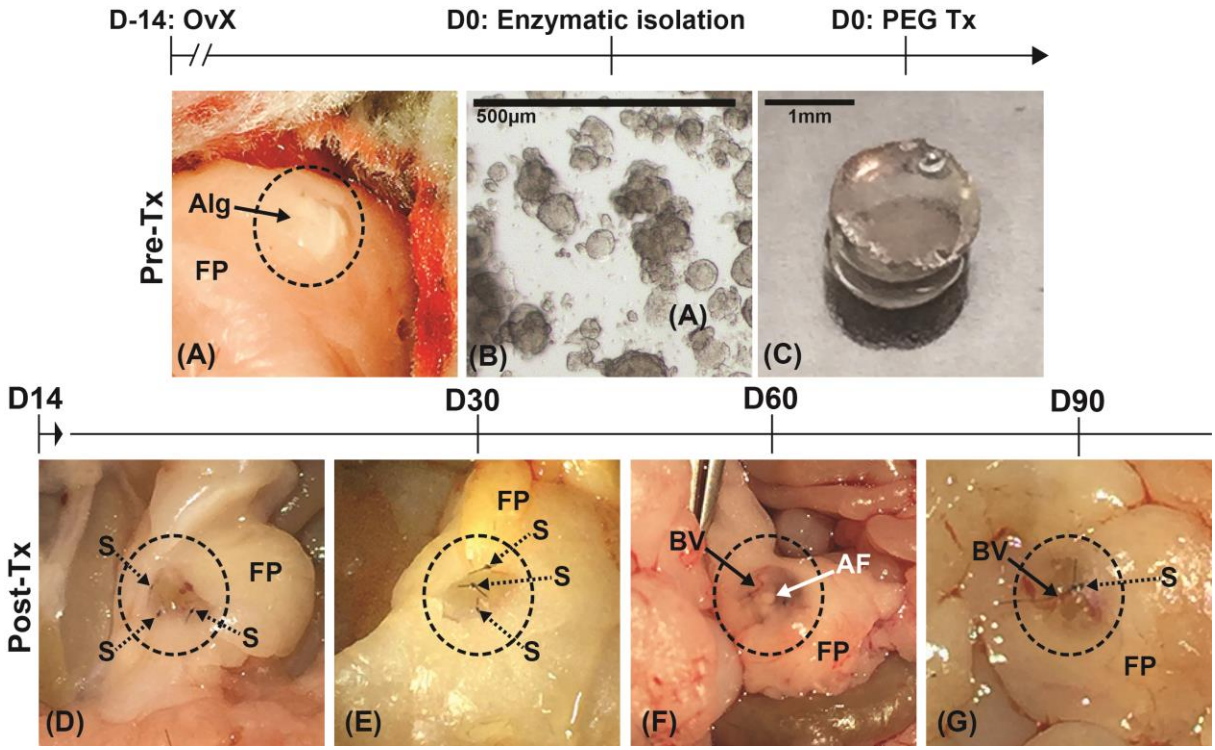

Figure 5.1 – The timeline for inducing premature ovarian failure and grafting artificial ovarian tissue: **(A)** A bilateral ovariectomy (OvX) was performed to induce premature ovarian failure in mice. In order to maintain the space within the bursa after OvX, inert alginate beads (black arrow) were inserted to prevent the collapse and adhesion. **(B)** Follicles were enzymatically isolated from three 6 or 7 days old female mice. **(C)** Follicles were encapsulated in 7% PEG-8VS (0.5mM RGD) crosslinked with LGPA hydrogels. One PEG grafts with enzymatically isolated follicles was transplanted (Tx) into each ovarian bursa, two implants per mouse. PEG grafts were retrieved **(D)** 14 (n_{mice}=11), **(E)** 30 (n_{mice}=6), **(F)** 60 (n_{mice}=6), and **(G)** 90 (n_{mice}= 5) days after Tx. [FP: Fat pad, S: Sutures (Dotted arrows), BV: Blood vessels, AF: Antral follicle]

5.2.2. Immature follicular pool sustained

We quantified the number and the distribution of follicles per gel before and after transplantation to evaluate the follicular reserve (Fig.5.3A, 5.3B). There was a decreasing trend of the primordial follicle number and an increasing trend of the antral follicle number over 60 days in grafts (Fig.5.3A). This was a result of primordial follicles entering the growing pool every estrous cycle and reaching fully mature pre-ovulatory follicles. The variability in the initial number of follicles encapsulated in the graft was due to the loss of follicles during the sedimentation and encapsulation processes. The expected decreasing trend of the early stage follicle numbers in grafts (Fig.5.3A) indicates a functioning graft that activates a small cohort of

follicles each estrous cycle. Multiple growing follicles at the primary and early secondary stages were observed 14 days after transplantation. As primordial follicles were recruited into the growing pool, a 51.4% decrease of primordial follicles occurred over 60 days *in vivo*. However, 60% of the immature follicular pool, including both primordial and primary follicles, was still present in the grafts at day 60 (Fig.5.3B). Based on histological analysis, both primordial and primary follicles were observed adjacent to secondary follicles (Fig.3C), showing selective activation and recruitment of primordial follicles into the growing pool.

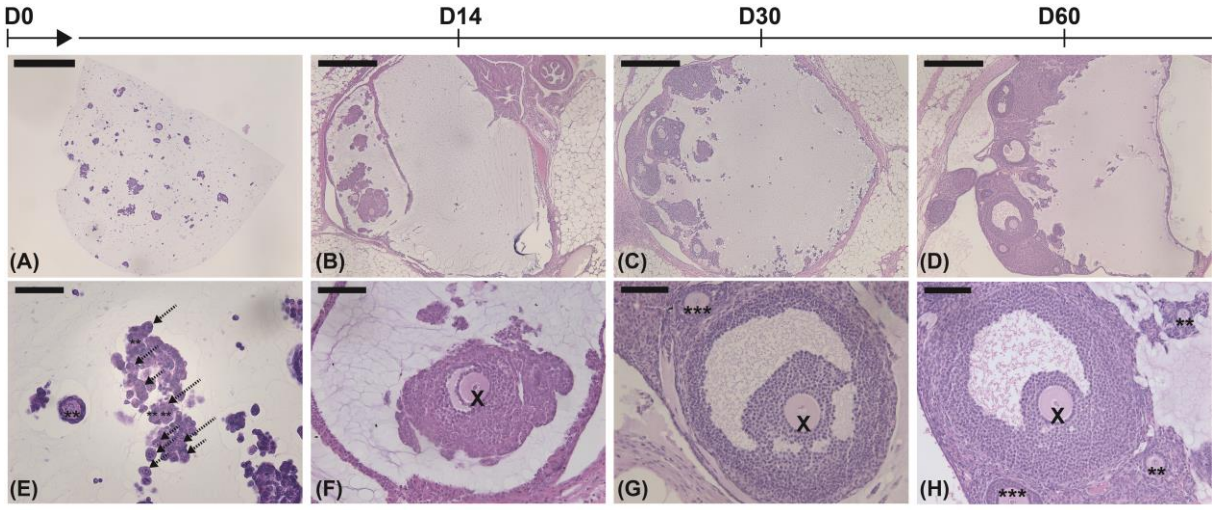

Figure 5.2 – Folliculogenesis in PEG grafts: **(A – D)** Over 60 days, massive volumetric expansion was observed during the complete folliculogenesis, beginning with the **(E)** mixed population of primordial and primary follicles to **(F - H)** antral follicles, and more tissue regeneration occurred. Antrum formation was observed by day 14. By day 30 and 60, multiple antral follicles were observed. [Primordial (dotted arrow), Primary follicle (**), Secondary follicle (***), Antral follicle (X)] Scale: 500µm (A – D), 50µm (E), 100µm (F – H).

5.2.3. Restoration of Hypothalamus-Pituitary-Gonadal (HPG) axis

Ovariectomy (OvX), and the subsequent absence of circulating gonadal hormones produced in the ovaries, disrupts the negative feedback loop of the hypothalamus-pituitary-gonad (HPG) axis. The most immediate and pronounced clinical outcome after removal of the ovaries is disruption and absence of regular estrous cycles as well as elevated FSH levels. To investigate

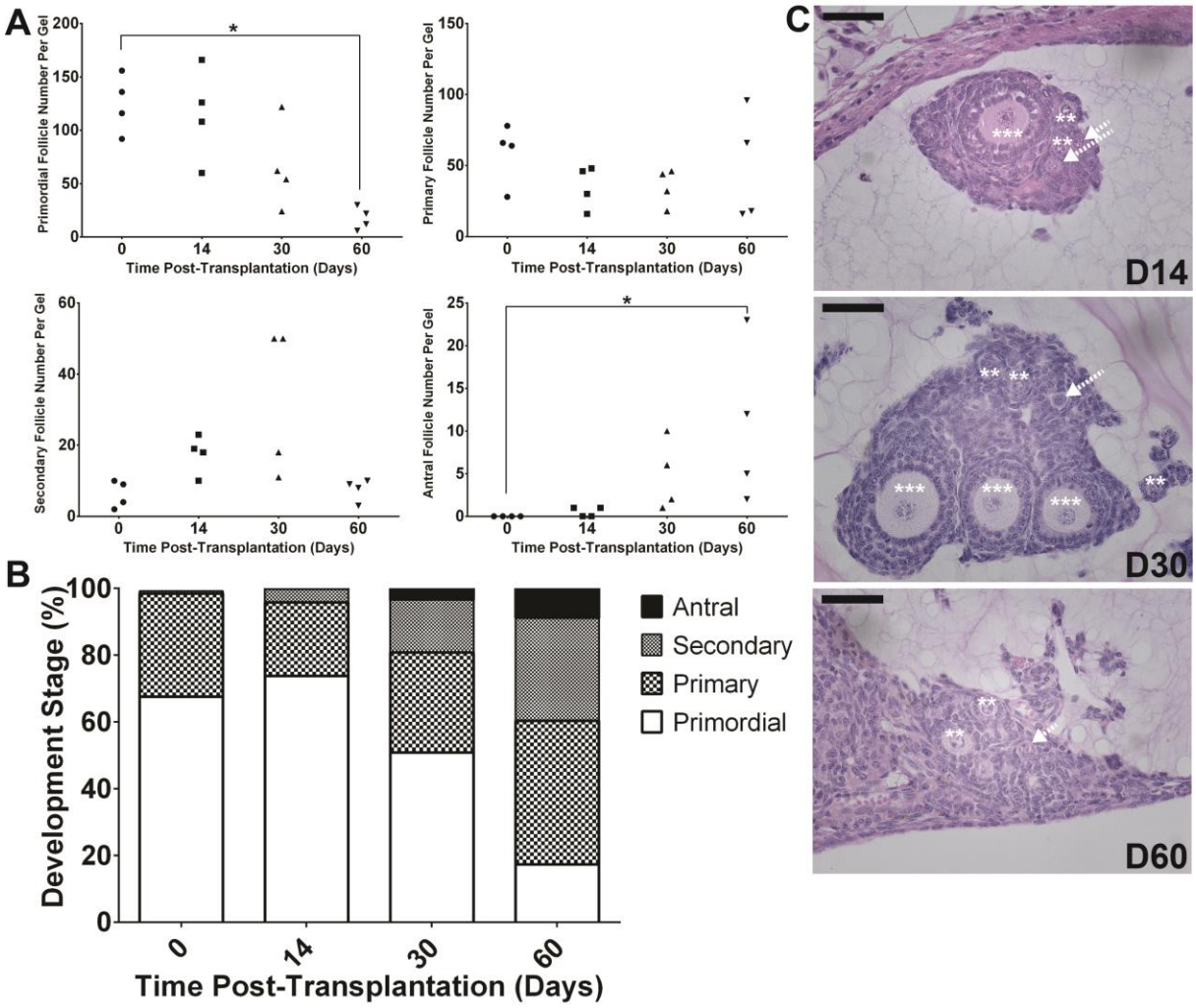

Figure 5.3 - Follicle development and progression through the developmental stages: **(A)** The number of follicles in each graft at different stages after transplantation. There was a decreasing trend of the primordial follicle number in grafts over 60 days as a result of entering the growing pool every estrous cycle, ovulate and become corpus lutea. The distribution in the follicle numbers before transplantation resulted due to the loss of follicles during encapsulation process. (n_{gel} = 4 from 4 mice, for each time point) Statistical significance was determined by the Kruskal-Wallis test followed by Dunn's post-test ($p < 0.05$). **(B)** Graft composition and percentage of the follicles at each developmental stage. After 14 days *in vivo* the majority of the implanted follicles were at primordial stage, similar to the graft composition at the implantation. After 30 days, 15% of the implanted follicles reached a pre-antral stage and 5% were antral. The percentage of primordial follicles decreased and the percentage of growing follicles increased over 60 days *in vivo*. 60% of immature follicular pool, including both primordial and primary follicles, was still presented in the grafts. **(C)** Primordial and primary follicles present at day 14, 30 and 60 after implantation. [Primordial follicles (dashed arrow), Primary follicle (**), Secondary follicle (***)] Scale: 50µm

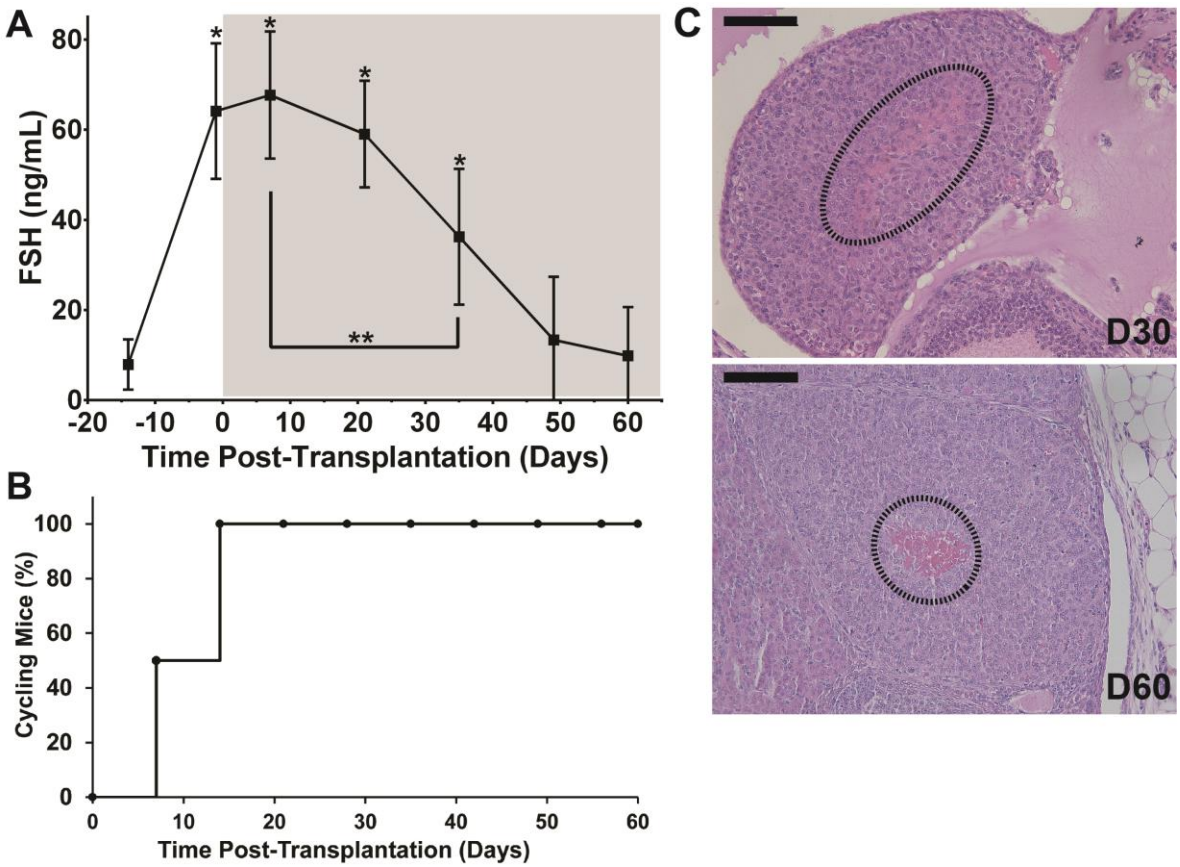

Figure 5.4 – Graft function: **(A)** FSH level significantly increased post-OvX, confirming the complete OvX. For the group transplanted with PEG graft, FSH level decreased beginning at 35 days post-Tx (**), and FSH level declined to Pre-OvX levels by 49 days post-Tx, confirming the restoration of HPG axis. High FSH level persisted throughout for the control group that did not receive PEG graft with follicles. All data is reported as mean ± S.D. [With PEG graft: D-14 ~ D28 (n_{mice} = 11), D35 ~ D60 (n_{mice} = 6)]. An asterisks (*) denoted significance within the group transplanted with PEG graft compared to pre-OvX (D-14). Statistical significance was determined by a one-way ANOVA followed by Tukey's test ($p < 0.01$). **(B)** Vaginal cytology demonstrated resumed cyclicity in 50% of mice after 7 days post-Tx and 100% by 14 days. Cyclicity was maintained up to 60 days, supporting 12 – 15 estrous cycles in mice. (n_{mice} = 4) **(C)** Corpora lutea (CL) were observed at 30 and 60 days post-Tx, in agreement with the FSH levels. CL formation suggests ovulatory events and they showed the typical characteristic of centrally located blood clot (dashed outline).

how the graft contributes to the restoration of HPG axis, follicle-stimulating hormone (FSH) levels were measured before and after transplantation (Fig.5.4A). As expected, serum FSH levels significantly increased post-OvX (from 8 ng/mL to 64 ng/mL) and the levels remained constantly elevated up to 14 days post-Tx.

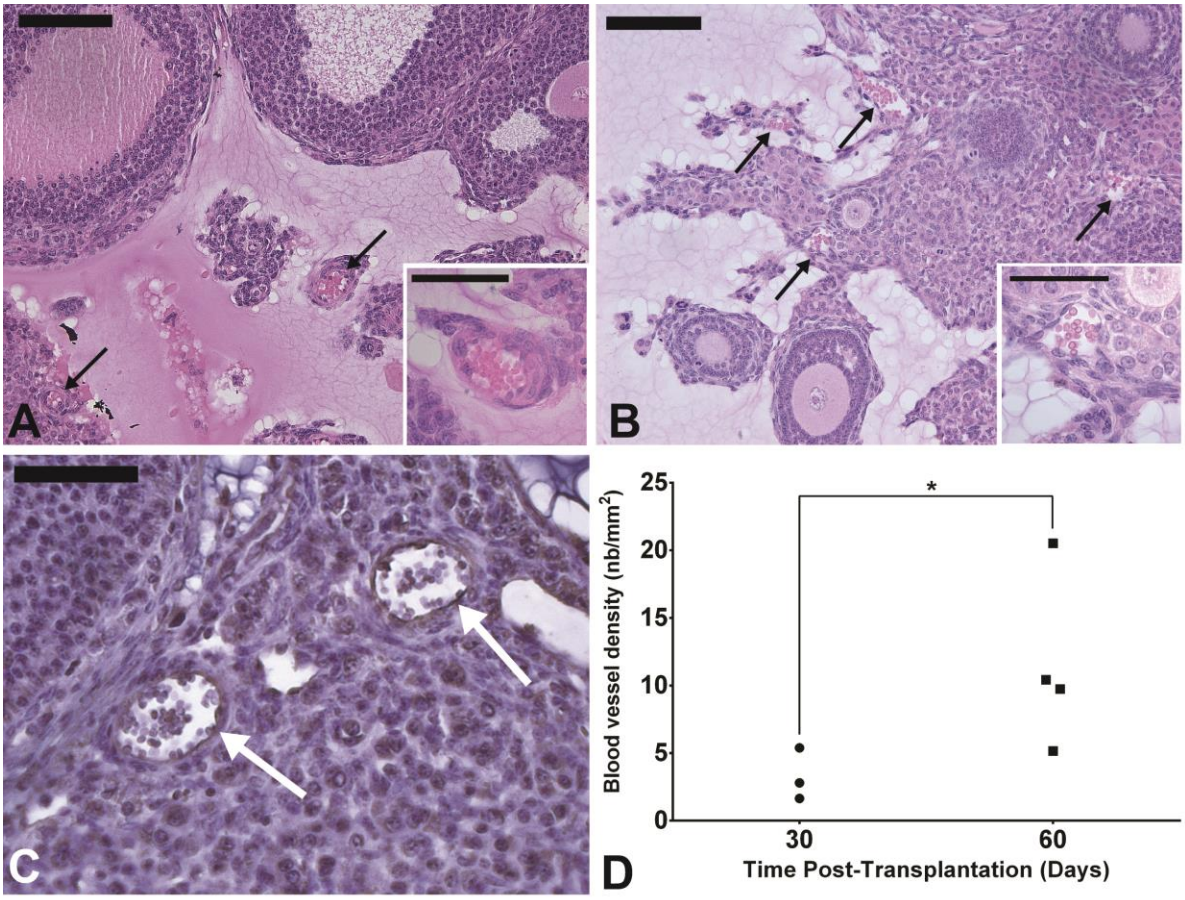

Figure 5.5 – Graft remodeling and revascularization: Functioning blood vessels (arrows) were found after **(A)** 30 days and **(B)** 60 days *in vivo*, as indicated by the presence of red blood cells (box). Scale bar: 100µm, box: 50µm **(C)** CD34 staining (arrows) confirmed the infiltration of blood capillaries into the graft. **(D)** Blood vessel density (number of blood vessel (nb)/mm^2) significantly increased from 30 days to 60 days post-Tx, confirming more progressed remodeling process. Neovascularization was observed in 3 out of 5 mice for 30 days post-Tx and 4 of 5 mice for 60 days. Statistical significance was determined by the Mann-Whitney test ($p = 0.1$).

The elevated FSH levels, ranged from 64 to 76 ng/mL, persisted without the implantation of PEG grafts throughout the study in the control group. However, FSH levels consistently decreased in mice that received the PEG grafts, as the transplanted follicles initiated folliculogenesis and steroidogenesis. The FSH levels declined to 36ng/mL by day 35 post-Tx, and 13ng/mL by day 49. The physiological levels of FSH were maintained up to day 60 (10ng/mL), confirming the restoration of the HPG axis. The resumption of the estrous cycle 14 days post-Tx in all the transplanted mice further confirmed the presence of functioning artificial

ovarian tissue (Fig.5.4B). Presence of CL in the histological sections collected after 30 and 60 days served as an important evidence of successful ovulation, which was consistent with regular estrous cyclicity (Fig.5.4C).

5.2.4. Graft remodeling and neovascularization

The degree of remodeling and neovascularization of the implanted PEG hydrogel directly impacts the graft longevity. Functioning blood vessels were found after 30 (Fig.5A) and 60 (Fig.5.5B) days post-Tx, which was indicated by the presence of red blood cells in the lumen of the vessels. The presence of the blood capillaries was confirmed by positive CD34 immunostaining (Fig.5.5C), indicating PEG hydrogel's capability of stromal cells and follicle driven remodeling. The density of blood vessels increased from 30 days post-Tx to 60 days post-Tx (Fig.5.5D), further indicating to continuous remodeling and folliculogenesis.

5.2.5. Graft longevity

The ovarian reserve of follicles declines because of the non-renewable nature of the follicles. At the onset of menopause, ovarian reserve reaches about 5-10% of the initial number of follicular reserve, the levels of estradiol decrease and levels of FSH increase. Thus, we hypothesized that a positive correlation between the number of implanted follicles and the longevity of implanted graft exists. We investigated the longevity of PEG grafts with an average of 376 encapsulated follicles up to 90 days post-Tx. Physiological FSH levels (Fig.5.6A) and regular estrous cycles (Fig.5.6C) were maintained up to 70 days. Increasing FSH levels and more spread-out estrous cycles were observed beginning at 77 days, similar to premenopause. Multiple antral follicles and corpora lutea were presented in histological sections retrieved 90 days post transplantation (Fig.5.6D); however, all primordial follicles were exhausted by 90 days (Fig.5.6B), concluding the graft longevity.

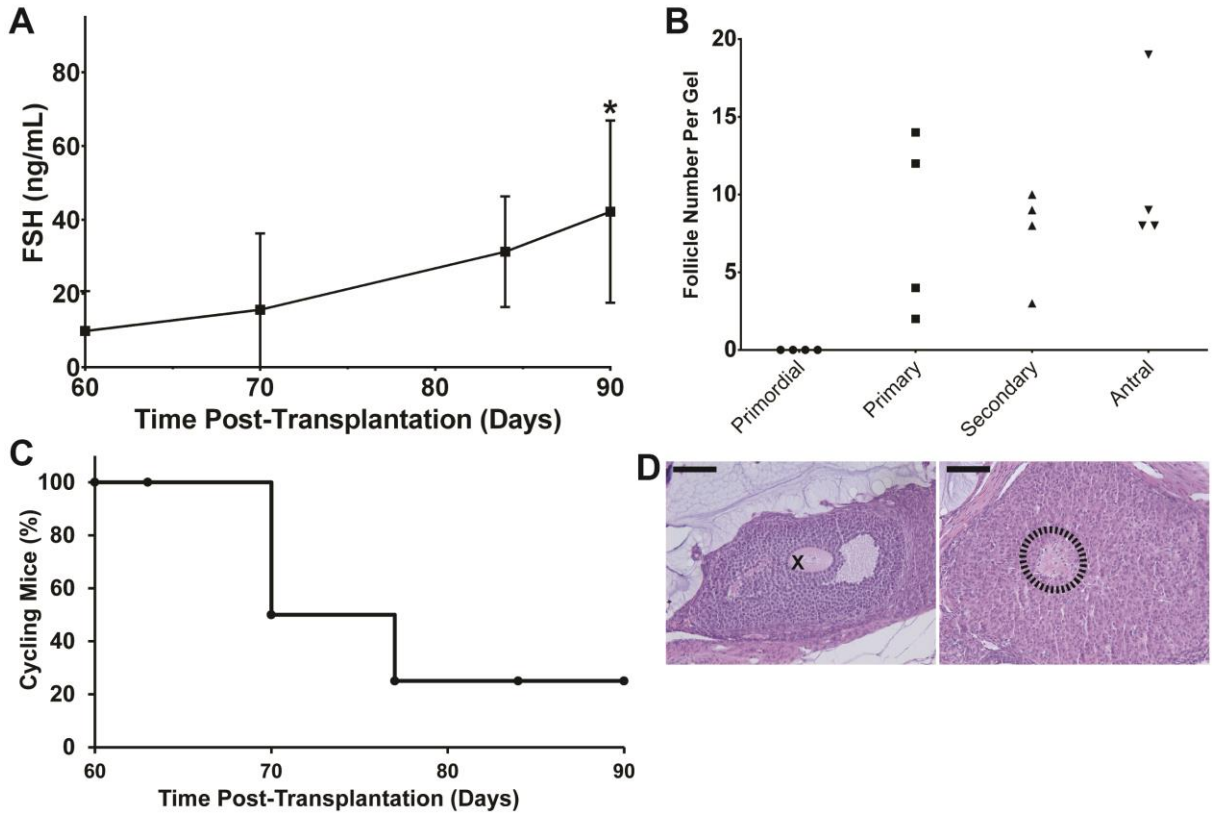

Figure 5.6 – Graft longevity: **(A)** FSH level that declined to physiological level increased beginning at 70 days post-Tx due to follicle exhaustion within the graft. All data is reported as mean ± S.D. (n_{mice} = 6). An asterisks (*) denoted significance within the group transplanted with PEG graft compared to D60. Statistical significance was determined by a one-way ANOVA followed by Tukey's test ($p < 0.01$). **(B)** The total number of follicles declined over 90 days as a result of follicles entering growing pool, ovulate or undergoing atresia after activation. **(C)** Cyclicity was maintained up to 70 days, supporting 12 – 15 estrous cycles in all mice. However, reduced and irregular cycles were observed starting at 77 days post-Tx, which in agreement with the FSH levels. (n_{mice} = 4) **(D)** Antral follicles and corpora lutea (CL) were still observed at 90 days post-Tx.

5.3. Discussion

In this study, we engineered a synthetic PEG hydrogel that supports implantation of isolated ovarian follicles and promotes ovarian function *in vivo*. Ovarian tissue from a blood borne cancer patient potentially could contain cancer cells and autotransplantation may lead to cancer recurrence. Our approach mitigates this problem because follicles are purified from the rest of the ovarian tissue by enzymatic tissue digestion. Several groups demonstrated that

enzymatically-isolated follicles could be sorted from the rest of the ovarian tissue resided with cancer cells using microfluidic device(34) or by sedimentation(21). However, the survival and the function of enzymatically-harvested primordial follicles are low due to the lack of a structural support and cell signaling from the surrounding matrix(35, 36). Therefore, we employed PEG hydrogels with the storage modulus of 5.2kPa, which mimicked the stiffness of soft stromal tissues (Fig.5S2). And here we demonstrated that PEG hydrogels can provide the physical support to preserve oocyte-somatic cell connections and the overall architecture of encapsulated follicles while enabling follicular expansion through degradation.

Volumetric expansion of the follicle is one of the key structural events during folliculogenesis. Starting at the primordial stage, the volumetric expansion of the growing follicle is approximately 300 folds in mice and about 10^5 fold in humans when the follicle reaches antral preovulatory stages(15, 28). As a result, the surrounding matrix of the encapsulated follicles must accommodate the volumetric expansion associated with the follicular growth, either through elastic expansion or degradation. Natural hydrogels, such as alginate and fibrin, provided an important platform to study folliculogenesis *in vitro* and *in vivo*. For example, alginate hydrogels support follicle growth and 3D culture of rodent follicles. Yet, the non-degradable nature of the alginate hydrogel was prohibitive in supporting the complete development of a human follicle, which typically reaches a diameter of 20 mm at the final stages(37). On the other hand, the fast degrading fibrin gels provided the required physical support for the remodeling and growth of the implanted follicles, but for a limited time(20). These examples emphasized the importance of material properties for the follicle growth and maturation. The synthetic tunable PEG hydrogels were able to accommodate massive volumetric

expansions of growing follicles within the graft as indicated by the presence of multiple fully-grown antral follicles.

We also observed the development of early-stage follicles into antral follicles and corpora lutea, concluding the final stage of folliculogenesis in PEG hydrogels after 30 days *in vivo*. The proportion of growing follicles continuously increased over the 60 days post implantation, while the total number of the follicles in the grafts decreased over the same period. The natural decline in follicle numbers occurs as immature follicles enter the growing pool every estrous cycle, then mature and ovulate. Maintaining high percentage of primordial and primary follicles after 60 days *in vivo* suggested a selective activation, rather than a burst activation and premature depletion of primordial follicles, which is believed to be a common cause of an early graft failure(11-13). This resembles behavior of the normal ovarian reserve where the majority of primordial follicles remain in quiescent state and only a small cohort activates each cycle(37).

Overall, multiple fully-grown antral follicles and the corpora lutea corresponded with the physiological levels of follicle-stimulating hormone (FSH). We measured the FSH levels to evaluate the function of the artificial ovarian tissue and the restoration of the endocrine hypothalamus-pituitary-gonad (HPG) axis. After the complete development of the early-stage follicles, granulosa cells of antral follicles produced high levels of estrogen, resulting in the restoration of feedback to reduce FSH secretion by the pituitary gland. We demonstrated that resumed cyclicity at 14 days, and significant decrease in FSH levels at 30 days post-Tx, which corresponded with the appearance of antral follicles in the histological sections. As the proportion of growing follicles continuously increased, FSH levels further declined reaching physiological levels, confirming the restoration of the HPG axis. Regular estrous cycles were

maintained up to 60 days, which is another indication of potential restoration of normal endocrine function.

The described ovarian PEG graft initially sustained follicle survival by diffusion of essential nutrients without active vasculature(38). However, vascularization of the graft is needed to prevent hypoxia in the long-term, control follicular quiescence, and inhibit atresia for a larger construct with multiple growing follicles(39). Human ovarian cortical strips are dense and have longer revascularization periods, which negatively affect the outcomes of ovarian grafts(12, 13). Similarly, within plasma clots, oocytes were lost by extrusion and necrosis, and more losses occurred after transplantation due to hypoxia before the graft was vascularized(40). The presence of functioning blood vessels containing red blood cells shows a promising result of cell driven remodeling and tissue regeneration within PEG hydrogels. The formation of a vascular network occurred mostly around follicles due to the presence of high concentration of proangiogenic growth factors, such as vascular endothelial growth factor (VEGF)(41). The presence of stromal cells is also likely to have contributed to vascularization process after grafting by regulating vascular remodeling and producing angiogenic factors(42). Neovascularization driven by endothelial and stromal cells of the host is a promising approach to reconstructing an artificial organ for long-term applications. These results demonstrate the promising role of synthetic PEG hydrogels as a platform for reproductive tissue engineering and regenerative medicine.

5.4 Conclusion

In summary, our study provides a systematic investigation of the first synthetic system for artificial ovarian tissue engraftment and regeneration. PEG hydrogels with tunable mechanical properties and controlled degradation successfully supported folliculogenesis and steroidogenesis

in vivo. After 30 days, grafts revealed multiple fully developed antral follicles and corpora lutea, which corresponded with regular ovulation cycles and follicle-stimulating hormone (FSH) levels. The elevated levels of FSH, caused by bilateral ovariectomy, were reversed by the implanted follicles and maintained at physiological levels for 60 days. Importantly, primordial and primary follicles still represented 60% of the follicular pool, demonstrating selective recruitment of primordial follicles into the growing pool. Functioning blood vessels in the grafts 30 and 60 days after implantation proved the capability of PEG hydrogels to undergo graft remodeling and revascularization. Our results demonstrate for the first time that PEG hydrogels with encapsulated immature ovarian follicles successfully functioned as an artificial ovarian tissue for 90 days *in vivo*.

5.5 Materials and Methods

5.5.1. Ovariectomy and orthotopic transplantation

A bilateral ovariectomy (OvX) was performed on 12 – 16 week-old mice (B6CBAF1) to mimic premature ovarian failure and absence of ovarian endocrine function. Animals were treated in agreement with the NIH Guide for the Care and Use of Laboratory Animals and the Institutional Animal Care and Use Committee (IACUC) protocol at the University of Michigan. All the surgical procedures were approved and performed according to the IACUC protocol (PRO00006459). Ovaries were removed from the ovarian bursa as previously described(43) with some modification. Briefly, a 1.5cm longitudinal midline incision was made in the abdominal wall using aseptic techniques and procedures. Then intraperitoneal space was exposed with an abdomen retractor. Before the ovary was removed, the ovarian blood vessels were tied to prevent bleeding after ovariectomy. To prevent the bursal cavity from collapsing, a 15μL alginate (1.0%

w/v) bead was placed inside the bursal cavity and closed with 10-0 non-absorbable sutures (Fig.5.1A). The same procedure was repeated for each ovary. The abdominal muscles and skin were closed with 5-0 absorbable sutures. Following recovery, the animal was housed in the animal facility for at least 14 days. Mice received analgesics for at least 48 hours after surgery or as needed. 14 – 21 days after ovariectomy, PEG hydrogels were transplanted into both orthotopic sites as described above, following removal of the alginate bead (Fig.5.1D-G). Ovariectomized mice were randomly assigned to a control group that did not receive PEG grafts post-OvX. The graft function was assessed through daily vaginal cytology, serum levels of follicle-stimulating hormone (FSH), and histology of the retrieved PEG-VS hydrogels after 14 (n_{mice}=11), 30 (n_{mice}=6), 60 days (n_{mice}=6) and 90 days (n_{mice}=4) after transplantation. Power analysis was performed using Graphpad StatMate (GraphPad Prism Software, La Jolla, CA) (alpha = 0.05, power > 80%) to determine the number of animals.

5.5.2. Enzymatic follicle isolation and viability assessment

For all experiments, ovaries were isolated from 6 – 7 day old female mice (B6CBA F1), separated from the connective tissues and enzymatically digested in 50μL (13 Wünsch units/mL) Liberase DH (Roche, Indianapolis, IN) in 500 μL L15 (Leibovitz's) media (Sigma-Aldirch) (Fig.5.1B). The total digestion time was 50min at 37^{o}C, followed by 20min gentle pipetting of enzyme-digested pieces. The enzyme digestion was arrested by adding 10% fetal bovine serum and the digest was transferred to a tube for sedimentation. The sedimentation velocity of primordial and primary follicles was calculated according to a previously published report(20). After 15min of sedimentation, the top half of the total media containing slower sinking arbitrary cells was removed. The rest of the media volume remaining follicular suspension was removed by centrifuging at 100G for 5min. To determine any deleterious effects of the isolation procedure

on the viability of enzymatically isolated follicles, double fluorescent labeling LIVE/DEAD Cell Imaging Kit (Invitrogen) was performed according to the manufacturer's protocol.

5.5.3 Encapsulation of enzymatically isolated follicles in PEG-VS hydrogels and graft preparation

The hydrogels were prepared by dissolving 8 arm PEG-Vinyl sulfone (PEG-VS, hexaglycerol, 40,000 g mol^{-1}, >99% purity, Jenkem Technology) in 0.05 M HEPES Buffer at pH 7.66 at room temperature, followed by addition of integrin-binding peptide (RGD) (GenScript). The hydrogels were formed via Michael-type addition (MTA) chemistry with MMP-sensitive tri-functional crosslinking peptides AcG**C***L*↓*GPA*G**C***L*↓*GPA***C**G (LGPA) (1217.45 g mol^{-1}, >90% purity, GenScript, cleavage site indicated by ↓, cysteines with reactive thiols are in bold). The stoichiometric ratio of -VS to thiol (-SH) groups was kept at 1:1 ratio for all experiments. PEG hydrogels were modified with the integrin-binding peptide G**C**GYG*RGD*SPG (RGD) (1067.10 g mol^{-1}, GenScript) to allow cell adhesion and migration. The modified PEG solution was kept at room temperature for 15min to allow the RGD peptide to chemically bind to the PEG precursor, and 6.5µL of the modified PEG solution was then pipetted into the concentrated follicle suspension and gently mixed. The LGPA crosslinker was dissolved in HEPES buffer and 5.5µL of the crosslinking peptide solution was added to the mixture of PEG-VS and follicle suspension. Two grafts with follicles (6.5µL each) were allowed to crosslink on a heating plate at 37 ^{o}C for 10min to complete the MTA reaction. Upon complete gelation, these hydrogels were transplanted immediately into the ovarian bursa (Fig.5.1C).

5.5.4. Functionality of the artificial ovarian tissue

5.5.4.1. Vaginal Cytology

The presence of estrous cycle in the transplanted animals was determined by daily vaginal cytology. The animals were gently restrained by the tail and 0.1 – 0.2mL of saline was pushed using a syringe or a pipette in and out of the vaginal opening to collect cells to identify cycle stage every day, before and after transplantation. The onset and cessation of cyclicity were determined by the cell population in the vaginal lavage.

5.5.4.2. Blood collection for measurements of follicle-stimulating hormone in serum

Lateral tail vein blood (0.5-1% volume of the total body weight: ~ 0.075-0.15 mL from a mouse weighing 15 grams) was collected every 2 weeks to compare FSH levels pre- and post-transplantation. The mouse was restrained in a mouse trap to allow easy access to the tail. The lower one half of the tail was cleaned with 70% alcohol and a small incision in the tail vein at the distal end of the tail was made using a sharp scalpel or razor blade. A new scalpel was used for each animal. 75 - 150μL blood was collected in a capillary tube and left at 4^{o}C overnight to allow blood to clot. Then 10 - 20μL serum was aspirated from the sample following centrifugation at 10,000rpm at 4^{o}C for 10min and stored at -20^{o}C. At the terminal time point of the experiment, the blood was collected via cardiac puncture. All samples were labeled numerically to blind any correlation to time points or group assignments. The FSH levels were measured with Radioimmunoassay at Ligand Assay and Analysis Core Facility at University of Virginia Center for Research in Reproduction.

5.5.5. Histological tissue analysis

After 14 (n_{mice}=11), 30 (n_{mice}=6), 60 days (n_{mice}=6) and 90 days (n_{mice}=4) following transplantation, PEG-VS hydrogels were retrieved and fixed in Bouin's fixative solution (Sigma-

Aldrich) overnight, and then transferred to 70% EtOH at 4 ^{o}C until processing. The number of follicles and their distribution on day 0 (pre-transplantation) was characterized using HistoGel^{TM} (Richard-Allan Scientific^{TM}) using a similar procedure for encapsulation in PEG. After fixation, all samples were processed at the Histology Core in Microscopy & Image Analysis Laboratory at the University of Michigan. Samples were embedded in paraffin and serially sectioned at a 7μm thickness and were stained with hematoxylin and eosin (H&E) to identify and count follicles at all the developmental stages. Primordial follicles were identified by the nucleus, which is surrounded by a single layer of flattened squamous follicular cells. A primary follicle was defined as an oocyte surrounded by a single layer of cuboidal granulosa cells (GCs). A secondary follicle has two or more layers of cuboidal GCs, but no antrum, and the presence of a fluid-filled antrum defined an antral follicle. Extensive permeation of red blood cells into the ovulated follicle and luteinized granulosa cells were defined as corpora lutea (CL).

Identified follicles were quantified by counting every-other section of every-other slide (4 sections per slide) to prevent counting a follicle more than once(20). Since every-other slide was counted, a correction factor was applied to adjust for the counting rules. The oocyte diameter for primordial and primary follicles averaged 14μm (44), meaning the same follicle would appear only on 2 consecutive sections. Therefore, the numbers of primordial and primary follicles were doubled since every-other slides was counted. Primary, secondary, and antral follicles were counted when the nucleolus of the oocyte was present. This was done to prevent double counting of large growing follicles (secondary and antral) and undercounting smaller follicles.

5.5.6. Immunohistochemistry

To analyze the neovascularization within transplanted PEG hydrogels, paraffin sectioned slides were stained for mouse endothelial cells. First, sections were deparaffinized with Xylene

and rehydrated in 100% Ethanol. Slides were incubated in 3% H_2O_2 for 30min at room temperature to block any endogenous peroxidase activity. Then, slides were incubated in 10mM Tris EDTA (pH 9) solution for 20min at 96^{o}C and additional 20min at room temperature for antigen retrieval. Afterwards, non-specific bindings were blocked by the protein block (Abcam) for 1 hr followed by overnight incubation at 4^{o}C with primary antibodies – rabbit anti-mouse CD34 antibody (1:500 dilution) (Abcam, catalog#ab81289) dissolved in TBS with 1% Normal Rabbit Serum (Sigma-Aldrich) and 0.1% Bovine Serum Albumin (Fisher Scientific). Following incubation overnight, slides were treated for 20min each with the Biotinylated Goat Anti-Polyvalent and Streptavidin Peroxidase, provided in Rabbit Specific HRP/DAP Detection IHC Kit (Abcam). Hematoxylin was used for counterstaining. Healthy mouse uterus was used as positive control and negative control slides were incubated without the presence of primary antibody (Fig.5S3). The identical procedure was followed for both positive and negative control as described.

5.5.7. Statistical Analysis

All statistical analyses were performed using GraphPad Prism (GraphPad Prism Software, La Jolla, CA) and power analyses were performed using GraphPad StatMate (GraphPad Prism Software, La Jolla, CA) (alpha = 0.05, power >80%). Homogeneity of variance was determined with an F test. For sample sizes ($n>5$), data are reported as mean ± standard deviation of measurements, and statistical analyses were performed with one- way ANOVA followed by Tukey's post-test. And statistical significance was set at $p<0.05$. For sample sizes ($n<5$), individual data points were plotted and the statistical analyses were performed with the Kruskal-Wallis test followed by Dunn's post-test (Fig.5.3A), or Mann-Whitney test (Fig.5.5D).

5.6 References

1. Resetkova N, Hayashi M, Kolp LA, Christianson MS. Fertility Preservation for Prepubertal Girls: Update and Current Challenges. Curr Obstet Gynecol Rep. 2013 Dec 1;2(4):218-25.

2. Smith MA, Altekruse SF, Adamson PC, Reaman GH, Seibel NL. Declining childhood and adolescent cancer mortality. Cancer. 2014 Aug 15;120(16):2497-506.

3. Meirow D, Nugent D. The effects of radiotherapy and chemotherapy on female reproduction. Hum Reprod Update. 2001 Nov-Dec;7(6):535-43.

4. Green DM, Sklar CA, Boice JD,Jr, Mulvihill JJ, Whitton JA, Stovall M, et al. Ovarian failure and reproductive outcomes after childhood cancer treatment: results from the Childhood Cancer Survivor Study. J Clin Oncol. 2009 May 10;27(14):2374-81.

5. Ethics Committee of American Society for Reproductive Medicine. Fertility preservation and reproduction in patients facing gonadotoxic therapies: a committee opinion. Fertil Steril. 2013 Nov;100(5):1224-31.

6. Jeruss JS, Woodruff TK. Preservation of fertility in patients with cancer. N Engl J Med. 2009 Feb 26;360(9):902-11.

7. Diller L. Clinical practice. Adult primary care after childhood acute lymphoblastic leukemia. N Engl J Med. 2011 Oct 13;365(15):1417-24.

8. Shuster LT, Rhodes DJ, Gostout BS, Grossardt BR, Rocca WA. Premature menopause or early menopause: long-term health consequences. Maturitas. 2010 Feb;65(2):161-6.

9. Donnez J, Dolmans MM. Ovarian cortex transplantation: 60 reported live births brings the success and worldwide expansion of the technique towards routine clinical practice. J Assist Reprod Genet. 2015 Aug;32(8):1167-70.

10. Fauser BC, Devroey P, Yen SS, Gosden R, Crowley WF,Jr, Baird DT, et al. Minimal ovarian stimulation for IVF: appraisal of potential benefits and drawbacks. Hum Reprod. 1999 Nov;14(11):2681-6.

11. Donnez J, Dolmans MM, Pellicer A, Diaz-Garcia C, Sanchez Serrano M, Schmidt KT, et al. Restoration of ovarian activity and pregnancy after transplantation of cryopreserved ovarian tissue: a review of 60 cases of reimplantation. Fertil Steril. 2013 May;99(6):1503-13.

12. Kim SS, Soules MR, Battaglia DE. Follicular development, ovulation, and corpus luteum formation in cryopreserved human ovarian tissue after xenotransplantation. Fertil Steril. 2002 Jul;78(1):77-82.

13. Donnez J, Squifflet J, Dolmans MM. Frozen-thawed ovarian tissue retransplants. Semin Reprod Med. 2009 Nov;27(6):472-8.

14. Dolmans MM, Luyckx V, Donnez J, Andersen CY, Greve T. Risk of transferring malignant cells with transplanted frozen-thawed ovarian tissue. Fertil Steril. 2013 May;99(6):1514-22.

15. Picton HM. Activation of follicle development: the primordial follicle. Theriogenology. 2001 Apr 1;55(6):1193-210.

16. Smitz J, Dolmans MM, Donnez J, Fortune JE, Hovatta O, Jewgenow K, et al. Current achievements and future research directions in ovarian tissue culture, in vitro follicle development and transplantation: implications for fertility preservation. Hum Reprod Update. 2010 Jul-Aug;16(4):395-414.

17. Nieman CL, Kazer R, Brannigan RE, Zoloth LS, Chase-Lansdale PL, Kinahan K, et al. Cancer survivors and infertility: a review of a new problem and novel answers. J Support Oncol. 2006 Apr;4(4):171-8.

18. West ER, Zelinski MB, Kondapalli LA, Gracia C, Chang J, Coutifaris C, et al. Preserving female fertility following cancer treatment: current options and future possibilities. Pediatr Blood Cancer. 2009 Aug;53(2):289-95.

19. Vanacker J, Dolmans MM, Luyckx V, Donnez J, Amorim CA. First transplantation of isolated murine follicles in alginate. Regen Med. 2014;9(5):609-19.

20. Smith RM, Shikanov A, Kniazeva E, Ramadurai D, Woodruff T, Shea LD. Fibrin-mediated delivery of an ovarian follicle pool in a mouse model of infertility. Tissue Eng Part A. 2014 May 7.

21. Kniazeva E, Hardy AN, Boukaidi SA, Woodruff TK, Jeruss JS, Shea LD. Primordial Follicle Transplantation within Designer Biomaterial Grafts Produce Live Births in a Mouse Infertility Model. Sci Rep. 2015 Dec 3;5:17709.

22. Chiti MC, Dolmans MM, Orellana R, Soares M, Paulini F, Donnez J, et al. Influence of follicle stage on artificial ovary outcome using fibrin as a matrix. Hum Reprod. 2016 Feb;31(2):427-35.

23. Shikanov A, Zhang Z, Xu M, Smith RM, Rajan A, Woodruff TK, et al. Fibrin encapsulation and vascular endothelial growth factor delivery promotes ovarian graft survival in mice. Tissue Eng Part A. 2011 Dec;17(23-24):3095-104.

24. Kim J, Kong YP, Niedzielski SM, Singh RK, Putnam AJ, Shikanov A. Characterization of the crosslinking kinetics of multi-arm poly(ethylene glycol) hydrogels formed via Michael-type addition. Soft Matter. 2016 Feb 21;12(7):2076-85.

25. Lutolf MP, Hubbell JA. Synthesis and physicochemical characterization of end-linked poly(ethylene glycol)-co-peptide hydrogels formed by Michael-type addition. Biomacromolecules. 2003 May-Jun;4(3):713-22.

26. Hern DL, Hubbell JA. Incorporation of adhesion peptides into nonadhesive hydrogels useful for tissue resurfacing. J Biomed Mater Res. 1998 Feb;39(2):266-76.

27. Howe A, Aplin AE, Alahari SK, Juliano RL. Integrin signaling and cell growth control. Curr Opin Cell Biol. 1998 Apr;10(2):220-31.

28. Shikanov A, Smith RM, Xu M, Woodruff TK, Shea LD. Hydrogel network design using multifunctional macromers to coordinate tissue maturation in ovarian follicle culture. Biomaterials. 2011 Apr;32(10):2524-31.

29. Vigen M, Ceccarelli J, Putnam AJ. Protease-sensitive PEG hydrogels regulate vascularization in vitro and in vivo. Macromol Biosci. 2014 Oct;14(10):1368-79.

30. Pratt AB, Weber FE, Schmoekel HG, Muller R, Hubbell JA. Synthetic extracellular matrices for in situ tissue engineering. Biotechnol Bioeng. 2004 Apr 5;86(1):27-36.

31. Lutolf MP, Weber FE, Schmoekel HG, Schense JC, Kohler T, Muller R, et al. Repair of bone defects using synthetic mimetics of collagenous extracellular matrices. Nat Biotechnol. 2003 May;21(5):513-8.

32. Ny T, Wahlberg P, Brandstrom IJ. Matrix remodeling in the ovary: regulation and functional role of the plasminogen activator and matrix metalloproteinase systems. Mol Cell Endocrinol. 2002 Feb 22;187(1-2):29-38.

33. McGee EA, Hsueh AJ. Initial and cyclic recruitment of ovarian follicles. Endocr Rev. 2000 Apr;21(2):200-14.

34. Lai D, Labuz J, Kim J, Luker G, Shikanov A, Takayama S. Simple multi-level micochannel fabrication by pseudo-grayscale backside diffused light lithography. RSC Advances. 2013 July, 29th, 2013;3(42):19467-73.

35. Hovatta O, Wright C, Krausz T, Hardy K, Winston RM. Human primordial, primary and secondary ovarian follicles in long-term culture: effect of partial isolation. Hum Reprod. 1999 Oct;14(10):2519-24.

36. Abir R, Fisch B, Nitke S, Okon E, Raz A, Ben Rafael Z. Morphological study of fully and partially isolated early human follicles. Fertil Steril. 2001 Jan;75(1):141-6.

37. Gougeon A. Regulation of ovarian follicular development in primates: facts and hypotheses. Endocr Rev. 1996 Apr;17(2):121-55.

38. Griffith CK, Miller C, Sainson RC, Calvert JW, Jeon NL, Hughes CC, et al. Diffusion limits of an in vitro thick prevascularized tissue. Tissue Eng. 2005 Jan-Feb;11(1-2):257-66.

39. Fortune JE, Cushman RA, Wahl CM, Kito S. The primordial to primary follicle transition. Mol Cell Endocrinol. 2000 May 25;163(1-2):53-60.

40. Gosden RG. Restitution of fertility in sterilized mice by transferring primordial ovarian follicles. Hum Reprod. 1990 Jul;5(5):499-504.

41. Geva E, Jaffe RB. Role of vascular endothelial growth factor in ovarian physiology and pathology. Fertil Steril. 2000 Sep;74(3):429-38.

42. Dissen GA, Lara HE, Fahrenbach WH, Costa ME, Ojeda SR. Immature rat ovaries become revascularized rapidly after autotransplantation and show a gonadotropin-dependent increase in angiogenic factor gene expression. Endocrinology. 1994 Mar;134(3):1146-54.

43. Liu L, Wood GA, Morikawa L, Ayearst R, Fleming C, McKerlie C. Restoration of fertility by orthotopic transplantation of frozen adult mouse ovaries. Hum Reprod. 2008 Jan;23(1):122-8.

44. Bristol-Gould SK, Kreeger PK, Selkirk CG, Kilen SM, Cook RW, Kipp JL, et al. Postnatal regulation of germ cells by activin: the establishment of the initial follicle pool. Dev Biol. 2006 Oct 1;298(1):132-48.

CHAPTER VI

Conclusion and Future Directions

6.1 Conclusion

This work demonstrated the design of synthetic hydrogels to mimic the components of tissues that provide mechano-biological cues to reconstruct and regenerate the structure and their function *in vivo*. The extracellular matrix (ECM) provides the three-dimensional (3D) structure and paracrine signals that regulate and promote cell adhesion and directs the cellular processes leading to tissue development(1, 2). ECM also affects morphology(3), cell communication(4, 5), survival(6, 7), proliferation(8) and steroidogenesis(9). Naturally derived and synthetic hydrogels have been extensively exploited in biomedical materials research due to their abilities in directing cellular behavior and function(10, 11). These hydrogels have been used to examine cell-matrix interaction and have the potential to modify the components and density of ECM proteins. Different cellular responses result from interactions with specific integrins and adhesion sequences(12). Each chapter demonstrated the role of various material properties of 3D matrices on cellular behavior, morphology, and growth, which contributed to reconstruction and regeneration of a desired tissue.

In Chapter II, we addressed three different components toward building an artificial ovarian tissue, from enzymatic isolation and purification of the early stage follicles to encapsulation in natural hydrogels. Follicle sorting using microfluidic device would serve as future potential applications of clinical treatment-scale separation of ovarian follicles from cancer cells. After follicle isolation, multiple previous studies(13-16) confirmed that re-implanting of isolated follicles using fibrin hydrogels has shown promising results; however, the rapid degradation and coupled mechanical and biological properties of fibrin hydrogels resulted in early graft failure. This result further confirmed the importance of a precise control of hydrogel properties to design the optimum environment for long-term applications.

In Chapter III, we explored the effect of mechanical properties of natural hydrogels like fibrin, fibrin-collagen, and collagen, on cellular growth and behavior. Fibrin degradation was controlled by using aprotinin to demonstrate the importance of a precise control of degradation rate. Throughout the different gel systems, more cell growth and more interconnected stromal network formation were observed when cells were in less rigid and more degradable environments, which allowed branching and cell remodeling. Unlike slow degrading collagen-containing gel systems, fibrin degradation rate was controlled with aprotinin, which provided the structural support while allowing them to migrate and remodel their microenvironment. This result demonstrated how the defined control over degradation rate can balance matrix degradation and cell proliferation and regulate cellular behavior.

As shown in Chapter III, natural hydrogels are compatible with live cells, support cell attachment, migration and remodeling; however, the mechanical and biological properties of these materials are closely tied. Supplementing the culture with aprotinin delayed fibrin degradation, yet for no longer than 10 days, limiting its long-term applications. In contrast to

natural hydrogels, biologically inert synthetic hydrogels, such as poly(ethylene glycol) (PEG), have tunable physical properties independent of their biological activity(17-22). Bioactive modification, such as incorporation of integrin binding sequences, affected the mechanical properties of multi-arm PEG gels, such as storage modulus and swelling, as a consequence of the macroscopic network changes. These changes were dependent on PEG functionality (4 vs. 8-arm) and PEG solid concentrations, which are directly related to the concentration of elastically active chains and the overall amount of binding sites.

Therefore, in Chapter IV, we explored the role of functionality and the effects of bioactive modification on the material properties of multi-arm PEG hydrogels. Overall, 8-arm PEG allowed a greater degree of modification and its macroscopic properties and crosslinking kinetics were less affected by the act of modification or quenching compared to 4-arm PEG. These advantages provide a finely tuned design for various biological applications with broad range of bioactive modification. And when human bone marrow stromal cells were encapsulated in 4 and 8-arm PEG hydrogels, different cellular phenotype and behavior was observed from spheroids formation in 4-arm PEG to dense and connected stromal networks formation in 8-arm PEG. And different cellular phenotype and behavior was observed from spheroids formation in 4-arm PEG to dense and connected stromal networks formation in 8-arm PEG. These results demonstrate that bioactive modification not only affects the PEG hydrogel's macroscopic properties, but also regulates cellular behavior. Overall, well-controlled biochemical and biophysical cues can mimic the complex components of ECM in synthetic hydrogels like PEG to function as a platform for diverse tissue engineering applications.

Lastly, in Chapter V, we utilized synthetic PEG hydrogels as a supportive matrix for follicle development and neovascularization to initiate the graft remodeling in mice, functioning as an

artificial ovarian tissue. The mechanism and kinetics of degradation of the synthetic PEG matrix mirrored follicle growth and function *in vivo*. The degradation rate of the hydrogel and its physical properties provided the structural support for the implanted tissue, yet allowed follicle growth and expansion, and cell migration to maximize engraftment and revascularization of the matrix surrounding implanted mouse follicles. The graft function was supported by resumed cyclicity starting at 14 days post-Tx and the physiological levels of FSH were maintained up to 84 days. In summary, this is the first study proving the concept of a fully functional artificial ovarian tissue transplant built on a platform of the synthetic PEG hydrogel. And this is also the first step towards a fully engineered synthetic hydrogel that will present a clinically translatable opportunity to preserve fertility and ovarian endocrine function in women with premature ovarian failure.

6.2 Future directions

Naturally derived and synthetic hydrogels have been extensively exploited in biomedical materials research as a platform for tissue engineering. There are many ongoing studies to understand the effect of biophysical and biochemical cues on cellular differentiation and function(23-25). However, there are still many mysteries to unfold to understand how each component in a complex set of tissues or organs play a role in regulating or maintaining the function. And PEG hydrogel can be utilized as a tool to unfold these mysteries by decoupling and isolating components of ECM and as a biomimetic platform for tissue engineering.

In this dissertation, we showed the importance of the defined control over material properties and the effects on cellular behavior and tissue regeneration. We demonstrated 8-arm PEG allowed a greater degree of modification and its macroscopic properties; however, further studies

will be needed to understand the effect of increasing functionality even more. The properties of star polymers are known to be affected steric hindrances(26); however, the threshold of functionality that results in complete gelation is still unknown. And plasmin-sensitive peptide YKNR and MMP-sensitive peptide LGPA were used in this study. However, bioactive modification with other protease sensitive peptide sequences and more than one peptide sequences at the same time can be investigated further, because different peptide sequences demonstrate different rate of degradation and specificity toward proteases(27). Other studies also have demonstrated the laminin-derived peptide YIGSR can be used in conjunction with fibronectin-derived RGD to enhance spreading on PEG gels(22, 28, 29). Further modification is possible by covalently bonding thiolated growth factors, which are incorporated into a PEG thiol-ene hydrogel promoting cell proliferation and matrix production(30). Incorporation of all of these components will allow better mimicking the complex system of tissue, which will further widen the scope of biomedical applications.

The PEG graft initially sustained follicle survival by diffusion of essential nutrients without active vasculature(31). However, faster vascularization of the graft will need to happen to prevent hypoxia, control follicular quiescence, and inhibit atresia for a larger construct with multiple growing follicles. Human ovarian cortical strips are dense and have longer revascularization periods, which negatively affect the outcomes of ovarian grafts. To initiate vascularization and remodeling process in earlier stage after transplantation, growth factors, such as vascular endothelial growth factor (VEGF)(32), can be incorporated. Also neovascularization driven by endothelial and stromal cells of the host is a promising approach to reconstructing an artificial organ for long-term applications.

PEG hydrogels with tunable mechanical properties and controlled degradation successfully supported folliculogenesis and steroidogenesis *in vivo* in mice. However, this study is only the first step towards a fully engineered synthetic hydrogel that will present a clinically translatable opportunity to preserve fertility and ovarian endocrine function in women with premature ovarian failure. First of all, the restoration of fertility was not demonstrated in this dissertation, which determines the full restoration of both endocrine and reproductive function. However, the live-birth was demonstrated using fibrin as a graft material, suggesting the approach of grafting of isolated follicles can be a solution to fertility preservation(16). And in the context of clinical translation, there are still many hurdles to overcome. Human ovaries are not located within the ovarian bursa unlike those of mice, which would require different approach of transplantation. Also the number of follicles that determine the graft quality and longevity will be significantly affected by the quality of tissue from patients.

6.3 Concluding Remarks

To conclude, we demonstrated the structural reconstruction and functional regeneration of lymphoid and ovarian tissues using natural and synthetic hydrogel as a platform. By controlling the degradation rate of fibrin, we successfully reconstructed lymphoid stromal network *in vitro*. By characterizing and utilizing tunable multi-arm PEG hydrogels, we successfully regenerated an artificial ovarian tissue *in vivo* that restored the estrous cycle and HPG axis. However, as I stated before, this is only the first step toward a fully engineered artificial ovary. This research started with a strong motivation to improve the quality of human life, especially young women. My desire is that the information gathered in this dissertation will be a cornerstone to many other

researches that are intended to improve the quality of human life and eventually, relieve the pain of many suffering individuals.

6.3 References

1. Giancotti FG, Ruoslahti E. Integrin signaling. Science. 1999 Aug 13;285(5430):1028-32.

2. De Arcangelis A, Georges-Labouesse E. Integrin and ECM functions: roles in vertebrate development. Trends Genet. 2000 Sep;16(9):389-95.

3. Ben-Ze'ev A, Amsterdam A. Regulation of cytoskeletal proteins involved in cell contact formation during differentiation of granulosa cells on extracellular matrix. Proc Natl Acad Sci U S A. 1986 May;83(9):2894-8.

4. Albertini DF, Kravit NG. Isolation and biochemical characterization of ten-nanometer filaments from cultured ovarian granulosa cells. J Biol Chem. 1981 Mar 10;256(5):2484-92.

5. Anderson E, Albertini DF. Gap junctions between the oocyte and companion follicle cells in the mammalian ovary. J Cell Biol. 1976 Nov;71(2):680-6.

6. Adams JC, Watt FM. Regulation of development and differentiation by the extracellular matrix. Development. 1993 Apr;117(4):1183-98.

7. Irving-Rodgers HF, Mussard ML, Kinder JE, Rodgers RJ. Composition and morphology of the follicular basal lamina during atresia of bovine antral follicles. Reproduction. 2002 Jan;123(1):97-106.

8. Rodgers HF, Irvine CM, van Wezel IL, Lavranos TC, Luck MR, Sado Y, et al. Distribution of the alpha1 to alpha6 chains of type IV collagen in bovine follicles. Biol Reprod. 1998 Dec;59(6):1334-41.

9. Kreeger PK, Woodruff TK, Shea LD. Murine granulosa cell morphology and function are regulated by a synthetic Arg-Gly-Asp matrix. Mol Cell Endocrinol. 2003 Jul 31;205(1-2):1-10.

10. Peppas NA, Langer R. New challenges in biomaterials. Science. 1994 Mar 25;263(5154):1715-20.

11. Hubbell JA. Biomaterials in tissue engineering. Biotechnology (N Y). 1995 Jun;13(6):565-76.

12. Humphries MJ. The molecular basis and specificity of integrin-ligand interactions. J Cell Sci. 1990 Dec;97 (Pt 4)(Pt 4):585-92.

13. Shikanov A, Zhang Z, Xu M, Smith RM, Rajan A, Woodruff TK, et al. Fibrin encapsulation and vascular endothelial growth factor delivery promotes ovarian graft survival in mice. Tissue Eng Part A. 2011 Dec;17(23-24):3095-104.

14. Smith RM, Shikanov A, Kniazeva E, Ramadurai D, Woodruff T, Shea LD. Fibrin-mediated delivery of an ovarian follicle pool in a mouse model of infertility. Tissue Eng Part A. 2014 May 7.

15. Chiti MC, Dolmans MM, Orellana R, Soares M, Paulini F, Donnez J, et al. Influence of follicle stage on artificial ovary outcome using fibrin as a matrix. Hum Reprod. 2016 Feb;31(2):427-35.

16. Kniazeva E, Hardy AN, Boukaidi SA, Woodruff TK, Jeruss JS, Shea LD. Primordial Follicle Transplantation within Designer Biomaterial Grafts Produce Live Births in a Mouse Infertility Model. Sci Rep. 2015 Dec 3;5:17709.

17. Hern DL, Hubbell JA. Incorporation of adhesion peptides into nonadhesive hydrogels useful for tissue resurfacing. J Biomed Mater Res. 1998 Feb;39(2):266-76.

18. Lutolf MP, Lauer-Fields JL, Schmoekel HG, Metters AT, Weber FE, Fields GB, et al. Synthetic matrix metalloproteinase-sensitive hydrogels for the conduction of tissue regeneration: engineering cell-invasion characteristics. Proc Natl Acad Sci U S A. 2003 Apr 29;100(9):5413-8.

19. Pratt AB, Weber FE, Schmoekel HG, Muller R, Hubbell JA. Synthetic extracellular matrices for in situ tissue engineering. Biotechnol Bioeng. 2004 Apr 5;86(1):27-36.

20. Lutolf MP, Hubbell JA. Synthetic biomaterials as instructive extracellular microenvironments for morphogenesis in tissue engineering. Nat Biotechnol. 2005 Jan;23(1):47-55.

21. van de Wetering P, Metters AT, Schoenmakers RG, Hubbell JA. Poly(ethylene glycol) hydrogels formed by conjugate addition with controllable swelling, degradation, and release of pharmaceutically active proteins. J Control Release. 2005 Feb 16;102(3):619-27.

22. Weiss MS, Bernabe BP, Shikanov A, Bluver DA, Mui MD, Shin S, et al. The impact of adhesion peptides within hydrogels on the phenotype and signaling of normal and cancerous mammary epithelial cells. Biomaterials. 2012 May;33(13):3548-59.

23. Engler AJ, Sen S, Sweeney HL, Discher DE. Matrix elasticity directs stem cell lineage specification. Cell. 2006 Aug 25;126(4):677-89.

24. Huebsch N, Arany PR, Mao AS, Shvartsman D, Ali OA, Bencherif SA, et al. Harnessing traction-mediated manipulation of the cell/matrix interface to control stem-cell fate. Nat Mater. 2010 Jun;9(6):518-26.

25. Burdick JA, Murphy WL. Moving from static to dynamic complexity in hydrogel design. Nat Commun. 2012;3:1269.

26. Kim E, Kim B, Kim S. Structural effect of linear and star-shaped poly(L-lactic acid) on physical properties. J Polym Sci B Polym Phys. 2004;42(6):939-46.

27. Turk BE, Huang LL, Piro ET, Cantley LC. Determination of protease cleavage site motifs using mixture-based oriented peptide libraries. Nat Biotechnol. 2001 Jul;19(7):661-7.

28. Boateng SY, Lateef SS, Mosley W, Hartman TJ, Hanley L, Russell B. RGD and YIGSR synthetic peptides facilitate cellular adhesion identical to that of laminin and fibronectin but alter the physiology of neonatal cardiac myocytes. Am J Physiol Cell Physiol. 2005 Jan;288(1):C30-8.

29. Fittkau MH, Zilla P, Bezuidenhout D, Lutolf MP, Human P, Hubbell JA, et al. The selective modulation of endothelial cell mobility on RGD peptide containing surfaces by YIGSR peptides. Biomaterials. 2005 Jan;26(2):167-74.

30. Sridhar BV, Doyle NR, Randolph MA, Anseth KS. Covalently tethered TGF-beta1 with encapsulated chondrocytes in a PEG hydrogel system enhances extracellular matrix production. J Biomed Mater Res A. 2014 Dec;102(12):4464-72.

31. Griffith CK, Miller C, Sainson RC, Calvert JW, Jeon NL, Hughes CC, et al. Diffusion limits of an in vitro thick prevascularized tissue. Tissue Eng. 2005 Jan-Feb;11(1-2):257-66.

32. Geva E, Jaffe RB. Role of vascular endothelial growth factor in ovarian physiology and pathology. Fertil Steril. 2000 Sep;74(3):429-38.

APPENDIX

Supplemental Materials

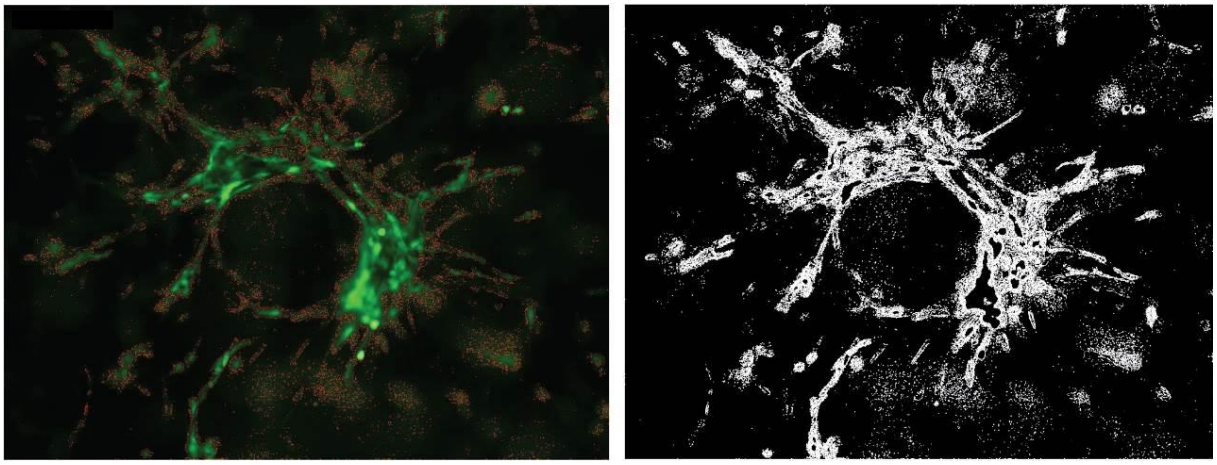

Figure 3A1. Network density measurement using GFP fluorescence. A MATLAB code was created using the Image Processing Toolbox in order to determine the approximate area of fluorescent. Specifically, the green channel was parsed out from each image before using image segmentation functions to create a gradient picture. Image segmentation relies upon differences in contrast in order to create a binary mask of the image. The binary mask image contains outlines of the cells and the mask is dilated and filled in order to cover the full area of each cell. Within the binary mask, white spots are denoted as cells, thus determining the number of white pixels in each image and converting this number to a micron size results in a calculated cell area. Additionally, superimposing the binary mask outline onto the original image ensures that cell area was detected appropriately and performs an optional check. All images analyzed were taken by Leica DMI3000B at 100x magnification and images were screened, selected and analyzed a double-blind manner.

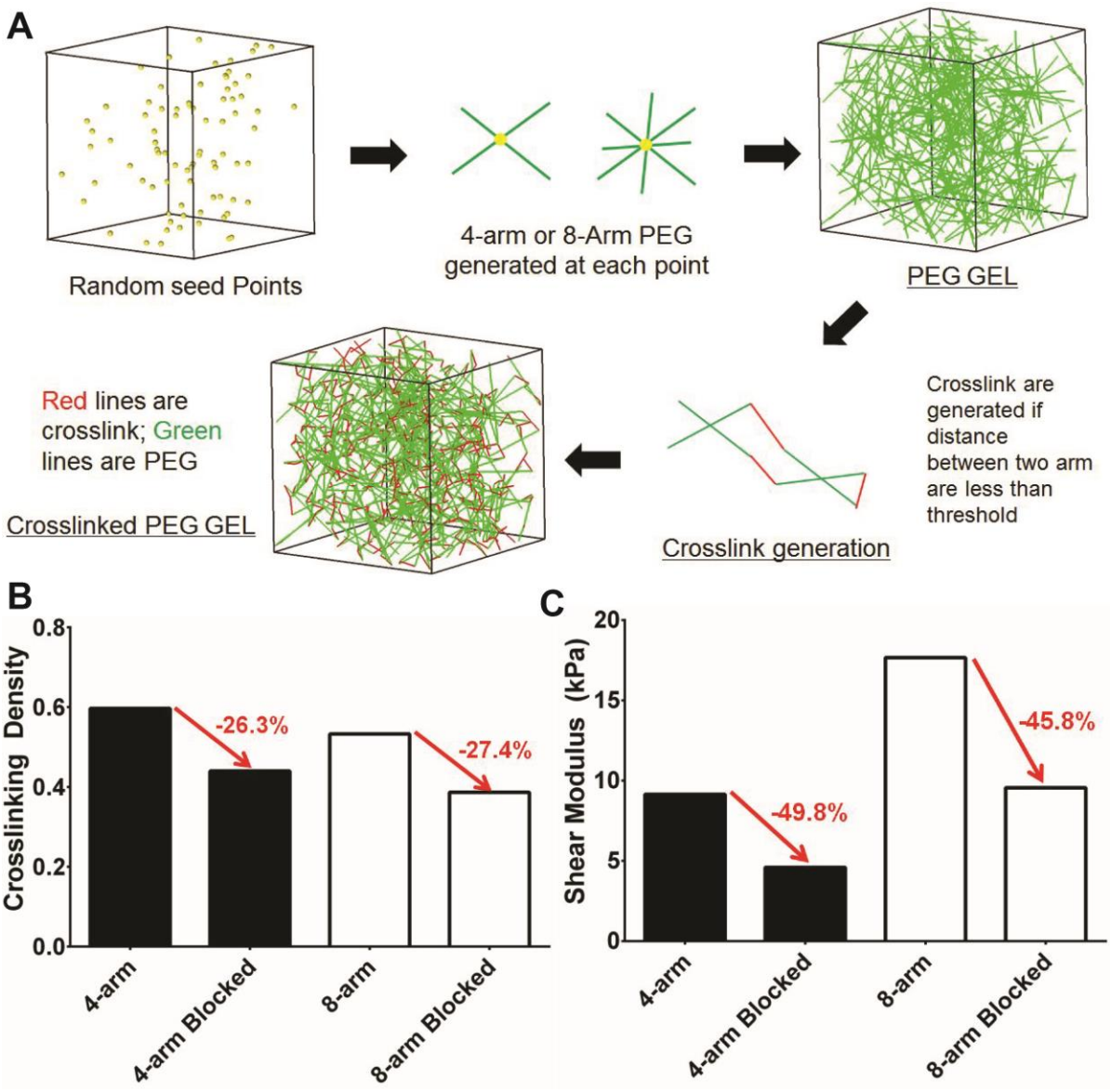

Figure 4A1. Computational modeling and simulation of 4 and 8-arm PEG hydrogels. **(A)** Model generation adapted from collagen model. Relative volume element (RVE) is 10µm in size length and the number of random points generated for 4-arm PEG is 200 and 100 for 8-arm PEG. Each arm length is set to 2µmwith crosslink threshold equal to 1µm. And total of four different models were simulated: 4-arm, 8-arm, 4-arm PEG blocked (one arm), and 8-arm PEG blocked (two arms). **(B)** Crosslinking density and **(C)** Shear modulus were simulated based on assumption of arm material property being 50MPa in elasticity and 31nm in diameter with 10% shear loading. According to simulation, 8-arm PEG is stiffer than the 4-arm PEG and is less susceptible to the arm block, following the trend of experimental results.

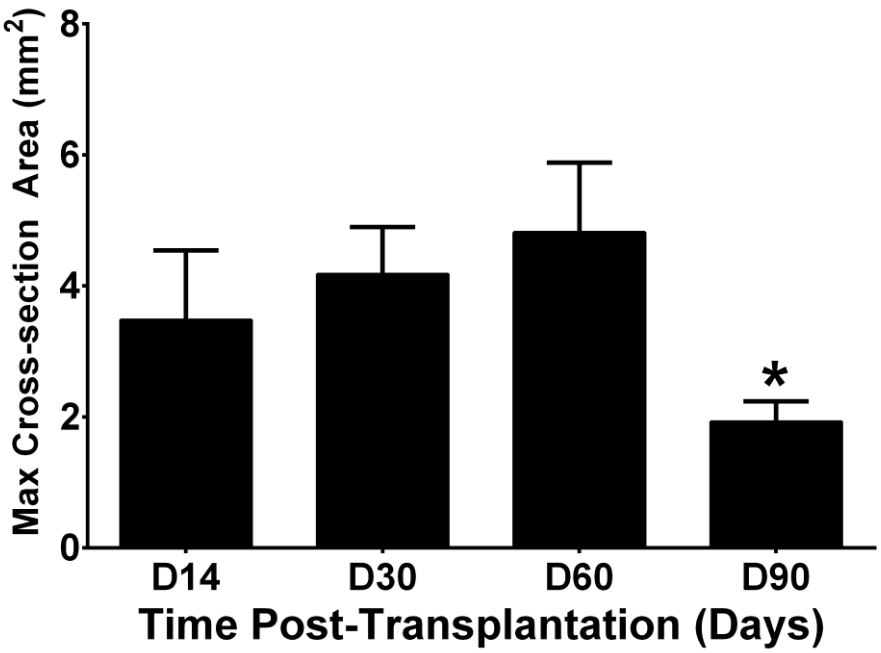

***Figure 5S1* – Maximum cross-section area of PEG hydrogels.** In order to analyze the PEG degradation, cross-section area measurements were taken from an H&E stained histological section of each sample. Each section at different time points was selected from the middle region of the entire sections. Measurements were performed using ImageJ 1.48v (U. S. National Institutes of Health, Bethesda, Maryland). PEG hydrogel implanted showed a bulk degradation behavior over 90 days *in vivo*. Statistical significance was determined by a one-way ANOVA followed by Tukey's test ($p < 0.05$).

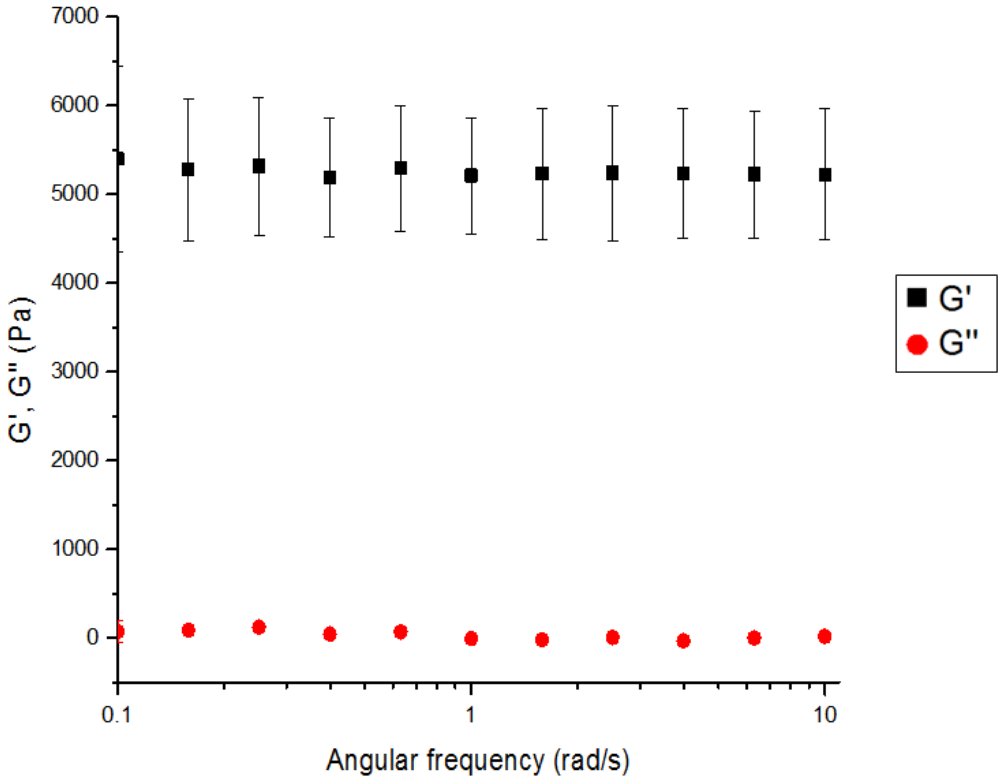

Figure 5S2 - Storage modulus (G') of 7% PEG-8VS (0.5mM RGD) crosslinked with LGPA: Frequency sweep test was performed at 10% strain to measure the storage modulus (G') of 7% PEG-8VS (0.5mM RGD) crosslinked with LGPA using AR-G2 rheometer (TA Instruments). These hydrogels were swollen in miliQ water for 24 hours before the measurement.

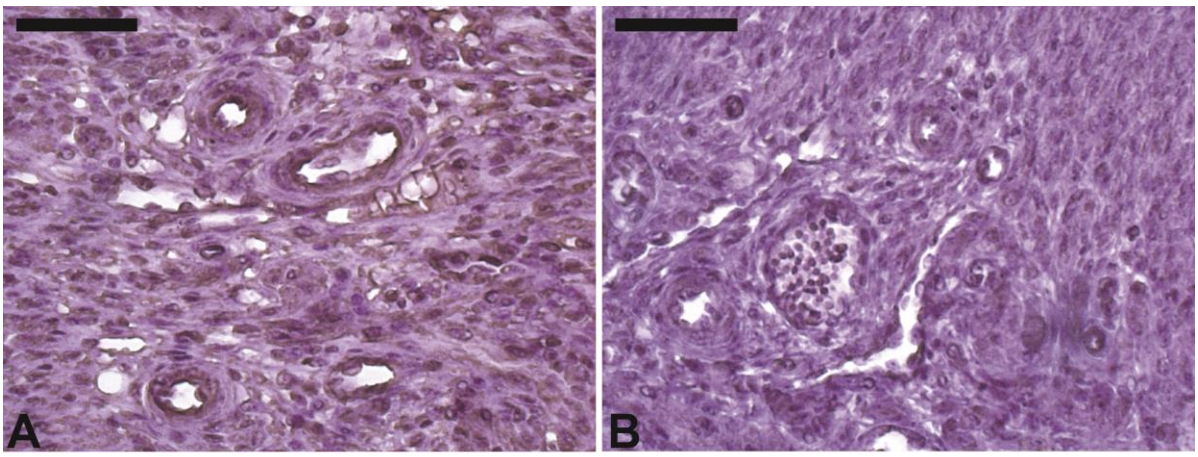

Figure 5S3 - Healthy mouse uterus was used as positive control **(A)** and negative control **(B)** slides were incubated without the presence of primary antibody. Positive CD34 staining was only observed with the presence of primary antibody, confirming its specificity. Scale bar: 50 µm.